

Evaluation of Different Immobilization Techniques of TiO₂ Particles in Sintered Glass Substrate (SGS) for the Degradation of Humic Acid Solutions

by

Sheila M. Arias Román

A thesis submitted in partial fulfillment of the requirements for the degree of

MASTER OF SCIENCE
in
CIVIL ENGINEERING
(Environmental and Water Resources Engineering)

UNIVERSITY OF PUERTO RICO
MAYAGÜEZ CAMPUS

2017

Approved by:

Pedro J. Tarafa Vélez, PhD
Chairperson, Graduate Committee

Date

Marcelo O. Suárez, PhD
Co-chair, Graduate Committee

Date

Sangchul Hwang, PhD
Member, Graduate Committee

Date

Juan Romero, PhD
Representative, Graduate School

Date

Ismael Pagán Trinidad, MSCE
Director, Department of Civil Engineering and Surveying

Date

ABSTRACT

It is well known that humic acids (HAs) have become one of the most extensively investigated organic material since they are considered one of the principal precursors of harmful compounds such as trihalomethanes (THMs). In the last few years, great efforts have focused in the development of treatment alternatives to mitigate the formation of THM's. In spite of the considerable attention devoted to the removal of HA from raw water its continuous presence increase the potential for THMs formation above acceptable levels. To overcome this problem it is urgent to develop a practical technology for the water treatment facilities for the removal of the HAs. Hence, the present research aimed to develop an alternative to remove or destroy HAs in an aqueous medium through a TiO_2 assisted photocatalytic degradation. Different techniques for the immobilization of TiO_2 porous glass substrate (SGS) and its efficiency in degrading HA were evaluated. Four approaches were investigated to incorporate the TiO_2 particles in the SGS: 1) TiO_2 particles embedded in the SGS; 2) TiO_2 immobilization by gravitational deposition and evaporation; 3) immobilization by TiO_2 coating over the SGS surface; and 4) TiO_2 immobilization with Polyvinyl Alcohol. The SGS optimal percolation rate, surface porosity and total porosity as function of sintering temperature and time were investigated. The effect of the thermal treatment in the polymorph structure of the TiO_2 particles and GTCs was also assessed. It was found that the sintering time and temperature were critical experimental parameters since a decrease in the SGS open porosity, total porosity, and percolation was observed as these parameters

increases. The thermal treatment used for the immobilization process did not affected the crystal structure of the TiO₂ since the anatase phase was confirm in the XRD diffractogram. The removal efficiency was greater under acid conditions due to effect of electrostatic attraction and further adsorption that leads to a photomineralization of HA. Despite the discrepancy in the immobilization techniques, the photocatalytic degradation experiments showed that the performance and photoactivity of each GTC were very similar.

RESUMEN

Ácidos húmicos (HAs) se han convertido en uno de los materiales orgánicos más investigados, ya que se consideran principales precursores de compuestos dañinos como los trihalometanos (THMs). En los últimos años, grandes esfuerzos se han centrado en el desarrollo de alternativas de tratamiento para mitigar la formación de THM. A pesar de la atención dedicada a la eliminación de HA del agua cruda, su continua presencia aumenta el potencial de formación de THMs por encima de los niveles aceptables. Para superar este problema es urgente desarrollar una tecnología práctica para las instalaciones de tratamiento de agua que permita eliminar los HA. Por lo tanto, la presente investigación tuvo como objetivo desarrollar una alternativa para eliminar o destruir HAs en un medio acuoso a través de una degradación fotocatalítica asistida por TiO_2 . Se evaluaron diferentes técnicas para la inmovilización TiO_2 sobre un sustrato de vidrio poroso (SGS) y su eficiencia en la degradación de HA. Cuatro enfoques fueron investigados para incorporar las partículas de TiO_2 en el SGS: 1) partículas de TiO_2 incrustadas en el SGS; 2) inmovilización de TiO_2 por deposición gravitatoria y evaporación; 3) inmovilización por recubrimiento de TiO_2 sobre la superficie de SGS; y 4) inmovilización de TiO_2 con alcohol polivinílico. Se investigaron propiedades óptima del SGS, como percolación, porosidad superficial y porosidad total en función de temperatura y tiempo de sinterizado. También se evaluó el efecto del tratamiento térmico en la estructura polimorfa de las partículas de TiO_2 y los GTC. Se encontró que el tiempo y la temperatura de sinterizado son parámetros experimentales críticos ya que se

observaba una disminución en la porosidad y percolación SGS a medida que estos parámetros aumentaban. El tratamiento térmico utilizado para el proceso de inmovilización no afectó a la estructura cristalina del TiO_2 ya que la fase de anatasa se confirmó en el difractograma de XRD. La eficiencia de remoción fue mayor en condiciones ácidas debido al efecto de la atracción electrostática y la adsorción que conduce a una fotomineralización de HA. A pesar de la discrepancia en las técnicas de inmovilización, los experimentos de degradación fotocatalítica demostraron que el rendimiento y la fotoactividad de cada GTC eran muy similares.

Copyright © 2017 by Sheila Marie Arias Román. All rights reserved. Printed in the United States of America. Except as permitted under the United States Copyright Act of 1976, no part of this publication may be reproduced or distributed in any form or by any means, or stored in a data base or retrieved system, without the prior written permission of the publisher.

ACKNOWLEDGEMENTS

The successful outcome of this thesis would not be possible without God's guidance and blessing. I learnt a lot from this experience and that would not be possible without all the people that somehow contributed immensely towards the end of this endeavor. First, I would like to extend my sincere appreciation to my mentor, Dr. Pedro Tarafa Vélez, for offering me the opportunity to pursue Master's Study and for the confidence placed in me.

I am particularly grateful to Maricely Nieves who made this process easier due to her comprehension, constant cheers and unconditional support, which was a key factor in the completion of this process. I would also like to thank my little sister, Vivianna Arias, for her help in the laboratory.

I would like to express my gratitude to Boris Renteria and Perla Torres whose help allowed me to carryout the experimental part of this research. In addition, I would like to thank to Dr. Marco de Jesus for sharing with me his knowledge. I am very thankful to Roberto Caraballo because his help was fundamental and his support meant a lot to me. I would like to acknowledge the contribution of all the undergraduate students whose not only contribute to the experimental part but also help me to become a better mentor.

Finally, I appreciate the financial support I received during my master's that was possible thanks to the Puerto Rico Water Resources and Environmental Research Institute, Dr. Jonathan Muñoz and Ismael Pagán Trinidad.

TABLE OF CONTENTS

Abstract	I
Resumen	III
Acknowledgements	VI
List of Tables	IX
List of Figures	X
1 Introduction	1
1.1 Background	1
1.2 Need of Research	4
1.3 Research Scope and Objectives	5
2 Literature Review	7
2.1 Definition and Description of Humic Acids	7
2.1.1 Structure and Composition	9
2.1.2 Properties and Characteristics	14
2.1.3 HAs Isolation and its Analogs	16
2.1.4 HAs Detection Methods	18
2.2 Photocatalytic Degradation	22
2.2.1 Mechanism of Photocatalytic Oxidation Using TiO ₂	23
2.2.2 TiO ₂ Properties and Polymorph Phases	28
2.2.3 Effect of Catalyst Load	31
2.2.4 Effect of Solution pH	33
2.2.5 Adsorption of HAs	34
2.3 Photocatalytic Reactors	35
2.3.1 Slurry	35
2.3.2 Immobilization of TiO ₂	36
3 Materials and Methods	40
3.1 Materials	40
3.2 Sintered Glass Substrates	40
3.2.1 Particle Size distribution of the RGP	41
3.2.2 Sintering Process	41
3.3 Immobilization of TiO ₂ Particles in the SGS	42
3.3.1 TiO ₂ Particles within the SGS body	42

3.3.2TiO ₂ Particles Immobilized on the SGS surface	44
3.4Characterization of Physical and Structural Properties	48
3.4.1Morphology	48
3.4.2Percolation.....	49
3.4.3Surface Porosity.....	51
3.4.4General Porosity	52
3.4.5Polymorph Structure of TiO ₂ Phase	53
3.5Degradation of Natural Organic Matter	54
3.5.1Preparation of the HA Solutions	54
3.5.2Photocatalytic Reactor	55
3.5.3Photodegradation Experiments	56
3.6Adsorption of Natural Organic Matter	57
4 Results and Discussion.....	59
4.1Immobilization of TiO ₂ Particles in the SGS.....	61
4.1.1TiO ₂ Particles within the SGS body	62
4.1.2Immobilization by Gravitational Deposition and Evaporation	66
4.1.3Immobilization by TiO ₂ Coating over the SGS Surface.....	72
4.1.4Immobilization with Polyvinyl Alcohol	74
4.2Physical and Structural Properties of the Glass composite	75
4.2.1Percolation.....	75
4.2.2Surface Porosity.....	79
4.2.3General Porosity	85
4.2.4Polymorph Structure of TiO ₂ Particles	89
4.2.5Morphology	96
4.3Degradation of Humic Acid.....	99
4.3.1Photolysis	99
4.3.2Photodegradation of HA by TiO ₂ Suspension.....	102
4.3.3Photodegradation of HA by GTC.....	106
4.4Adsorption of Natural Organic Matter	118
4.5Fluorescence Spectra of HAs	120
5 Conclusions	122
References	126

LIST OF TABLES

Table 2-1. Typical index of atomic ratios for HA (based on Janknecht et al., 2009)	11
Table 2-2. Elemental composition of HAs extracted from different sources	12
Table 2-3. Elemental composition of commercial HAs (adapted from Uyguner-Demirel and Bekbolet, 2011)	18
Table 2-4. Major bands characteristics of FT-IR spectra of Humic Substances (modified from Matilainen et al., 2011)	22
Table 2-5. Properties of TiO ₂ crystalline structures	28
Table 2-6. Commercial TiO ₂ and their properties	30
Table 2-7. Influence on TiO ₂ concentration on photodegradation of HAs	32
Table 2-8. Methods for the immobilization of TiO ₂ on different substrates	37
Table 4-1. Granulometry of the MG-30 recycled glass powder	59
Table 4-2. TiO ₂ Particles deposited onto glass beads.....	63
Table 4-3. Porosity of the GTC prepared at pH 1.7.....	88
Table 4-4. Porosity of the GTC prepared at pH 5.....	88
Table 4-5. Photocatalytic removal of HA by Method 1 at pH 3	107
Table 4-6. Photocatalytic removal of HA by Method 1 at pH 6	107
Table 4-7. Photocatalytic removal of HA by Method 2 at pH 3	108
Table 4-8. Photocatalytic removal of HA by Method 2 at pH 6	108
Table 4-9. Photocatalytic removal of HA by Method 3 at pH 3	109
Table 4-10. Photocatalytic removal of HA by Method 3 at pH 6	109

LIST OF FIGURES

Figure 2-1. Structures of humic acid as proposed by: a). Stevenson (1982) (Retrieved from Peña-Méndez et al., 2005); and b). Schulten & Schnitzer (1993).....	10
Figure 2-2-2. Diagram of the mechanism of TiO ₂ photocatalysis (modified from Nakata & Fujishima, 2012).....	24
Figure 2-3. Process occurring during the photodegradation of HAs (modified from Dong et al., 2015)	27
Figure 3-1. Schematic of the percolation system.....	50
Figure 3-2. Schematic of the photocatalytic reactor box.....	56
Figure 4-1. Grain size distribution.....	60
Figure 4-2. RGP particle cumulative distribution curve	61
Figure 4-3. TiO ₂ mass loss as a function of pH and initial mass	64
Figure 4-4. Total TiO ₂ mass embedded onto the glass beads	65
Figure 4-5. Effect of TiO ₂ initial mass	67
Figure 4-6. TiO ₂ Mass deposited on the SGS: a) pH 1.7, and b) pH 5.....	69
Figure 4-7. TiO ₂ Mass Immobilized on the SGS for different temperatures.....	71
Figure 4-8. Percolation rate of SGS	76
Figure 4-9. Response surface for the percolation rate of SGS	77
Figure 4-10. Hydraulic conductivity as a function of sintering parameters	79
Figure 4-11. Surface micrograph for SGS sintered at 950°C for 45 minutes.....	81
Figure 4-12. Surface micrograph for SGS sintered at 975°C for 45 minutes.....	82
Figure 4-13. Surface micrograph for SGS sintered at 1000°C for 45 minutes.....	82
Figure 4-14. Surface micrograph classified using ImageJ	83
Figure 4-15. Characterization of the surface porosity of SGS samples.....	84
Figure 4-16. Response surface for surface porosity of SGS.....	85
Figure 4-17. Characterization of the total porosity of SGS samples.....	86
Figure 4-18. Porosity of the SGS as a function of calcination temperature	87
Figure 4-19. X-ray diffractogram of pure TiO ₂ powder	89
Figure 4-20. XRD diffractogram of TiO ₂ particles calcinated at: (a) 1000°C, (b) 975°C, (c) 950°C, (d) 900°C, (e) 800°C, and (f) 105°C	90
Figure 4-21. Effect of calcination temperature in TiO ₂ crystallinity	91
Figure 4-22. Effect of TiO ₂ mass deposited onto glass beads in the relative crystallinity: a) 10wt.%, b) 3wt.%, and c) 1wt.%	92
Figure 4-23. XRD diffractogram for TiO ₂ -glass beads sintered at 950°C for: (a) 90 min, (b) 75 min, and (c) 60min.....	93

Figure 4-24. XRD diffractogram for TiO ₂ -glass beads sintered at 975°C for: (a) 90 min, (b) 75 min, and (c) 60min	94
Figure 4-25. XRD diffractograms for GTC prepared by different TiO ₂ immobilization methods: (a) immobilized on the SGS surface with pH 5 at 900°C, (b) immobilized on the SGS surface with pH 5 at 800°C, (c) immobilized on the SGS surface with pH 1.7 at 900°C, (d) immobilized on the SGS surface with pH 1.7 at 800°C, and (e) pasting the SGS at 800°C	95
Figure 4-26. SEM micrographs of uncoated SGS.....	97
Figure 4-27. SEM micrographs of GTC prepared by method: (a) pasting the SGS, (b) immobilized on the SGS surface with pH 1.7, (c) immobilized on the SGS surface with pH 5, (d) TiO ₂ -glass beads sintered at 975°C with 1g of TiO ₂	98
Figure 4-28. Evaluation of photolysis, in terms UV absorbance, of HA at: (a) 20 mg/L, (b) 15 mg/L, and (c) 10 mg/L.....	100
Figure 4-29. Evaluation of photolysis, in terms TOC, of HA at: (a) 10 mg/L, (b) 15 mg/L, and (c) 20 mg/L	101
Figure 4-30. HA residuals levels in terms of absorbance as quantified by UV-vis spectrometry for three different initial HA concentrations in TiO ₂ in suspension exposed to UV light at pH 3	103
Figure 4-31. HA residuals levels in terms of absorbance as quantified by UV-vis spectrometry for three different initial HA concentrations in TiO ₂ in suspension exposed to UV light at pH 6	103
Figure 4-32. HA residuals levels in terms of TOC for three different initial HA concentrations in TiO ₂ in suspension exposed to UV light at pH 3	104
Figure 4-33. HA residuals levels in terms of TOC for three different initial HA concentrations in TiO ₂ in suspension exposed to UV light at pH 6	104
Figure 4-34. Effect of the photocatalytic degradation of different concentration of HA at pH 3 on the UV absorbance with TiO ₂ particles within the SGS body	112
Figure 4-35. Effect of the photocatalytic degradation of different concentration of HA at pH 6 on the UV absorbance with TiO ₂ particles within the SGS body	112
Figure 4-36. Effect of the photocatalytic degradation of different concentration of HA at pH 3 on the TOC with TiO ₂ particles within the SGS body.....	113
Figure 4-37. Effect of the photocatalytic degradation of different concentration of HA at pH 6 on the TOC with TiO ₂ particles within the SGS body.....	113
Figure 4-38. Effect of the photocatalytic degradation of different concentration of HA at pH 3 on the UV absorbance with TiO ₂ particles immobilized by Method 2.....	114
Figure 4-39. Effect of the photocatalytic degradation of different concentration of HA at pH 6 on the UV absorbance with TiO ₂ particles immobilized by Method 2.....	114
Figure 4-40. Effect of the photocatalytic degradation of different concentration of HA at pH 3 on the TOC with TiO ₂ particles immobilized by Method 2.....	115
Figure 4-41. Effect of the photocatalytic degradation of different concentration of HA at pH 6 on the TOC with TiO ₂ particles immobilized by Method 2.....	115

Figure 4-42. Effect of the photocatalytic degradation of different concentration of HA at pH 3 on the UV absorbance with TiO₂ particles immobilized by Method 3..... 116

Figure 4-43. Effect of the photocatalytic degradation of different concentration of HA at pH 6 on the UV absorbance with TiO₂ particles immobilized by Method 3..... 116

Figure 4-44. Effect of the photocatalytic degradation of different concentration of HA at pH 3 on the TOC with TiO₂ particles immobilized by Method 3..... 117

Figure 4-45. Effect of the photocatalytic degradation of different concentration of HA at pH 6 on the TOC with TiO₂ particles immobilized by Method 3..... 117

Figure 4-46. Degradation experiments in the absence of UV light with HA concentration of 20 mg/L at pH 6..... 119

Figure 4-47. Degradation experiments in the absence of UV light with HA concentration of 20 mg/L at pH 3..... 120

Figure 4-48. Fluorescence spectra of HA as a function of irradiation time 121

1 INTRODUCTION

The primary objective of a water treatment plant (WTP) is to protect and ensure the quality of drinking water by eliminating or reducing pollutants that may have adverse effects in the people's health. Disinfection is a crucial process that integrates a conventional water treatment to remove or inactivate disease-causing organism in water such as pathogens. In fact, the most commonly disinfection treatment method is chlorination in which the disinfectant agent is chlorine. Even though this practice has reduced many waterborne diseases, the process has become a major challenge. Specifically, for treatment processes in which the predominant water supply comes from surface waters (e.g.; rivers, lakes and reservoirs). These water sources tend to have high naturally occurring organic matter (NOM) which in turn may compromise drinking water quality since NOM can interact with chlorine to create potentially hazardous disinfection by-products (DBPs). The formation of DBPs has been of great concern because they are considered carcinogenic substances. Consequently, for WTP, it is essential to pursue an optimal balance between the removal of pathogens (i.e. chlorination) and the potential formation of DBPs.

1.1 BACKGROUND

It is well known that humic acids (HAs) have become one of the most extensively investigated organic material since they are considered one of the principal precursors of harmful compounds such as trihalomethanes (THMs) (Dziedzic et al., 2010; Matilainen et al., 2011;

Mosteo et al., 2009). HA consists of a mixture of molecules that originate from the chemical and bacterial degradation of vegetable and natural residues. It is primarily found in a variety of neutral and alkaline systems such as soils, water, lignite, brown coals and leonardite. The common definition of HAs is as the fragment of the humic substances that are soluble at pH levels greater than 2. This property may be influenced by several characteristics that comprise HA molecules such as ionic strength, structural conformation and pH values (de Melo et al., 2015). Since HAs represent the major fraction of the organic matter in aquatic environments they have been extensively used as model compound for investigation regarding NOM.

Although NOM is ubiquitous in terrestrial and aquatic environments, its presence in water supply sources is a primary concern. The complex matrix of organic materials may produce adverse health impacts in drinking water when they are subject to existing water purification processes such as chemical disinfection; hence, compromising the quality of drinking water (Baghoth, 2012; Liu et al., 2008; Wang et al., 2014). This is because HA serves as precursor for the formation of THMs, haloacetic acids (HAAs) and haloacetobitriles (HANs), which are human carcinogens (Uyguner & Bekbolet, 2005; Wang et al., 2014; Wiszniowski et al., 2002). Essentially, these three are the groups of DBPs most likely found in drinking waters (Krasner et al., 2006).

Other than the DBP-related problems, the excessive presence of HAs may affect physical characteristics of water producing undesirable taste, odor and color. Besides to aesthetic problems, it negatively impacts water treatment methods such as oxidation, coagulation, membrane filtration and adsorption (Baghoth, 2012; Sillanpää, 2014). HA increases the

demand of coagulants as well as disinfectants dosage, and are identified as the main responsible of membrane fouling during micro- and ultrafiltration process thus increasing the cost of water treatment (Huang et al., 2008; Wang et al., 2014; Xu et al., 2017). Furthermore, this organic molecule comprises particulate and colloidal particles that may have a strong attraction with heavy metals, pesticides, and herbicides increasing the toxicity of the water and also promote microbial growth (Bekbolet et al., 2002; Yigit & Inan, 2009).

Conventional water treatment consists of a combination of processes that include coagulation, flocculation, sedimentation, filtration and disinfection. A fraction of the HAs can be removed from the raw water in the processes preceding disinfection. However, these mechanisms are not very effective since it can only remove 10 to 50 percent of the total NOM, in terms of TOC (Reguero et al., 2013). To overcome this problem it is urgent to develop a practical technology for the water treatment facilities for the removal of the NOM.

Among the DBPs found in chlorinated waters, of particular concern are the THMs since they are more often present at elevated concentrations in drinking water. The potential formation of THMs has become a main problem in WTP facilities, not only in the United States (US), but other countries around the world. THMs can cause adverse effects on the liver, kidney, heart, central nervous system and can increase the incidence of cancer. As a result, the US Environmental Protection Agency (EPA) has set maximum contaminant levels (MCL) of 80 ppb for drinking water (United States Environmental Protection Agency, 2012). This MCL is for total THMs produced in the chlorination, which are: chloroform (CHCl_3),

dichlorobromomethane (CHBrCl₂), chlorodibromomethane (CHClBr₂) and bromoform (CHBr₃).

The formation of THMs in the drinking water is influenced by the composition and amount of the HAs. THMs are formed when the chlorine species, used as a disinfectant, react with the HA existing in the raw water. The THMs are chemical compounds in which a halogen replaces the hydrogen atoms of methane. The rate of THMs formation depends on many parameters such as disinfectant dosage, precursor's concentration, reaction or contact time, water pH and temperature. In general, the production of THMs increases as a function of each parameter. A general reaction of the THMs formation is presented in Eq. 1 (as cited by Benítez, 1991).



1.2 NEED OF RESEARCH

Removal of THMs from the treated water is a complex task. One of the most implemented strategies consists in reducing the chlorine doses. This effort has been quite successful, however, the continuous presence of HA in the raw water increase the potential for THMs formation above acceptable levels. Another approach to address this issue can be to reduce or remove NOM levels before the chlorination step. Numerous attempts have been made to develop techniques for the removal of THM's precursors from raw waters. Among the proposed processes are biodegradation of the organic matter, chemical coagulation, advanced oxidation, membrane separation and adsorption (J. Wang et al., 2014). However,

many of these techniques are not completely effective or are very expensive for the treatment facility. Hence, the development of cost-effective methods for the control of THMs is completely necessary.

In recent years, many researches have proposed the use of aqueous suspension of titanium dioxide (TiO_2) particles, also known as titania slurry, as an alternative method for the photodegradation of organic pollutants such as HA. Nevertheless, the use of the slurry system has brought a particular problem considering that the TiO_2 particles induce contamination in the treated water. Furthermore, this method is not completely effective since it produces the need of expensive further treatments in order to separate the TiO_2 particles from water.

One approach to overcome this limitation could be the immobilization of the TiO_2 particles in a solid, porous matrix. In this sense, water could be filtered through the porous media while the immobilized TiO_2 can support a photocatalytic reaction for the destruction of THM precursors under the influence of an ultraviolet (UV) light source. Hence, the aim of this research was to develop and evaluate a filter-like glass/ TiO_2 composite (GTC) for degradation of HA as an alternative for THMs control.

1.3 RESEARCH SCOPE AND OBJECTIVES

The present research sought for an alternative to remove or destroy HAs in an aqueous medium through a TiO_2 assisted photocatalytic degradation. The initiative consisted in developing a solid, porous matrix made out of sintered glass to support TiO_2 nanoparticles to undergo photodegradation of the HA solution. Different techniques for the immobilization of

TiO₂ and its efficiency in degrading HA were evaluated. The structural and morphology properties for the glass as well as for the sintered glass substrates (SGS) and GTC were also investigated. The specific objectives of this study were to:

1. Conduct a sieve analysis to determine the particle size distribution for the glass.
2. Obtain a performance map of the SGS that specifies optimal percolation rate, surface porosity and total porosity as function of sintering temperature and time.
3. Determine the polymorph structure and morphology of the pure TiO₂ particles and GTCs.
4. Examine the adsorption properties of HA onto the SGS, TiO₂ particles and GTC,
5. Investigate the photolysis of the HA at different concentrations.
6. Establish the photocatalytic degradation efficiency of TiO₂ suspensions as a function of solution pH, photocatalyst dosage and initial HA concentration.
7. Perform quantitative and qualitative comparisons on different methods for the immobilization of TiO₂ in the glass substrate. The methods were: a. TiO₂ particles embedded in the SGS; b. TiO₂ immobilization by gravitational deposition and evaporation; c. immobilization by TiO₂ coating over the SGS surface; and d. TiO₂ immobilization with Polyvinyl Alcohol.
8. Assess the photocatalytic activity on the different TiO₂ immobilization methods by means of the photomineralization of HA quantified and characterized by the measurement of TOC and adsorption of UV light at the wavelength of 254 nm (UV₂₅₄).

2 LITERATURE REVIEW

In view to suppress the formation of a considerable number of DBPs due to chlorine-based disinfection process, numerous researches have investigated this phenomenon. In the last few years, great efforts have focused in the development of treatment alternatives to mitigate the formation of DBPs as well as to study their toxicity in drinking waters. Therefore, this chapter will be devoted to summarize the most significant details and progress of the scientific research on DBPs precursors such as HAs. In an effort to establish the importance of this topic, it will be discussed the origins, properties and characterization methods for HAs as well as, health concerns. Some fundamentals concepts regarding the process of photocatalytic degradation of HA and TiO₂ immobilization techniques are also described.

2.1 DEFINITION AND DESCRIPTION OF HUMIC ACIDS

NOM, also referred to as DBPs precursors, is a complex heterogeneous combination of organic molecules resulting as consequence of biochemical reactions during the decay of animals, and plants, among many others activities of microorganisms (J. Wang et al., 2014). NOM is present abundantly in different environments such as soils, sediments, surface waters and ground waters. The structure, characteristics and concentration of NOM vary according to its environment and are widely influenced by the biogeochemical processes and the physicochemical properties in the terrestrial or aquatics systems. The primary parameters affecting the presence and quantity of NOM are the origins of the organic materials, the

geology and climate of the surrounding environments which influence the amount of precipitation, water temperature, quality and pH, and also sediments solubility (Matilainen et al., 2011; Sillanpää, 2014).

In raw natural waters, the NOM is derived from a diverse list of sources; therefore, its composition and concentration in water varies from source to source. The chemical composition of the DBPs precursors present in natural waters comprises different functional groups such as phenolic, carboxylic, hydroxyl, amino, and nitroso (Sillanpää, 2014). The typical concentration of NOM in surface water range from 0.1 to 20 mg/L (Janknecht et al., 2009). The high content of NOM corresponds to large rainfall events and high flow conditions.

NOM can be partitioned in hydrophobic and hydrophilic compounds being the humic substances (HSs) the main components of the hydrophobic fraction and the major constituent of NOM (Valencia et al., 2013). It is estimated that these hydrophobic acids constitute over 50% of the total organic compound (TOC) in aquatic systems. HSs are considered highly chemically reactive; however, they are identified as recalcitrant with respect to biodegradation.

HSs are described as yellow to black colored species that comprise three fractions: humic acids (HAs), fulvic acids (FAs) and humin. The solubility of the HSs depends on the pH level of the natural water. Humin is the portion of HSs that is insoluble under any pH conditions whereas, the FA is soluble at all pH values (Klavins & Purmalis, 2013). The HAs, which is the most reactive fraction and predominant type of NOM in aqueous systems, are soluble under

alkaline conditions, insoluble in acidic conditions and partially soluble in neutral conditions (de Melo et al., 2015).

2.1.1 Structure and Composition

In spite of the considerable attention devoted to the investigation of HAs its exact structure is still unknown due to the great variability of the properties according to its origin. The HAs is mostly composed of compounds with complex structure having dense molecular mass, however, its chemical composition is significantly influenced by the origin of its precursor materials, climate and biological conditions (Chiu & Tian, 2011). HAs are macromolecules that comprise a mixture of weak aliphatic and aromatic organic acids. This fraction of the HAs contains carboxylic acid (COOH), phenolic (OH), enolic (OH), alcoholic (OH), ether, quinone and hydroxylquinone functional groups connected with carbons chains and rings (Motta et al., 2016; Wan Ngah et al., 2008). The carboxylic and phenolic groups are the predominant functional groups in HAs structures (de Melo et al., 2015; Klavins & Purmalis, 2013). In addition, many researchers have suggested that the HAs comprises polymers of polyhydroxybenzoic acids, polyhydroxybenzenes, polycarboxylic acids, sugars and N-bases. Despite the fact that the HAs have a complex identity, some investigators have proposed molecular structure for this substance. Figure 2-1 shows two proposed structure for HAs.

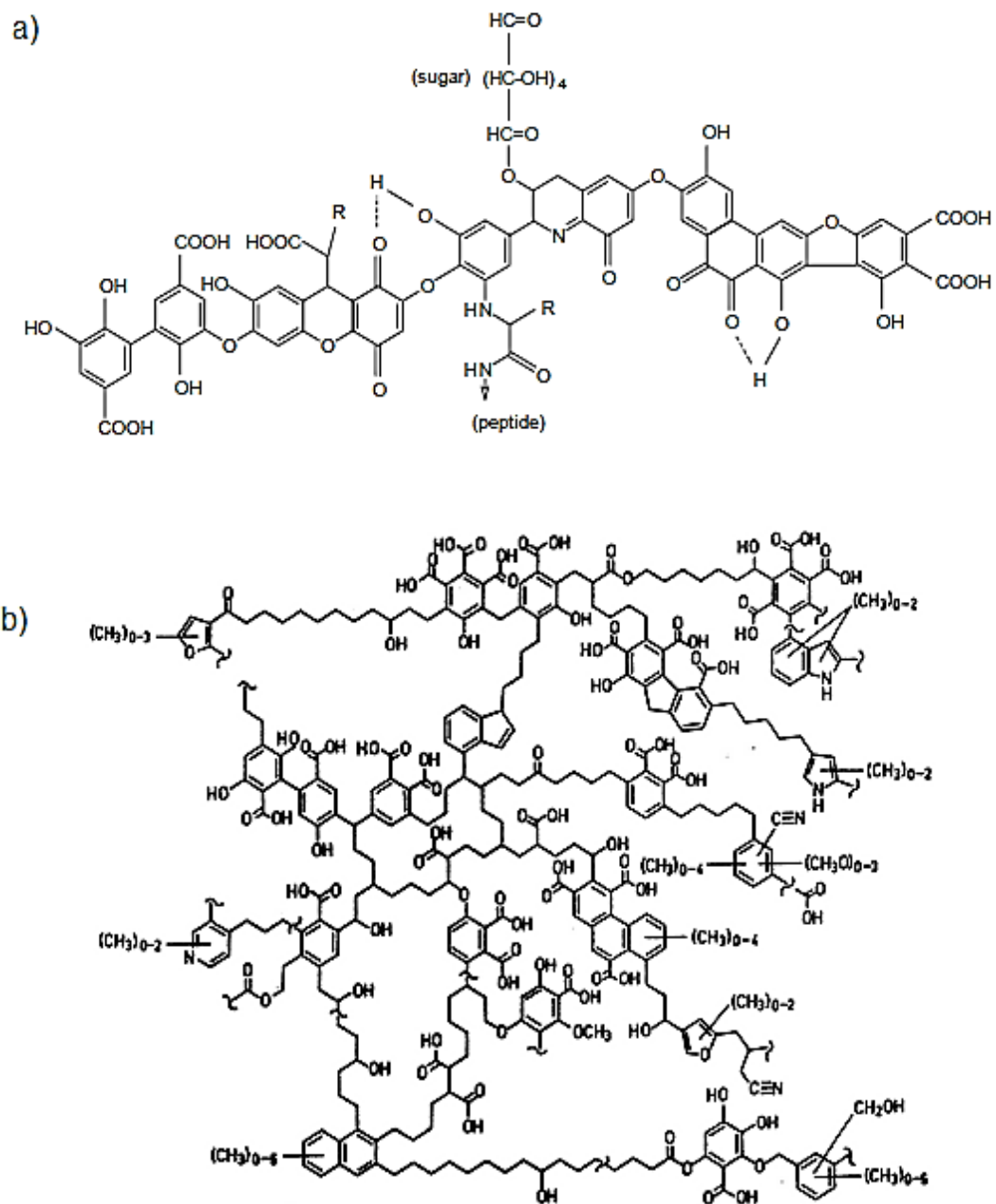


Figure 2-1. Structures of humic acid as proposed by: a). Stevenson (1982) (Retrieved from Peña-Méndez et al., 2005); and b). Schulten & Schnitzer (1993)

The TOC content has been extensively used as a chemical method to quantify HA in natural waters. Several investigators have reported organic carbon content in the HAs ranging from 50 to 60% (Uyguner-Demirel & Bekbolet, 2011). The elemental analysis has been commonly employed in studies to characterize non-stoichiometric substances such as HAs and gain a better understanding of their composition (Amir et al., 2004; Chiu & Tian, 2011; Janknecht et al., 2009; Klavins & Purmalis, 2013; Matilainen et al., 2011). This technique is useful for determining the contents of the major elements in the composition of HAs which are of carbon (C), hydrogen (H), nitrogen (H), sulfur (S) and oxygen (O) as well as the index of the atomic ratios: hydrogen-carbon (H/C), nitrogen-carbon (N/C) and oxygen-carbon (O/C). Theoretically, these indexes provide essential information regarding the structure and composition of HAs (Table 2-1).

Table 2-1. Typical index of atomic ratios for HA (based on Janknecht et al., 2009)

Atomic Ratio	Indicator of	Typical Range
Hydrogen-Carbon (H/C)	Amount of saturation of Carbon or degree of aromatic rings	1.23-1.46
Nitrogen-Carbon (N/C)	Quantity of proteinaceous compounds within the molecule	0.036-0.070
Oxygen-Carbon (O/C)	Carbohydrate content and degree of oxidation	0.55-0.63

A variety of reports in the literature demonstrate the inconsistency of the elemental contents of HAs according to its origin. For instance, Klavins and Purmalis (2013) compared the elemental analysis of peat HAs from similar sources, namely Eipurs, Dižpurvs and Dzelve. In this study the authors supported that the HA composition varies with its source of origin.

Concentrations of the functional groups such as carboxyl and phenolic and other properties of the macromolecule are also affected by the origin. Table 2-2 covers the information of the peat humic acids elemental composition as well as the results reported by others authors.

Table 2-2. Elemental composition of HAs extracted from different sources

Humic Acid Origin	Elemental Composition, %					References
	C	H	O	S	N	
Weathered Coal	50.82 - 60.83	3.71 - 5.00	33.62 - 44.49	na	0.94 - 1.28	Zhang et al., 2017
Sediments	43.70 - 53.80	4.10 - 5.80	31.10 - 37.10	na	3.50 - 6.20	van Rensburg, 2015
Eipurs Peat	55.30	4.49		1.01	2.48	Klavins & Purmalis, 2013
Dižpurvs Peat	58.11	4.78	na	0.90	3.10	
Dzelve Peat	59.49	3.98		0.68	2.02	
Sewage Sludge	52.80	6.80	33.90	0.10	6.50	Klavins & Purmalis, 2010
Peat Bog	57.40 - 59.00	4.30 - 4.50	35.30 - 36.60	na	1.50 - 1.60	Gondar et al., 2005
Sewage Sludge	48.76	6.59	40.00	na	4.68	Amir et al., 2004
Soil	55.40	4.80	36.00	0.80	3.60	Rice & MacCarthy, 1991
River	51.20	4.70	40.40	1.90	2.60	
Peat	57.10	5.00	35.20	0.40	2.80	

na = information not available

As mentioned earlier, due to the conformational variability it can be concluded that there is no unique substance of HA. Early effort to establish the compositional differences of humic matter was based on their characterization accordingly to the used extraction method. Thus, the high degree of heterogeneity in the compositional and structural properties of the HAs is

not only related to nature of the material source but to the fractionation or extraction procedures implemented to isolate the macromolecule (Asing et al., 2009; de Melo et al., 2015; Timofeevna Shirshova et al., 2006). Asing et al. (2009) have outlined in their study that the HAs chemical characteristics is influenced by different parameters regarding the extraction techniques such as the frequency of extraction, extracting agent, temperature and drying procedure.

Trubetskaya et al. (2013) isolated HAs using two different methods aiming to compare the influence of these isolation procedure in the HAs characteristics. Significant difference in the yield of HAs extracted, elemental composition and atomic ratios were evident. They also showed that the hydrophobicity and optical properties of HAs present remarkable variance according the isolation method. Zhang et al. (2017) have demonstrated that the pH of the extraction solutions plays an important role not only in the elemental composition of the extracted fractions but also in the contents of functional groups. In general, the presence of functional groups, primarily carboxyl and acidic groups, decreased with an increment in pH extraction solution. Indeed, the pH is a contributing factor in the dissociation of functional groups which is based on their ability to protonate and deprotonate. Therefore, as the pH values decreases the acidic functional groups become more protonated decreasing the effects of repulsion which leads to aggregation and further precipitation (Motta et al., 2016; Uyguner-Demirel & Bekbolet, 2011). Additionally, the HAs fractions extracted under acidic and neutral conditions yield greatest carbon content. Although several researchers have compared the properties of HAs isolated with many processes, concluding remarks regarding

the difference in composition require further work relating the extraction procedure with the material source.

2.1.2 Properties and Characteristics

The understanding of such macromolecule as HA result in a complicated task due to its variability of functional groups content, molecular size, weight and interaction with other substances. The HA possesses an undefined structure divided in hydrophobic and hydrophilic components, being the aliphatic chains and aromatic rings the hydrophobic part, and the OH groups the hydrophilic fraction. HAs are amorphous, polydispersed and polyelectrolyte mixture described as a dark brown to gray black organic compounds (Klučáková, 2016; S. Zhang et al., 2017). The molecular weight (MW) is another property that varies according to the ecosystem. For instance, in aquatic systems the MW is estimated to be in the range of 1500 to 5000 Da, while in soils is about 50,000 to 500,000 Da (McDonald et al., 2004).

The pH plays an important role in the ionic strength, solubility and dissociation capacity, sorption and desorption ability, and its capability of chelate formation with metals (Klučáková, 2016). Generally, HA solubility is proportional to pH value and they are considered to be soluble under neutral to alkaline conditions. The dissolution rate of HAs under alkaline pH reaches a steady state faster than in acidic conditions (Brigante et al., 2009). This behavior is related to the protonation and deprotonation process of HAs surface. Under neutral and alkaline media, the functional groups are deprotonated and tend to have negative charges causing an increment in the electrostatic repulsion of HAs molecules. Therefore, promoting a

colloidal suspension in the aqueous medium. The opposite occurs in acidic conditions and the HAs presents surfactant characteristics since its structure develops a micelle-like arrangement in which the hydrophobic parts are in the interior of the structure and the hydrophilic parts are exposed to the aquatic system (de Melo et al., 2015).

As the principal component of HAs, the functional groups relates to the many properties and characteristics this macromolecule possess (de Melo et al., 2015; Motta et al., 2016). In aqueous solutions, the HA colloids present a negative zeta potential, which is directly affected by the dissociation ability of the phenolic and carboxylic functional groups (Boguta et al., 2016; Zhu et al., 2014). In fact, these functional groups are responsible for the weakly acidic characteristic of HAs (Andayani & Bagyo, 2011). Moreover, they are capable of producing reactive oxygen species which is mainly attributable to the quinones functional groups (Motta et al., 2016). The functional groups that comprise the HAs structure constitute the main contributing factor for their fungicidal, antimutagenic, antioxidant, and anti-inflammatory activities that makes the HAs relevant in the pharmaceutical and biomedical fields. Most of the information indicates that humic matter are one of the most important components of soil on regard the agricultural enhancement (Boguta et al., 2016). The remarkable properties and capabilities of the humic matter play a vital role in plant growth since they have the ability to transfer micronutrients from soil to plants, promotes water retention and produce stable organic clay (Peña-Méndez et al., 2005).

As pointed out, the heterogeneous composition of the structure of the HAs promotes the formation of aggregates by means of electrostatic attraction, water bridging, and chelation.

These properties provide HAs the capability to transport hydrophobic organic chemicals, heavy metals and other pollutants (Trubetskaya et al., 2013). Electrostatic attraction is the responsible for the high sorption capacity for cations of HAs. Negative charges sites on HAs surface function to attract and dissolve cations. In addition, the presence of the anionic sites can bind trace minerals that further function as ion exchange. The complexing ability of the HAs involve a complex reaction in the surface of the substance with heavy metal cations. The metal cation binds itself to more than one negative charge site since two anionic site attract the metal.

Recently, it was demonstrated that the HAs-metal binding is influenced by several parameters such as concentration, molecular weight and material source of HAs as well as the metal concentration (Christl et al., 2001). However, others result also indicates that the pH of the media affect the interaction between the HA and the metal. Boguta et al. (2016) verified the effect of the content of the carboxylic and phenolic groups as well as the pH in the interaction between HA and copper ions. It was found that the complexation capacity was higher in neutral conditions, and an increase in the contents of functional groups promotes a significant increase in the interaction HA-Cu (II).

2.1.3 HAs Isolation and its Analogs

HAs are ubiquitous in terrestrial and aquatics environments such as sediments, soils and freshwaters. However, the isolation and extraction of HAs from these systems results in a very complex and time consuming process. Moreover, specialized equipment and knowledge

is necessary in order to isolate the humic substances. Isolation and fractionalization of the HAs have been commonly employed for the following reasons: 1) to characterize these substances and obtain a better understanding of their composition, and 2) adopted in investigations as the source material regarding natural organic matter.

Available techniques and procedure for the isolation and extraction of the humic substances include reverse osmosis, ultrafiltration, solvent extraction, freeze-drying (Matilainen et al., 2011), however many of these methods tend to yield low amount of HAs (Timofeevna Shirshova et al., 2006). One of the most common procedure for the isolation of HAs is based on alkaline extraction (Gieguzynska et al., 2009; Saito & Seckler, 2014; Trubetskaya et al., 2013). In this method, a strong base is implemented to extract the alkaline-soluble materials, followed by the removal of components that are not soluble under these conditions. Then, acidification of the solution promotes the precipitation of HA.

Besides the isolation of the natural organic materials, the use of commercial HAs has become commonly among researchers in the last few decades. The investigators have used these products to represent the soils or aquatic humic acids as well as natural organic matter avoiding unnecessary delays in the experimental part. Some of the commercial HAs products cited in investigations were reported by Uyguner-Demirel and Bekbolet, 2011. Table 2-3 shows the average results of the elemental analysis of commercially available HAs.

Table 2-3. Elemental composition of commercial HAs (adapted from Uyguner-Demirel and Bekbolet, 2011)

Humic Acid Brand	Elemental Composition, %				
	C	H	O	S	N
Sigma Aldrich	68.98	5.26	43.45	4.24	0.74
Roth	57.90	5.40	31.70	2.80	1.70
Fluka	65.79	5.51	37.79	3.16	0.71
International Humic Substance Society (IHSS)	52.55	4.40	42.53	0.58	1.19

2.1.4 HAs Detection Methods

The study of the composition of the natural organic materials may constitute one of the most relevant aspects in order to address the water quality problem associated to this pollutant. The precise understanding of the characteristics and properties possesses by the HAs macromolecule is a primary task in the development of new treatments for the prevention of the formation of DBPs. In the last few years, a number of different characterization techniques and advanced instrumentation has been introduced to provide a better understanding of the nature of the organic matter (Sillanpää, 2014). Many of these useful methods are mostly based on spectroscopy and chromatographic approaches. Some of the methods used to describe diverse features of the humic matter in this research are summarized below:

- (i). **Total Organic Carbon and Dissolved Organic Carbon** – Because of the high content of organic carbon in the HAs structure, the concentration of this substance is

often represented by means of the total and/or dissolved organic carbon. The total organic carbon in a substance can be described as follows:

$$TOC = POC + DOC \quad (2-1)$$

Where POC is the particulate organic carbon and DOC is the dissolved organic carbon. The POC constitute a minor fraction of the TOC, generally below 10 percent (Baghoth, 2012), whereas the DOC is defined as the organic carbon in a solution able to pass a 0.45µm porosity membrane filter. In contrast, the POC is the fraction retained in the membrane filter. Since the TOC and DOC concentrations can be measured directly, they have become the primarily comprehensive measurement parameters intended to discern information about the quantity of the organic matter. They are usually measured using a TOC analyzer in which the organic carbon is determined by high temperature pyrolysis system and low-temperature photochemical system.

(ii). UV-Vis – A feature of particular interest of HAs is the ability to absorb light across a broad region of the electromagnetic spectrum, e.g. ultraviolet and visible. Hence, the ultraviolet and visible (UV-Vis) absorption spectroscopy, in the wavelength of 200-800nm, can be used as a quantitative indicator of HAs compounds in water (Uyguner & Bekbolet, 2005). When light hits the surface of the HAs, part is absorbed by its chromophores. UV-Vis absorbance can be recorded at a certain wavelength or over a spectral region, the results will be accordingly the chromophores in the HA structure since they do not possess a unique absorption spectrum. In general, the absorbance

capacity of HAs decreases with increasing wavelength (Matilainen et al., 2011). The main advantage of the absorption spectroscopy technique compared to general quantitative method, such as TOC, is the significant information provided by this method regarding the substance composition for the elucidation of HAs. UV absorbance at 254 nm (UV_{254}) has been typically implemented to monitor HAs concentrations and is primarily due to the following points (Matilainen et al., 2011; Uyguner-Demirel & Bekbolet, 2011):

- It has been identified a surrogate parameter for representing the organic carbon content in NOM, thus it is highly correlated to TOC and DOC in natural waters,
- Provides information related to the aromaticity of the NOM since the molecules that absorb light at this wavelength belongs to the aromatic groups with various degrees of variation,
- There is a minimal or negligible interference from inorganics compounds, and
- Reliability and sensitivity of the absorbance of NOM.

(iii). Fluorescence – The use of fluorescence spectroscopy to determine chemical properties of HAs has grown rapidly during the last few years. Fluorescence provides a simpler method for describing the structural and conformational characteristics of humic matter (Baghoth, 2012; Matilainen et al., 2011; Sillanpää, 2014). The HAs comprise fluorophores that emit radiation when are excited by UV light at a certain

wavelength. Hence, the fluorescence spectroscopy instrument detects the emitted radiation at different wavelength when the sample is excited at a specific wavelength. The emitted radiation intensity and properties is affected by the characteristic of the aqueous system such as pH, ionic strength and temperature as well as the humic matter concentration and composition. The fluorescence spectra of HAs are characterized by broad peaks within emission wavelengths between 380 to 475nm when the sample is excited in a range of 310-320 nm (Baghoth, 2012).

(iv). Fourier Transform Infrared Spectrometry – In FT-IR analysis, infrared radiation is passing through the humic matter in which some of the irradiation is absorbed by the sample and the other part is transmitted. Therefore, this produces a spectrum with absorption or transmitted peaks that correspond to frequencies of vibrations between the bonds of atoms that comprise the molecule. Since every sample contains a unique combination of atoms the infrared spectrum is considered an exclusive fingerprint of the analyzed material allowing to detect functional groups within the compound. For this reason, FT-IR has been commonly employed for the characterization of natural organic matter. Some of the general bands for compositional features of humic substances are shown in Table 2-4.

Table 2-4. Major bands characteristics of FT-IR spectra of Humic Substances (modified from Matilainen et al., 2011)

Band (cm-1)	Interpretation
1095 and 1030	C-O Stretch, alcohols and aliphatic ethers
1260 and 1220	C-O Stretch, carboxylic groups, phenols, aromatic, unsaturated ethers
1410	O-H Bend, carboxylic groups
1630	C=C Stretch, alkenes and aromatic rings
1720	C=O Stretch, carboxylic groups
2620	O-H Stretch, Hydrogen-bonded carboxylic groups
3400	O-H Stretch, alcohols, phenols, carboxylic groups

2.2 PHOTOCATALYTIC DEGRADATION

In recent years, a considerable attention has been focused in the use of heterogeneous photocatalytic oxidation for the degradation of organic pollutants (Umar & Aziz, 2013). Conventional treatments process such as adsorption, coagulation, flocculation, and reverse osmosis are not capable of completely decompose or destroy these pollutants (Dong et al., 2015; Zhang et al., 2012). Thus, the photocatalytic properties of some compounds have been used to decompose recalcitrant organic pollutants. These compounds are identified as catalyst mainly a semiconductor capable of induce a series of reductive and oxidative reactions on its surface by the adsorption of light. This process is referred as photocatalysis which is a predominant advanced oxidation process (AOP) that relies on the generation of reactive species.

In general, the heterogeneous photocatalytic is a process in which a UV light radiation is used to promote the excitation of a photocatalyst in the presence of oxygen. Oxidizing species,

either as free holes or hydroxyl radicals, are generated upon irradiation of the catalyst leading to the oxidation and mineralization of organic pollutants. Among many candidates for photocatalytic reactions, TiO₂ has been extensively studied for the degradation of NOM using HAs as model compound (Uyguner-Demirel & Bekbolet, 2011). This is because, as a catalyst, TiO₂ has been considered to have the most efficient photoactivity, the highest stability, nontoxicity and lowest cost compared with other photocatalysts and is important for the treatment of polluted water (Pansamut et al., 2013).

2.2.1 Mechanism of Photocatalytic Oxidation Using TiO₂

The photoactivity of TiO₂ has been widely reported in many researches since the pioneering work of Fujishima and Honda in 1972 (Hashimoto et al, 2005; Nakata & Fujishima, 2012; Zaleska, 2008). The discovery of the Honda-Fujishima effect involving the electrochemical photolysis of water on TiO₂ electrodes were the primarily steps towards the development of TiO₂ photocatalysis (Diebold, 2003; Lin et al., 2006; Zhang et al., 2012). Basically, the mechanism of the photooxidation of the HAs involves five fundamentals phases or reactions on the surface of the catalyst: 1) photoexcitation by the adsorption of photons ($h\nu$), 2) diffusion, 3) trapping, 4) recombination, and 5) oxidation and reduction (Dong et al., 2015). The diagram of these fundamentals steps is presented in Figure 2-2.

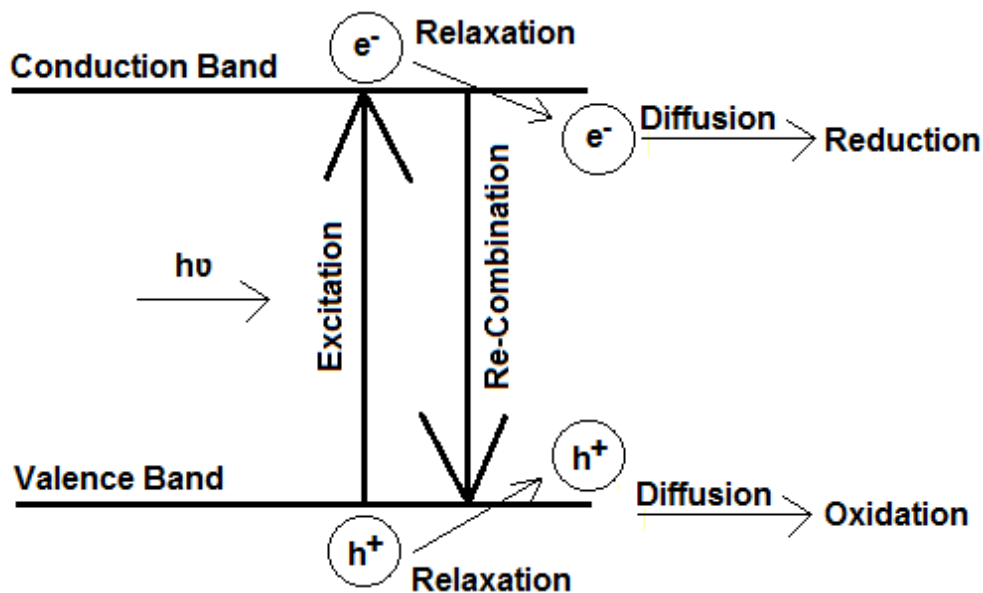


Figure 2-2-2. Diagram of the mechanism of TiO₂ photocatalysis (modified from Nakata & Fujishima, 2012).

The photocatalysis is initiated when the TiO₂ surface is irradiated with UV light to photogenerate charge carriers, namely electrons (e^-) and holes (h^+). The production of the electrons and holes (e^-/h^+) pair occurs when the TiO₂ absorbs photons with an energy equal to or greater than its bandgap energy (Dong et al., 2015). This photon energy is produced by an incident wavelengths equal or lower than 390 nm. At that moment, the electrons from the valence band (VB) are promoted to the conduction band (CB). As a results, there is a production of highly oxidative holes in the valence band and the formation of hydroxyl radicals ($\bullet OH$) and superoxide radical ions. The formation of hydroxyl radicals is due to the reaction between the adsorbed water molecules and the holes form the valence band that diffuse to the TiO₂ surface (Eqs.2-6 and 2-7). The reactions involved in the TiO₂ photocatalysis are presented by the following equations (2-2 to 2-10).

Charge Carrier Generation:



Charge Carrier Trapping (TR):



Electron/Hole Re – combination:



Oxidation of Hydroxyls:



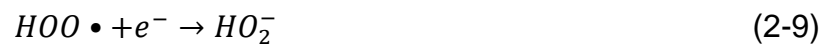
Photoexcited e^- scavenging:



Protonation of Superoxides:



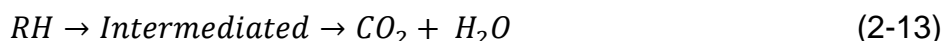
e^- scavenging:



Formation of H₂O₂:



There are two photochemical reactions occurring on the TiO₂ surface under UV light illumination: photo-induced redox reactions of adsorbed pollutants and photo-induced hydrophilic conversion of catalyst itself (Hashimoto et al., 2005). The generated holes, electrons and hydroxyl radicals are the responsible for the decomposition of the organic compounds. The holes and the hydroxyl radicals reacts with the organic pollutants adsorbed by the catalyst resulting in their oxidation, while the reduction process is produced by the electrons in the conduction band. Moreover, the superoxide radical ions (O_2^-) are formed when oxygen (O_2) react with these electrons. An increase in the contact time between the TiO₂ and the organic compounds results in the degradation of the pollutant and eventually mineralized them to carbon dioxide (CO₂) and water (H₂O) as presented by the following equations:



In the equations 2-11 to 2-13 the RH represent the organic pollutant in which a hydroxyl radical attacks by either one of the following ways: 1) adding itself to an unsaturated carbon, or 2) removing an accessible hydrogen atom to produce H₂O (Hoffmann et al., 1995). Taking this into account, the present study is focused on the degradation of HAs, hence, in our

particular case RH denotes the HA. The illustration of these equations is presented in Figure 2-3.

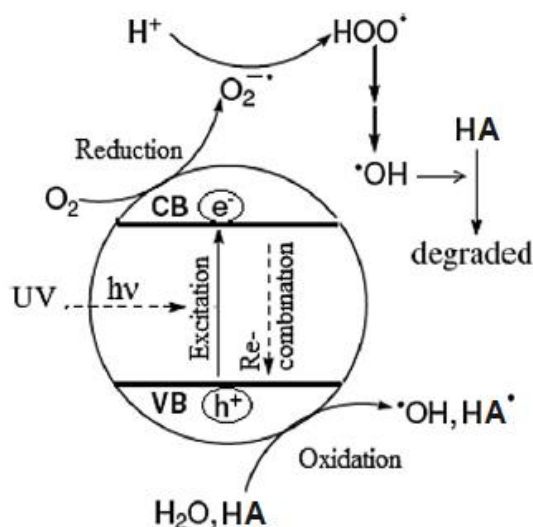


Figure 2-3. Process occurring during the photodegradation of HAs (modified from Dong et al., 2015)

For an efficient photocatalytic reactions and degradation, it is necessary to evade electron-hole recombination. In these photocatalytic reactions a recombination of electron in the conduction band and holes in the valence band can affect the electroneutrality of the TiO₂ particles, hence producing an ineffective degradation (Hanaor & Sorrell, 2011; Nakata & Fujishima, 2012). As consequences, it is important to promote the presence of dissolved oxygen in order to ensure that the reduction process occurs simultaneously with the oxidation process. It has been shown that the surface trapped valence band electron (e_{TR}^-) and conduction band hole (h_{TR}^+) reduce the recombination rate (Furube et al., 2001). Moreover, the presence of electrons scavengers can enhance the photocatalysis since they can make the recombination process slower (Dong et al., 2015).

2.2.2 TiO₂ Properties and Polymorph Phases

It has been shown that the photocatalytic performance of TiO₂ depends on many factors, including the catalyst properties such as particle sizes, specific surface area, crystalline phase, among others (Nakata & Fujishima, 2012). As mentioned before, the development of the photocatalysis depends on the band gap energy that TiO₂ possess. However, this energy varies depending the TiO₂ crystal structure, therefore this property has been identified as the most influenced in the photocatalytic activity. TiO₂ is a polycrystalline material that crystallizes in three polymorphs phases: rutile, anatase and brookite, being anatase and rutile the main polymorphs (Diebold, 2003; Hanaor & Sorrell, 2011). Each of these crystal structures presents different properties that impact the photocatalytic activity of the material. Table 2-5 outlines some of the basic properties of anatase and rutile. The electron is photoexcited with wavelength equal to or less than 413 nm corresponding to bandgap energy greater than 3.0 eV, whereas for the band gap energy of anatase (3.2 eV) it is necessary an incident light equal or less than 387 nm (Lin et al., 2006; Umar & Aziz, 2013).

Table 2-5. Properties of TiO₂ crystalline structures

Properties	Polymorph Phase		References
	Anatase	Rutile	
Crystal Structure	Tetragonal	Tetragonal	Hanaor & Sorrell, 2011
Crystal Surfaces	101, 100, 001	110, 100, 001	
Lattice Parameter a, nm	0.3733 - 0.3785	0.4584 - 0.4594	Diebold, 2003; Hanaor & Sorrell, 2011
Lattice Parameter c, nm	0.937 - 0.9514	0.2953 - 0.2959	
Band Gap Energy, eV	3.2	3.0	Umar & Aziz, 2013
Density, kg/m ³	3830	4240	Diebold, 2003

The crystalline phase is strongly influenced by the synthesis methods and parameters of the TiO₂ particles being the temperature the primarily factor defining the phase (Hanaor & Sorrell, 2011; Zhang et al., 2012). Amorphous TiO₂ is transformed to either of its polymorph phases usually at temperatures greater than 400°C (Zhang et al., 2012). Additionally, it was reported that the phase transformation not only depends on the temperature but on the impurities, particle size, oxygen vacancies as well as the defect concentration and grain boundary concentration (Mor et al., 2006).

Many studies for the photodegradation of organic pollutants have been focused on the use TiO₂ either as rutile or as anatase. In spite of that, rutile is described as the most thermodynamically stable form of TiO₂. However, the anatase phase exhibits a best photocatalytic reactivity (Hanaor & Sorrell, 2011; Lin et al., 2006).

An energy level who exceeds the energy difference between the conduction band and the valence band (e.g. band gap) is fundamental for the oxidation and reduction of the reactants. Since anatase has band gap greater than rutile, it requires a lower UV wavelength radiation to increase the oxidation potential of the electrons while promotes the electron transfer from the catalyst to the adsorbed compound. Furthermore, it has been shown that anatase possess an indirect band gap minor than its direct band gap, whereas rutile exhibits direct and indirect band gap very similar. As a result, anatase exhibit longer charge carrier life that leads to a better probability that these (e⁻) and (h⁺) become parts of the oxidation/reduction processes (Luttrell et al., 2014).

The anatase form is the most widely used in the photocatalytic degradation of HAs. Uyguner-Demirel and Bekbolet (2011) wrote an overview on photocatalytic oxidation of natural organic matter. The most common commercially available TiO₂ used by researchers in relation of the degradation of HAs are presented in Table 2-6. Among them, Degussa P25, which is a mixture of anatase and rutile, is often more used in the studies (Bekbolet et al., 2002; Huang et al., 2008; Uyguner-Demirel & Bekbolet, 2011; Uyguner & Bekbolet, 2005; Yigit & Inan, 2009).

Table 2-6. Commercial TiO₂ and their properties

TiO ₂ Band	BET Surface Area, m ² /g	Average Primary Particle Size, nm	Point of Zero Charge (pHzpc)	Crystal Structure	Reference
Degussa P25	50 ± 15	21	6.3	Anatase 70-80%, Rutile 20-30%	Huang et al., 2008; Uyguner-Demirel & Bekbolet, 2011
Sigma Aldrich	200 ± 20	25	na	Anatase 100%	Yigit & Inan, 2009
Hombikat UV-100	>250	10	6.0	Anatase 100%	Bekbolet et al., 2002; Uyguner-Demirel & Bekbolet, 2011

na = information not available
 BET = Brunauer, Emmett and Teller

Although Degussa P25 is not a pure form of anatase it has been postulated by many researchers that its photocatalytic reactivity is superior than pure anatase crystal form. Yigit and Inan (2009) compared the oxidation of HAs using Degussa P25 versus Sigma Aldrich and they found that the photocatalytic oxidation with the mixed-phase TiO₂ (e.g. Degussa P25) worked better. Bekbolet and co-workers (2002) also investigated the efficiency of Degussa P25 versus Hombikat on the photodecolorization of HAs and their findings were

consistent with Yigit and Inan results as the optimal degradation rate was achieved with Degussa P25.

The variations might be elucidated by the morphological properties of TiO₂ considering that each sample have different surface area and impurities that will affect generation and recombination rate of electron-hole pairs and the adsorption capacity of the organic compound. Moreover, the fact that rutile is dispersed within the anatase structure increase the photocatalytic performance because rutile photogenerate charge carriers that will be excited to the anatase form, thus reducing the e⁻/h⁺ recombination.

2.2.3 Effect of Catalyst Load

The effectiveness of TiO₂ photocatalytic oxidation and further mineralization of HAs is highly influenced by the catalyst dosage (Le-Clech et al., 2006). Extensive research on the effect of the TiO₂ concentration in suspension on the degradation kinetics of HA has been carried out (Dziedzic et al., 2010; Huang et al., 2008; Le-Clech et al., 2006; Wiszniowski et al., 2002). Data in Table 2-7 shows the experimental conditions used for the evaluation of catalyst loading in the removal of HAs. It should be emphasized that the list is presented to provide information for the elucidation of the influence of TiO₂ dosage considering that a direct comparison between these investigations may be difficult because of the variability of operational parameters.

Table 2-7. Influence on TiO₂ concentration on photodegradation of HAs

Model Compound	Concentration, mg/L	TiO ₂ Loading Range, g/L	Optimum Loading, g/L	References
Fluka HA	20	1.0 - 4.0	4.0	Li et al, 2002
Aldrich HA Sodium Salt	100	0.1 -2.0	1.0	Wiszniewski et al., 2002
River HA	2.3 as TOC	0 - 0.5	0.1	Le-Clech et al., 2006
IHSS HA	10 as TOC	0.1 - 1.0	1.0	Huang et al., 2008
Aldrich HA Sodium Salt	40	0.1 -2.0	1.0	Dziedzic et al., 2010
Aldrich HA Sodium Salt	100	0.17 - 0.5	0.3	Riungu et al., 2012)

In general, the photodegradation rate of the HAs increases with increasing the TiO₂ concentration. However, further increase in catalyst dosage may lead to an inefficient photocatalytic degradation of humic substances. It has been shown that when the amount of catalyst concentration exceeds certain level it negatively influences the amount of UV light transmitted to the solution (Wiszniewski et al., 2002). Increasing the quantity of TiO₂ particles creates a suspension with high turbidity leading to light scattering and promotes aggregation of particles. Thus, the catalyst surface area exposed to illumination is reduced and the photons adsorbed decrease. The reduction in photons adsorbed becomes important as their role is to initiate the photogeneration of charge carriers. The above explanation implies that there is an optimum TiO₂ dosage, yet this value is a function of the experimental conditions. Although there is no unique optimum concentration of TiO₂ many researchers have reported that the ideal loading is 1 g/L (Le-Clech et al., 2006).

2.2.4 Effect of Solution pH

It has been reported that the photocatalytic rates of the HAs increase with decreasing the solution pH (Le-Clech et al., 2006; Li et al., 2002; Yigit & Inan, 2009). This behavior is mostly due to the role of the electrostatic attractions between the catalyst and the reactant and charge carriers generated (Bahnemann et al., 2007). It is well known that the solution pH has a direct effect on the TiO₂ and HAs surface, depending on its value they may present a positive, negative or no charge. The pH where the net total charge for TiO₂ is zero is around 5.8 and 6.6 according to the type (Bekbolet et al., 2002; Yigit & Inan, 2009). This point is defined as the point of zero charge (pH_{pzc}) and below this point the TiO₂ surface is positively charge and negatively charge when is higher according to the following equations (Bahnemann et al., 2007; Zhang et al., 2012):



Equation 2-14 produce TiO₂ particles with a surface positively charge due to the H^+ in the solution, whereas equation 2-15 leads to negatively charged particles due to the OH^- in the media. Most studies have been presented with a focus on the interpretation of the pH effect on the photodecomposition of HAs. It has been found that the ideal conditions for the mineralization of the HAs is under acidic media (Le-Clech et al., 2006; Li et al., 2002; Yigit & Inan, 2009). For instance, Yigit and Inan (2009) studied the degradation under different pH

values, namely 3,5,6 and 9. The HA concentration decreased almost 80% after 1 hour of agitation under pH 3. In contrast, away from the pH_{pzc} the mineralization rate becomes slower.

2.2.5 Adsorption of HAs

Adsorption experiments are commonly conducted to evaluate the interaction between the TiO_2 and HA as well as the UV irradiation effect. Although adsorption of HAs onto TiO_2 surface is a very complex subject it is considered to be a necessary initial phase toward an effective photodegradation (Bekbolet et al., 2002). Adsorption is a process that occurs at the surface of the catalyst in which the HAs molecules becomes attached onto the TiO_2 surface. Therefore, some studies have related the adsorption ability of TiO_2 particles with the pH of the media as well as the electrostatic properties of the surface. According to Le-Clech and co-workers (2006), TiO_2 exhibits a better adsorption capacity under acidic medium. This may be attributed to the following: in acidic media ($\text{pH} < \text{pH}_{\text{pzc}}$), TiO_2 particles are protonated and the HA tend to have a neutral to negative charge thus the electrostatic attraction between them become much stronger. Upon increasing the pH, both TiO_2 particles and HAs macromolecule becomes deprotonated, and the effects of attraction are minimized. In this stage, the catalyst and the solute are negatively charge, therefore, the adsorption between them is less likely to occurs. Huang et al. (2008) reported that the adsorption equilibrium of HAs was reached in less than 5 minutes and under the same operational conditions a negligible change in adsorption was observed with TiO_2 concentrations above 1 g/L.

2.3 PHOTOCATALYTIC REACTORS

The photocatalytic decomposition and mineralization of organic pollutants, such as HAs, is significantly influenced by the experimental system in which the reaction will occur, e.g. photocatalytic reactor. The reactor design involves, at least, the selection of an appropriate UV source, magnetic stirrer and a glass container that yield the maximum degradation. According to literature, two approaches are usually employed for the removal of organic pollutants using TiO_2 as photocatalytic. These methods involve either the suspension or the immobilization of the TiO_2 particles.

2.3.1 Slurry

The most commonly configuration employed when using TiO_2 for photodegradation of organic compounds is the suspension system. In this method, an aqueous suspension or a slurry is prepared using certain concentration of TiO_2 powders. It has been shown that this technique has a removal efficiency greater than 90% (Dong et al., 2015). Moreover, since the TiO_2 particles are suspended over a unit volume the total surface area exposed for the degradation of the pollutants is greater than the particles attached to a substrate (Umar & Aziz, 2013). Despite the many benefits of using a TiO_2 slurry, this method is not completely suitable for industrial purposes. This is because, although the pollutant is destroyed, the solution becomes contaminated due to the suspended TiO_2 particles. Hence, a filtering process is necessary in order to remove the TiO_2 from the treated water. However, there still a major challenge to remove and recover the dispersed particles from the liquid after the degradation

process mostly due to the small particle size (Lazar et al., 2012). Therefore, the treatment with this method results in a complex process that will involve an inconvenient and expensive procedure to separate the TiO₂ particles.

2.3.2 Immobilization of TiO₂

Recently, some researchers have been proposing the immobilization of the catalyst onto several substrates in order to solve the problem generated by the TiO₂ slurry. Thus, avoiding the post treatment for the separation of the TiO₂ particles. Despite the fact that the photocatalytic performance of this reactors is generally negatively affected considering that the surface area is reduced, the immobilization of TiO₂ has been successfully achieved on glass fibers, glass, quartz, activated carbon, polymers, stainless steel and alumina (Dong et al., 2015; Kumar & Bansal, 2012). In an effort to immobilized the TiO₂ particles different techniques have been evaluated such as chemical vapor deposition, slip coating, dip coating, electrospinning and dip-evaporation (Lazar et al., 2012). Information about recent investigations in relation to the immobilization of TiO₂ is provided in Table 2-8. One of the most commonly used preparation method is the sol-gel process in combination with dip coating of the substrates. In this method, a chemical solution that act as the TiO₂ precursor is used to developed a gel-like containing a liquid and solid phase (Tseng et al., 2010). A thermal treatment is applicate to remove the liquid and to enhance the properties of the gel. Afterwards, the gel is used as a coating solution for the deposition of TiO₂.

Table 2-8. Methods for the immobilization of TiO₂ on different substrates

Photocatalyst Type	Immobilization Method	Substrate	References
Titanium Isopropoxide	Chemical Vapour Deposition	Silica and Quartz	Kaliwoh et al., 2002)
Titanium Butoxide	Sol-Gel	Silica	Z. Wang et al., 2002
Tetra-n-butylorthotitanate	Sol-Gel and Dip Coating	Glass	Paez & Matoušek, 2003
Titanium Oxysulfate	Sol-Gel and Dip Coating	Sintered Glass Plates	Hidalgo et al., 2004
Degussa P25	Dip Coating	Sintered Glass Cylinders	Mansilla et al., 2007
Degussa P25	Evaporation	Glass Plates, Perlite, and Steel Fibers	Hosseini et al., 2008
Degussa P25	Sol-Gel	Nut Shell Carbon	Shi et al., 2009
Titanium Tetraisopropoxide	Sol-Gel and Dip Coating	Quartz	Zhuang et al., 2010
Anatase Powder	Gel- Dipping	Ceramic Tiles	Santacruz et al., 2012
Titanium Isopropoxide	Sol-Gel and Dip Coating	Soda Lime and Indium Tin Oxide Glass	Pinar et al., 2014
Titanium Butoxide	Heterogenous Nucleation Method	Glass Beads	M.-Q. Wang et al., 2013

In general, the synthesis of TiO₂ layers onto a substrate comprises the following phases: 1) preparation of TiO₂ dispersion, 2) deposition of catalyst particles, 3) evaporation, and 4) thermal treatment. A colloidal suspension of the particles has been widely used for preparing coatings on different substrates (Hosseini et al., 2008; Mansilla et al., 2007; Santacruz et al., 2012). This suspension, also referred as TiO₂ slurry, is prepared by the mixture of TiO₂ powder and a solvent, usually an alcohol due to high rate of evaporation. The dip coating is a practical technique for the deposition of TiO₂ particles. This technique consists in the immersion of the substrates in the solution for a certain amount of time and withdraw at a constant velocity (Hidalgo et al., 2004; Zhuang et al., 2010). The evaporation steps encompass the removal of the solvent from the substrates and within the TiO₂ pores. The evaporation of the liquid phase is usually performed at room ambient temperatures or close

to the boiling point of the solvent (Hidalgo et al., 2004; M.-Q. Wang et al., 2013). The thermal treatment is the final step in the immobilization of TiO₂ particles consisting of the calcination of the substrates temperatures greater than 400°C.

Although there is a significant amount of material that can be used as a substrate the immobilization of TiO₂ has been mostly conducted on glass surfaces as presented before (Table 2-8). The main reason of this is that the glass is a transparent material that allow the penetration of radiation, thus enhance the harvesting of light by the attached particles (Hidalgo et al., 2004; Lazar et al., 2012). Furthermore, the TiO₂ particles haven been successfully attached onto the glass surface due to oxygen bridges formed between OH groups and the TiO₂ surface during the calcination process (Hosseini et al., 2007). Hence, a mechanically stable coating is produced by this mean.

Early efforts to immobilized the TiO₂ on glass are based on nonporous surface (Hosseini et al., 2008). Nevertheless, the use of highly porous substrates may enhance the photocatalytic performance of the immobilized material as it will produce a large surface area for adsorption (Stathatos et al., 2012). As discussed before, the adsorption of the organic compounds onto the surface of the catalyst plays a critical role in the photodecomposition of the pollutant. Among the applications of the glass powder is the generation of sintered glass plates to develop a solid porous substrate (Bernardo et al., 2010). The glass powder will be transform into a solid glass substrate by sintering, which is defined as the process of compacting a solid mass by heat or pressure. This process is achieving by heating the powder to a temperature of 50 to 80 percent of its melting temperature.

Recently, Mansilla et al. (2007) developed a novel photocatalytic system by immobilizing TiO₂ particles on sintered glass cylinders. The support surface was prepared using powdered silicate glass and sintered at temperature below 700°C. Additionally, the coated sintered glass was found to be effective for the photocatalytic degradation of the antibiotic flumequine. Photoactive TiO₂ coatings on sintered glass plates was reported for the assessment of glucose degradation (Hidalgo et al., 2004). The TiO₂ coatings were found to be highly stable since no significant changes were observed in the coating surface after 4000 hours of continuous operation.

3 MATERIALS AND METHODS

In the preparation of the GTC specimens, TiO₂ particles were immobilized in the SGS by different methods. The immobilization of the micro- and nanopowdered TiO₂ has many parameters that can affect the degradation of the HAs. In order to understand the influence of the experimental parameters, the present study was conducted in several parts as described below.

3.1 MATERIALS

Glass, MG-30 type, which comprises 100% recycled glass was provided by Vitro Minerals. Commercially titanium (IV) oxide anhydrous was obtained from fisher chemical. Humic acid was supplied by Sigma Aldrich Company. HA stock solution was filtered using a 0.45 μm mixed cellulose ester filter membranes (Whatman). Alfa Aesar supplied anhydrous ethanol (EtOH), HPLC grade with purity greater than 90%. Solution pH was adjusted using nitric acid (HNO₃) from ACROS Organics and/or sodium hydroxide obtained from fisher chemical.

3.2 SINTERED GLASS SUBSTRATES

The ultimate goal of this endeavor is to design a filter-like composite made out of sintered glass embedded with TiO₂ particles. First, a solid, porous glass substrate is established by sintering recycled glass powder (RGP). This section describes the methodology used to characterize the RGP and the sintering process.

3.2.1 Particle Size distribution of the RGP

This test aimed to investigate the percentage of different grain size contained within the MG-30 RGP. The particle size distribution was determined according to the Standard Test Method for Particle-Size Analysis of the ASTM. This test consists of a sieve analysis in which a pre-weighted sample of the material is placed upon the top of a group of sieves. The sieves that were used for this analysis, listed in descending size of opening, are 4, 10, 20, 60, 100, and 200. The sieve with the largest screen opening was placed at the top and the screen opening size decrease with each sieve down to the bottom sieve. Once the sieves were placed in the appropriate order the sample was shake for a period of time in order to promote that the particles were either retained on a sieve or passed through. After shaking, the sample material retained on each of the sieve was weighted. The following characteristics are determined from the gathered data: effective size (D_{10}), median size (D_{50}), finer size (D_{60}), and uniformity coefficient (UC).

3.2.2 Sintering Process

It has been shown that the addition of the TiO_2 particles can cause significant changes in the solidification process of the glass powder (Cuadrado, 2014). These changes are directly related to the physical and mechanical properties of the solid glass composite such as porosity and compressive strength. Therefore, in order to assess this effect, a control glass substrate was prepared with glass powder as the only component. The RGP was transform into a solid glass substrate by sintering, which is defined as the process of compacting a solid mass by heat or pressure.

Several SGS were fabricated as function of sintering time and temperature. The SGS samples were obtained by placing the RGP into a cylindrical ceramic mold. The mold produces circular SGS with the following dimensions: diameter equals to 2 inches and thickness of 0.5 inches. After the RGP were placed in the mold, it was compacted at high temperatures in the range of 950°C to 1000°C but avoiding reach the melting point of the RGP. The selected sintering times were 45 to 75 minutes with 15 minutes' intervals. The resulting samples were tested to obtain a performance map of the SGS in function of its porosity and water percolation.

3.3 IMMOBILIZATION OF TiO₂ PARTICLES IN THE SGS

Two approaches were investigated to incorporate the TiO₂ particles in the SGS: 1) within the SGS body, and 2) on the SGS surface. This section provides a description of the methodology implemented to immobilize the TiO₂ particles in the SGS in order to fabricate the GTC.

3.3.1 TiO₂ Particles within the SGS body

In this method, TiO₂ particles were embedded into the RGP in order to immobilize the particles onto the glass powder particles (beads) surface. The procedure for this immobilization technique consisted of two principal phases: preparation of a TiO₂-glass suspension and then sintering. As first step, the recycled glass beads were washed and dry at 105°C for 1 hour in order to remove any contaminant and dust. A TiO₂ suspension was prepared by adding titanium (IV) oxide anhydrous powder to 40 mL of ethanol. Three different masses of titanium powder were evaluated: 0.30, 1, and 3 grams. The titania slurry (TiO₂ + EtOH) was

magnetically stirred at room temperature (23°C) for 1 hour with the purpose of obtain a uniform suspension without TiO₂ powders aggregates.

Afterwards, 20 to 30 g of MG-30 are added to the well-mixed TiO₂ suspension. The glass beads were mixed for 1 hour and then left at room temperature for 24 hours to promote an adequate contact and adsorption of the catalyst on the substrate surface. After this period, the slurry was heated at 105°C for 45 minutes to allow evaporation of EtOH. Subsequently, the dried TiO₂ and glass beads mixture were sintered for the desired time and temperature. These temperatures ranged from 950°C to 975°C with sintering times varying from 1 to 6 hours. The sintering process allows the TiO₂ particles to be strongly attached to the glass beads surface. In this process, a circular shape sintered GTC was obtained.

The effect of pH in this immobilization method was also studied. For this pH assessment, the titania slurry was prepared as mentioned before but with the addition of nitric acid (HNO₃). Acidification of the slurry was conducted in order to provide a more disperse suspension with stable TiO₂ colloids. The recycled glass beads were then added and sintered as described before. At last, the quantity of TiO₂ particles embedded and immobilized onto the glass beads were determined by weigh difference. After the titania and glass beads mixture were poured in the mold a certain amount of catalyst remained in the beaker surface. Hence, this mass was not adhered onto the glass beads. Therefore, the total TiO₂ mass impregnated was quantified by subtracting the beaker initial weight to its final weight.

3.3.2 TiO₂ Particles Immobilized on the SGS surface

3.3.2.1 Immobilization by Gravitational Deposition and Evaporation

The general procedure for preparing the TiO₂ deposition with this method has been described elsewhere (Hosseini et al., 2007). However, the procedure was modified in order to obtain a proper TiO₂ film onto the SGS. The aim of this immobilization technique is to deposit the photocatalyst onto the SGS surface by a combination of evaporation and gravitational precipitation processes. Cedillo-González et al. (2014) demonstrated that the glass surface roughness has an influence in the adhesion of the TiO₂ coatings onto the substrate surface. The roughness of the SGS is affected by the sintering time and temperature. Therefore, the adherence of the coating in function of sintering time and calcination temperature was an investigation variable.

This deposition method was carried out in four consecutive steps. The first step consisted in prepare the SGS as described in Section 3.2. For this particular case, the sintering temperature was 975°C and the sintering time was 45 or 75 minutes. The SGS samples were washed with acetone and deionized water with the intention of remove any pollutant and dried at 105°C for 30 minutes.

In the second step, it was elaborated a slurry consisting of a colloidal suspension of TiO₂ particles. The TiO₂ powder particles were mixed with ethanol as the solvent in which the catalyst was dispersed. In order to provide a suitable suspension, the pH of the slurry was adjusted to 1.7 adding 3% HNO₃. After each of the components were poured in a beaker, the

TiO₂ slurry was magnetically stirred in order to provide a well dispersed viscous suspension. Different masses of TiO₂ particles were evaluated to determine the optimal quantities for the slurry suspension. These masses of TiO₂ ranged from 1 to 5 grams. The amount of nitric acid depend on the initial pH and the quantity needed to decrease it.

The third step, consisted in covering the SGS surface with the TiO₂ slurry obtained from the previous step. This process comprises immersion, deposition and evaporation. First the SGS was submerged in the TiO₂ slurry. The immersion of the substrate was performed slowly. After the SGS was submerged into the slurry, it remained in the suspension for 6 or 24 hours leading to the deposition of the TiO₂ particles. The period time of immersion was the ageing time which is identified as an experimental variable. After this time has elapsed, the SGS was retrieved from the suspension and an adequate evaporation time was provided in order to vaporize the volatile solvent.

The fourth and final step of this immobilization technique consisted in calcinating, the coated SGS at 800°C or 900°C for 3 hours. The purpose of the calcination process was to promote a good adherence of TiO₂ particles on the SGS surface while obtaining a strong and uniform coating. This final step leads to the production of the GTC.

The amount of TiO₂ immobilized on the SGS surface was quantified by weight difference. First, the SGS was weighted after the washing procedure described above. Prior calcination process the GTC was washed in deionized water assisted by stirring in a beaker for 90 minutes and subsequently dehydrated at 105°C for 1 hour. The intention of this procedure

was to remove any TiO₂ particle that was not attached to the surface. Once the GTC was completely dried, it was weighted. This weight comprises the initial SGS mass and the mass of the TiO₂ particle attached. The difference between the initial and final weight represents the mass of TiO₂ attached on the SGS surface.

3.3.2.2 Immobilization by TiO₂ Coating over the SGS surface

In this method, a TiO₂-based coating was elaborated by treating the TiO₂ particles with a strong acid. The immobilization is then achieved by pasting the coating over the SGS surface and further calcination. The final TiO₂ mass attached on the SGS surface was estimated by weight difference as described in Section 3.3.2.1 It is very important to carry out the sintering and coating process using the same procedure implemented in the others immobilization techniques to ensure an equivalent performance and comparison between the GTC develop by each methods.

The sintering process of the recycled glass powders was conducted following the same procedure earlier in order to obtain the SGS. However, the SGS was sintered at 975°C for 45 minutes. The TiO₂-based coating is obtained by treating the TiO₂ particles with HNO₃. The treatment consisted in mixing together a fixed amount of 3.0 g of TiO₂ with 40 mL of diluted HNO₃ (3%). The mixture was magnetically stirred for 1 hour and then left at room temperature for 48 hours. Subsequently, the HNO₃-treated TiO₂ particles were dehydrated for 90 minutes at 105°C. Then 5 mL of EtOH are added to end up with a viscous colloidal paste which is the TiO₂ coating.

The coating was stirred vigorously for 1 hour at 23°C in order to provide a uniform colloidal paste. Then a TiO₂ film was prepared by pouring the colloidal paste into the SGS to produce a thin layer. Afterward, the coated glass substrate was dried at room temperature for 24 hours and annealed at 105°C for 1 hour. As a final step, the sample was calcined at 800°C for 1 or 3 hours. In order to evaluate the influence of the acid treatment, the colloidal paste was also prepared by mixing the untreated particles with the same volume of EtOH.

3.3.2.3 Immobilization with Polyvinyl Alcohol

It has been shown that the synthetic polymer polyvinyl alcohol (PVA) has the capacity to promote adhesion of TiO₂ onto glass substrate surfaces (Kumar & Bansal, 2012). Therefore, in this method an immobilized film of TiO₂ particles were prepared using PVA as a binding agent to improve the adhesion of the catalyst. The creation of the film was produced by a dip coating process. Consequently, this impregnation procedure was divided in four stages: 1) fabrication of SGS, 2) preparation of TiO₂/PVA suspension, 3) dip coating process, and 4) annealing process.

The SGS was obtained by implementing the procedure described in Section 3.3.2.2. The TiO₂/PVA suspension was prepared by adding titania powder and PVA in a mixture of deionized water. The amount of catalyst used in this method was also 3 g. Similarly, a mass of PVA that range from 2 to 6 g was used. The mass of these components was added in 40 mL of water or water. Next, the solution was magnetically stirred for 3 hours at room temperature in order to obtain a well dispersed suspension. After this period of time, an

enhancement of the suspension was achieved by adjusting the pH with HNO₃. By adding nitric acid, the pH of the suspension was at different values ranging from 1.7 to 1.8. Thereafter, the adjusted TiO₂/PVA suspension was agitated by stirring for 2 hours at 80°C.

After stirring, the suspension was ready for the preparation of the TiO₂ films on the glass substrate. In this stage, the SGS was coated in the solution using dip coating process. The sample was submerged in the TiO₂/PVA suspension at a constant rate and slowly withdrew after 10 minutes of contact time. The coated glass substrate was annealed at 105°C for 24 hours.

3.4 CHARACTERIZATION OF PHYSICAL AND STRUCTURAL PROPERTIES

It was expected that each of the TiO₂ immobilization techniques produced different properties and structures in the GTCs. Therefore, microscopy and spectroscopy characterization methods were implemented to assess physical and structural characteristics such as percolation and porosity to both SGS and GTC. This evaluation yielded essential information related to the surface and crystalline structure of the TiO₂ films deposited on the glass substrate according to immobilization method.

3.4.1 Morphology

The morphology assessment was conducted to study the changes in the surface of the SGS produced by the immobilization of the TiO₂. This was achieved by using a JEOL 5410 JV Scanning Electron Microscope (SEM). The application of this microscope introduced micrographs of the TiO₂ films of the GTC fabricated. The goal of this examination was to

evaluate the characteristics of TiO₂ coatings surface such as homogeneity, composition and roughness.

Control micrographs were elaborated to identify the modifications to the sintered glass surface generated by the TiO₂ films. To achieve this, control specimen, which are the uncoated SGS, was made with RGPs using the sintering parameters established for the preparation of GTC. As a result, the sintering temperature was 975°C and the sintering time was 45 minutes. The data collected from this evaluation included information related of the morphology of coated and uncoated SGS.

3.4.2 Percolation

Percolation is defined as the process in which a liquid flux passes through a porous media. The purpose of this experiment was to evaluate the efficacy of the glass composites to percolate water. In this test, the behavior of the percolation through the uncoated sintered glass substrates as a function of sintering time and temperature was evaluated. The results obtained identified the optimal combination of sintering time and temperature for a better percolation.

The percolation capacity was measured using a custom-made percolation system designed by our team. The system consisted of three main components: funnel, a PVC pipe and a PVC male adapter union. A schematic of the percolation systems is presented in Figure 3-1.

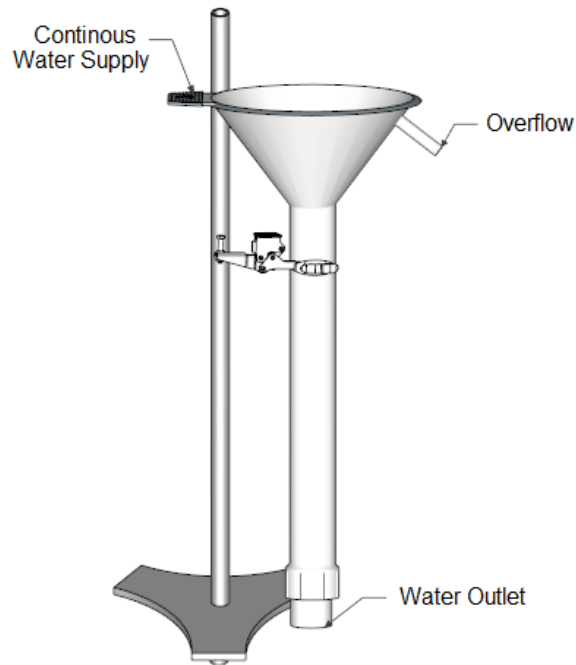


Figure 3-1. Schematic of the percolation system

The percolation system allows obtaining one directional water flux with a constant head in order to provide a constant flow. The constant head is produced by an overflow weir. The weir is represented with a hole in the funnel to produce a constant overflow at all times. The water inlet was at the funnel and the SGS or GTC were placed at the opposite side of the pipe in the PVC male adapter union. The water flow was discharged at this point; hence the male adapter union is the water outlet. The percolation capacity was defined as the ratio of water volume change and time. This was determined by recording the time to obtain a volume of water, namely 200 millimeters.

3.4.3 Surface Porosity

According to the sintering theory, the time and temperature selected to perform this process has a direct effect in the porosity of the SGS. It was expected that as sintering time and temperature increases there was a continuous reduction of the pore size until the pore is eliminated. Therefore, an evaluation of the effect of sintering time and temperature was desirable. For this assessment sintered glass substrates were prepared at temperatures from 950°C to 1,000°C at 25°C intervals. For each temperature the sintering time was 45, 60 and 75 minutes.

The preparation of the samples for the surface porosity quantification was as follows. The surface area of the prepared SGS were embedded in epoxy resin to produce an epoxy laminates. All samples were polished with sandpaper that has the following grit size: 60, 240, 320, 400, 600, 800 and 1200. After the SGS were covered with epoxy resin, the samples were divided in four section and surface micrographs were obtained randomly at five locations of each section using a Nikon SMZ 1500 optical microscope with a magnification of 5x. Hence, 20 micrographs were produced for each samples. The images comprise the red, green and blue (RGB) bands, have a resolution of 1,500 x 1,129 pixels in size.

For the image analysis assessment, the SGS surface porosity was estimated using ImageJ which is a Java software of public domain. This software has a collection of tools very useful for image analysis applications. Images of 8-bit, 16-bit and 32-bit can be displayed, edited processed and saved. The surface porosity was evaluated by manually drawn a polygon over

the pore until all the porous area were drawn. Then, a proper threshold to gray-scale was applied to the image to extract the pore from the sintered glass particles (background) based on the degree of contrast between the components. An image with regions black and white was produced. All the pixels in the black and white regions have a threshold of zero and one, respectively. The white regions were identified as pore and the black as sintered glass particles. The area of the image and the pore regions were determined with the analyze tool in ImageJ. The surface porosity, ε_s (%), was calculated with the following equation:

$$\varepsilon_s = \frac{A_p}{A_t} \times 100\% \quad (3-1)$$

where A_p is the total area of pore (white regions) in the optical microscope image and A_t is the total area of the optical microscope image.

3.4.4 General Porosity

For this assessment, the porosity of the samples was investigated using Archimedean porosimetry, which is based on the Archimedes buoyancy principle. In this method, the SGS needs to be immersed in a fluid for a long period of time until the pores are occupied with the fluid. The porosity of the SGS was determined as the ratio of the pore volume to the total geometrical volume of the sample. The samples were weighted before and after they were immersed in the fluid in order to obtain the dry mass and wet mass. As first step, the samples were washed and dry at 105°C for 1 hour in order to obtain the dry mass and eliminate moisture. Subsequently, the samples were immersed a vacuum chamber system containing

the fluid. In this case, the fluid was water since it has a low surface tension, hence was easily removed from the sample. Pumping was provided until there was no evidence of air bubble emerging from the samples. The pore volume is the difference between the wet mass and the dry mass divided by the density of the water. Mathematically this can be expressed as,

$$V_p = \frac{M_s - M_d}{\rho_w} \quad (3-2)$$

where M_s is the wet mass, M_d is the dry mass and ρ_w is the water density. The pore volume is represented with the volume of water occupying the total porous network. Knowing that the porosity is defined as the ratio of the pore volume to the total volume, the porosity, ε was calculated using the following equation:

$$\varepsilon = \frac{M_s - M_d}{AT\rho_w} \times 100\% \quad (3-3)$$

where A is the SGS superficial area and T is the SGS thickness.

3.4.5 Polymorph Structure of TiO₂ Phase

It has been shown that the polymorph phase of anatase in TiO₂ has a superior photocatalytic performance than rutile. The immobilization technique described in section in the previous employs temperatures between 950°C to 975°C. The phase of TiO₂ depends on many parameters such as the particle size and shape, surface area, atmosphere, volume of sample, impurities among others. Although this process is influence by these parameters, it was

necessary to determine if the sintering time and temperature impacted a phase transformation from anatase to rutile.

The study was carried out using GTC specimens obtained from the several immobilization methods. An X-Ray diffraction (XRD) instrument will be used to determine the polymorph structure of TiO₂ phase. The XRD analysis were performed to the TiO₂ powder before sintered and to the GTC. Also pure TiO₂ powder was exposed to sintering time and temperature to determine if the transformation occurs, as a control. Moreover, an XRD analysis were performed to the GTC developed by each of the propose immobilization methodologies in order to identify the presence of TiO₂ on the surface of the immobilized sintered glass substrates. This test produced information related to the quality of the coatings in terms of their crystalline structure. The tests were carried out at room temperature with the followings parameter: 2θ range from 15° to 75°, increasing steps of 0.02 s⁻¹, and step time of 1 second.

3.5 DEGRADATION OF NATURAL ORGANIC MATTER

The present thesis investigates the photocatalytic decomposition and mineralization of HAs. Therefore, this component of the research focuses in the evaluation of the photodegratation capacity of the TiO₂ powder as well as GTC by degrading HA.

3.5.1 Preparation of the HA Solutions

A synthetic stock solution of HA, representative of NOM found in raw waters, was prepared. The stock solution was prepared using the procedure introduced by Urano et al. (1983) in which the HA is dissolved by the addition of NaOH (referenced by Uyguner-Demirel &

Bekbolet, 2011). The materials needed for the preparations of this sample are: humic acid powder, distilled water, NaOH, and a microfilter (0.45 μ m).

The procedure consisted in adding and dissolving 0.1 g of HA powder in 100 mL of distilled water. The solution was stirred for 10 minutes in order to produce a homogeneous solution. Then the pH of the solution was adjusted to 10 by the addition of NaOH 1 M. After being stirred for 24 hours, the solution was then filtered through a 0.45 μ m filter membrane with the purpose of isolating the soluble organic matter fraction. Appropriate HA dilutions were prepared at different concentrations (10-20 mg/L) in order to mimic the content of NOM in natural waters. Thereafter, the HA solution was ready for the degradation experiments.

3.5.2 Photocatalytic Reactor

The photodegradation experiments were conducted in a photocatalytic reactor box as shown in Figure 3-2. The reactor consisted of a wood box, a magnetic stirrer plate and an UV lamp. The irradiation was carried out using a 4W PL series compact UV lamp that was placed at the top of the box. This UV lamp emit radiation wavelength of 365 nm as a result it is belong to the region of the electromagnetic spectrum refers as UVA. The intensity of the incident light is 1,000 μ w/cm².

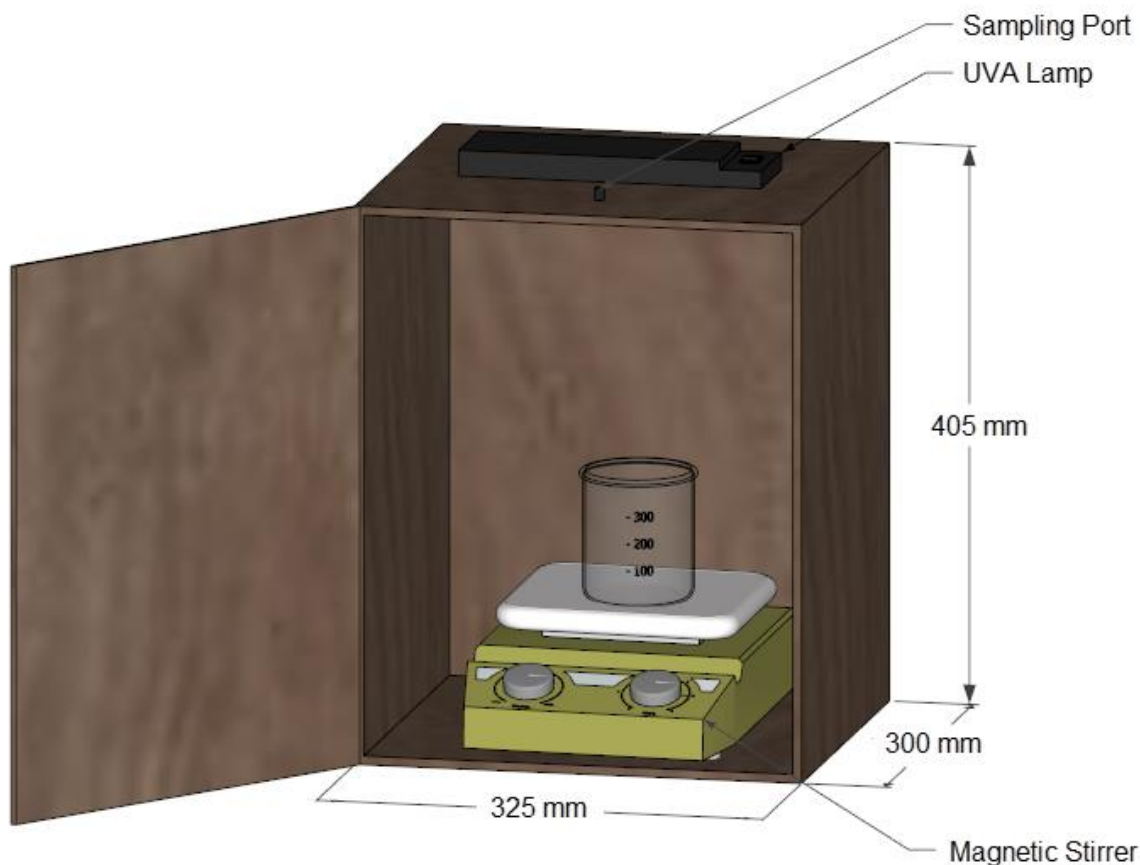


Figure 3-2. Schematic of the photocatalytic reactor box

3.5.3 Photodegradation Experiments

The catalytic performance of the GTCs and TiO_2 in suspension were assessed by means of the photodecomposition and photomineralization of the HAs. The degradation performed with each GTC and TiO_2 powder was identified as a treatment. The HA levels in the solution evaluated was quantified by means of TOC concentration, UV-Vis absorption and fluorescence spectroscopy. The TOC concentration was measured using a Teledyne Tekmar TOC Fusion Analyzer. UV-vis measurements were acquired from a Beckman Coulter DU 800

Spectrophotometer using a quartz cell. Fluorescence spectra of the sample were recorded on a Shimadzu RF-5301 Spectrofluorophotometer. For the slurry system, the TiO₂ was removed prior to analysis using a 0.45µm porosity membrane filter. The effect of the UV light and irradiation time were evaluated as well. Each experiment was conducted in the presence of UV light at different contact times.

The degradations experiments consisted in suspending GTCs in a beaker containing 225 mL of HA solution. The solution was continuously agitated by a magnetic stirrer. In order to evaluate the reaction kinetics several initial values of the investigated parameters were used. The HAs starting concentrations were of 10, 15, and 20 mg/L. The pH conditions evaluated were 3, natural pH of the solution (pH_{average} 6.5) and 10. For the TiO₂ suspensions experiments, the amounts of catalyst used were 0.5, 1.0 and 1.5 g/L. During the experiments, the solution and the GTC were irradiated for a maximum of 8 hours and samples solution were collected at 60 min intervals in order to determine the effect of the irradiation and contact time.

3.6 ADSORPTION OF NATURAL ORGANIC MATTER

It was also desired to evaluate the adsorption capacity of the SGS as well as GTC for the dissolved organic matter in water. Hence, an adsorption study was developed to confirm or discard any effect of the SGS as well as GTC in the HA levels. Consequently, one can determine if the degradation of the organic matter, if any, can be attributed due to adsorption.

The experiments consisted in placing a SGS or the GTC in HA solution for a maximum of 8

hours in the absence of UV light. The HA solution concentrations were of 10, 15, and 20 mg/L. A sample was extracted and analyzed for TOC at 60 min intervals.

4 RESULTS AND DISCUSSION

In ceramic processing, such as the fabrication of glass substrates, the final product is highly dependent on the physical properties of the particulate material. The initial powder particle size and distribution has a great influence in the sintering process such as the required sintering time and temperature. Therefore, it will have an effect in the resultant porosity of the substrate. In order to assess the particle size distribution that comprises the RGP a gradation test was conducted. The granulometric composition of glass powder is presented in Table 4-1. For this assessment, three different samples were analyzed. Hence, the results are reported as the average of the three measurements.

Table 4-1 Granulometry of the MG-30 recycled glass powder

Sieve No.	Sieve Opening, mm	Mass Retained, grams	Partial Retained, p_3 %	Cumulative Retained, %	Percent Finer, Q_3 %
4	4.75	0.00	0.00	0.00	100.00
10	2.00	0.00	0.00	0.00	100.00
20	0.85	142.10	28.42	28.42	71.58
40	0.43	345.00	69.00	97.42	2.58
60	0.25	11.70	2.34	99.76	0.24
100	0.15	0.20	0.04	99.80	0.20
200	0.07	0.20	0.04	99.84	0.16
Tray	-	0.80	0.16	100.00	0.00

There are two basic approaches for the representation of the particle size distribution: 1) histogram and 2) cumulative frequency curve. The histogram represent the partial retained fraction (p_3) and the cumulative frequency curve is the percent finer (Q_3). The granulometric

size distribution of the RGP is shown in Figure 4-1. The figure shows how closely the sampling approximates to a normal distribution. The greatest fraction of the tested specimens, around 69%, results with different values of particle size ranging from 0.43 to 0.85 mm.

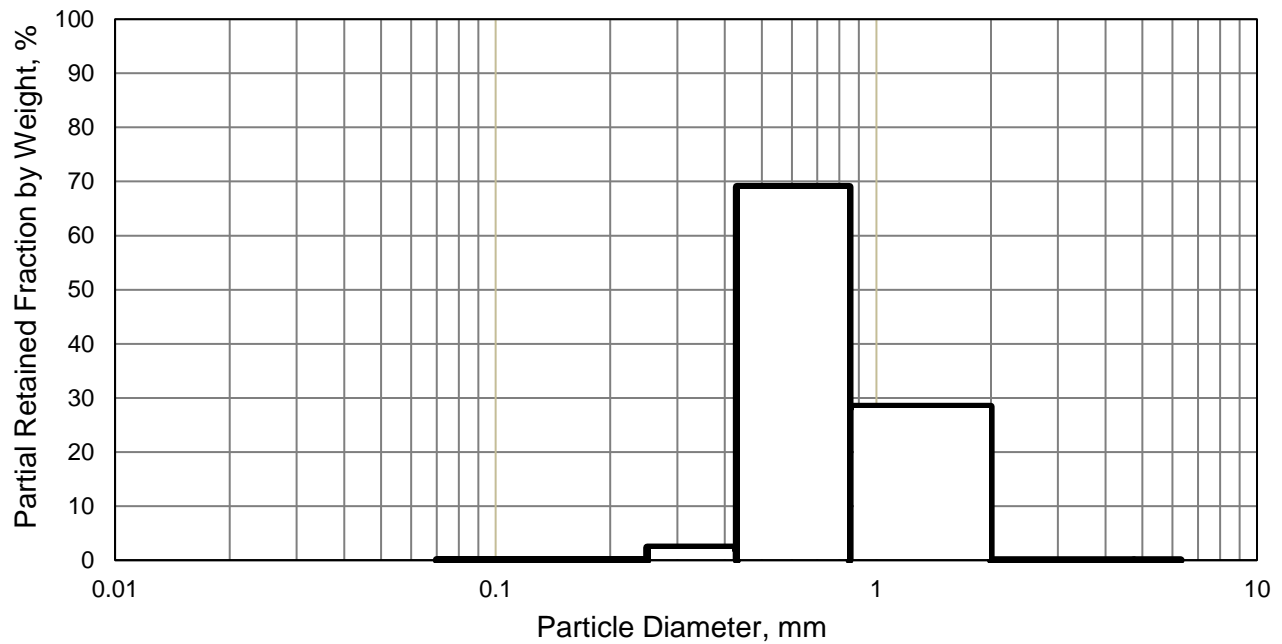


Figure 4-1. Grain size distribution

The characteristic particle diameters D_{10} , D_{50} , and D_{90} have been obtained from the cumulative distribution curve present in Figure 4-2. The corresponding grain size of the median of the distribution (D_{50}) is 0.72 mm, which means 50% of the sample are smaller or larger than 0.72 mm. The finer grain size (D_{60}) of the RGP is around 0.78 mm. 90 percent of the sample has a particle size smaller than 1.595 mm, which is defined as D_{90} . Only 10% of the RGP lies below the effective size (D_{10}) that is equal to 0.47 mm. The uniformity coefficient

of the samples is 1.57, therefore the RGP is considered to be poorly graded and the mass consists of only a limited range of particles sizes.

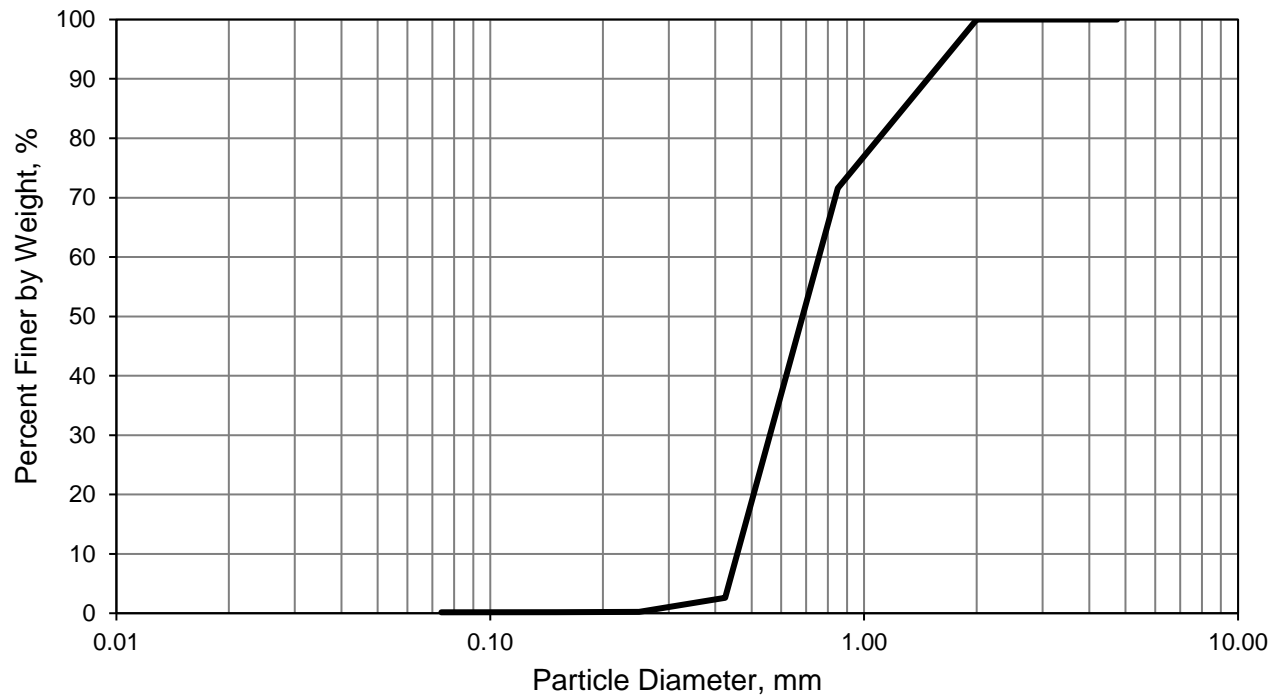


Figure 4-2. RGP particle cumulative distribution curve

4.1 IMMOBILIZATION OF TiO₂ PARTICLES IN THE SGS

This section is intended to provide a quantitative and qualitative comparison of the produced GTC by different techniques in order to define the better approach. The purpose of immobilized or impregnated TiO₂ on the recycled glass is to provide a clean decant thereby evading the complications related to the separation of the catalyst powder from the treated water.

Several procedures were implemented with the intention to determine which immobilization technique provides a stable adhesion of the TiO_2 and a further efficient photocatalytic activity. Therefore, it was very important to conduct every procedure and examination under similar experimental conditions so that an appropriate relation can be made. For each of the different routes implemented the TiO_2 deposition was prepared at least twice to ensure reproducibility of experimental results.

4.1.1 TiO_2 Particles within the SGS body

The principal objective of this method was to deposit TiO_2 particles on the surface of glass beads to further develop a GTC. This composite comprises a SGS with TiO_2 particles embedded in its body. The circular shape sintered GTC was prepared changing different experimental parameters, such as the initial TiO_2 mass, pH of the slurry, as well as the sintering time and temperature. In order to assess the effect of the initial TiO_2 quantity, several slurries were prepared varying the initial mass in the range of 0.30-3.0 grams. The amount of TiO_2 particles deposited and embedded on the glass beads were determined by weighing the beaker before and after the preparation of the titania and glass beads mixture. This value, i.e. mass of catalyst embedded, was calculated based on the assumption that the TiO_2 residues found in the beaker were the only percent of mass not attached to the glass beads surface.

Table 4-2 covers the average amount of TiO_2 deposited onto the glass beads surface. The results have been reported in function of the TiO_2 initial mass and the slurry pH and were calculate before the sintering process. No noticeable differences in mass calculation results

for the prepared samples at the same TiO₂ initial mass level. Therefore, the obtained data at each of the level produce a considerably small standard deviation as presented in the reported data. This is particular important for the reproducibility of the data and the conditions of the experimental procedure.

Table 4-2. TiO₂ Particles deposited onto glass beads

TiO ₂ Initial Mass, g	Average TiO ₂ Mass Embedded, g	
	pH 1.7	pH 5
0.3	0.17 ± 0.013	0.14 ± 0.055
1.0	0.87 ± 0.041	0.72 ± 0.024
3.0	2.69 ± 0.14	2.36 ± 0.077

In order to evaluate the influence of the pH, the TiO₂ suspension was prepared without making any change to its initial pH value. Therefore, the pH of the as-prepared slurry is report as the pH value obtained after magnetically stirring the TiO₂ with ethanol. The average pH value obtained in this case was 5 ± 15. The percentage of TiO₂ mass attached to the glass beads surface increased by decreasing the pH value to 1.7. As it can be observed in Figure 4-3, the greater TiO₂ mass loss was achieved at pH value of 5. This behavior could be explained by the stability of the colloidal system. In general, the overall stability of a colloidal suspension increased with a decrease in pH. Indeed, the pH is a contributing factor in the interaction of colloids that is based on their ability to protonate and deprotonate. Therefore, as the pH values decreases the TiO₂ particles become more protonated decreasing the effects of attraction which leads to a more stable suspension and smaller TiO₂ particles. Upon increasing the pH, generally greater than 3, the TiO₂ particles are likely to be deprotonated resulting for more

agglomeration. Consequently, particles with greater size are produced. Therefore, the greatest deposition was achieved under acidic conditions since smaller particles tend to have large surface area, which produce a greater contact area between the TiO_2 and the glass beads.

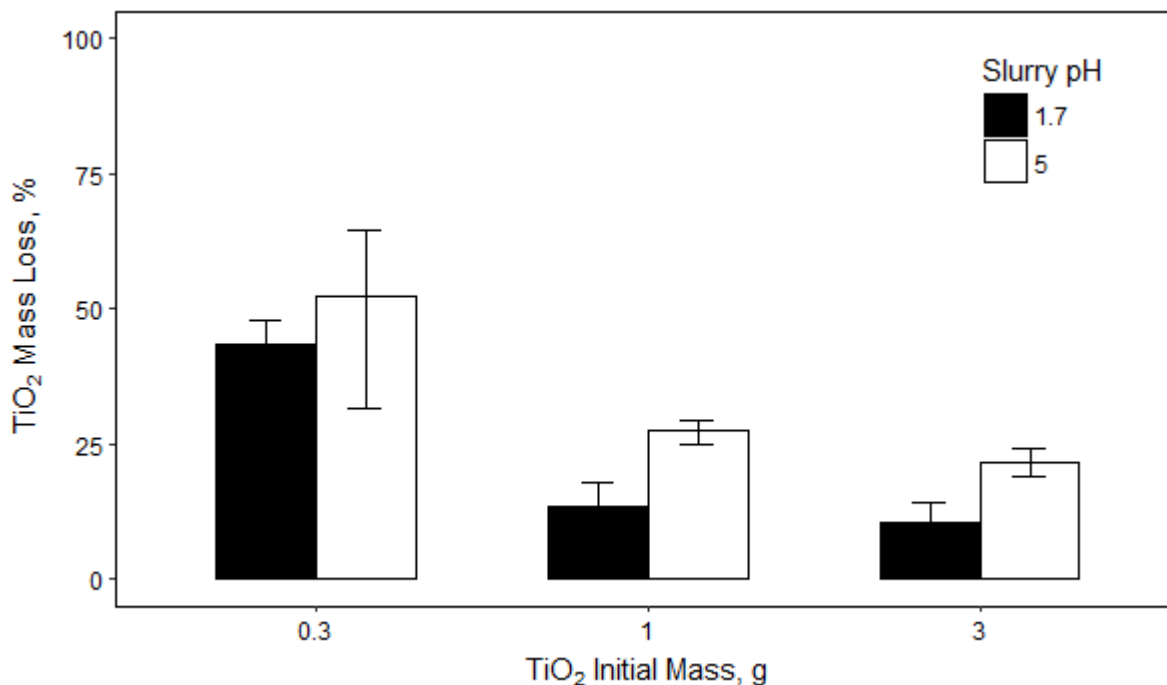


Figure 4-3. TiO_2 mass loss as a function of pH and initial mass

Figure 4-4 shows the effect of the initial mass amount on the quantity of the impregnated mass. It can be observed that the amount of TiO_2 particles impregnated onto the glass beads is highly influenced by the initial mass of TiO_2 used. There is a linear increase in the TiO_2 mass embedded. As it was expected, 3.0 g represents the amount of TiO_2 yielding the most

significant mass deposited onto the glass beads. Nevertheless, the addition of a higher amount of TiO_2 mass complicated further thermal treatment to embed the catalyst.

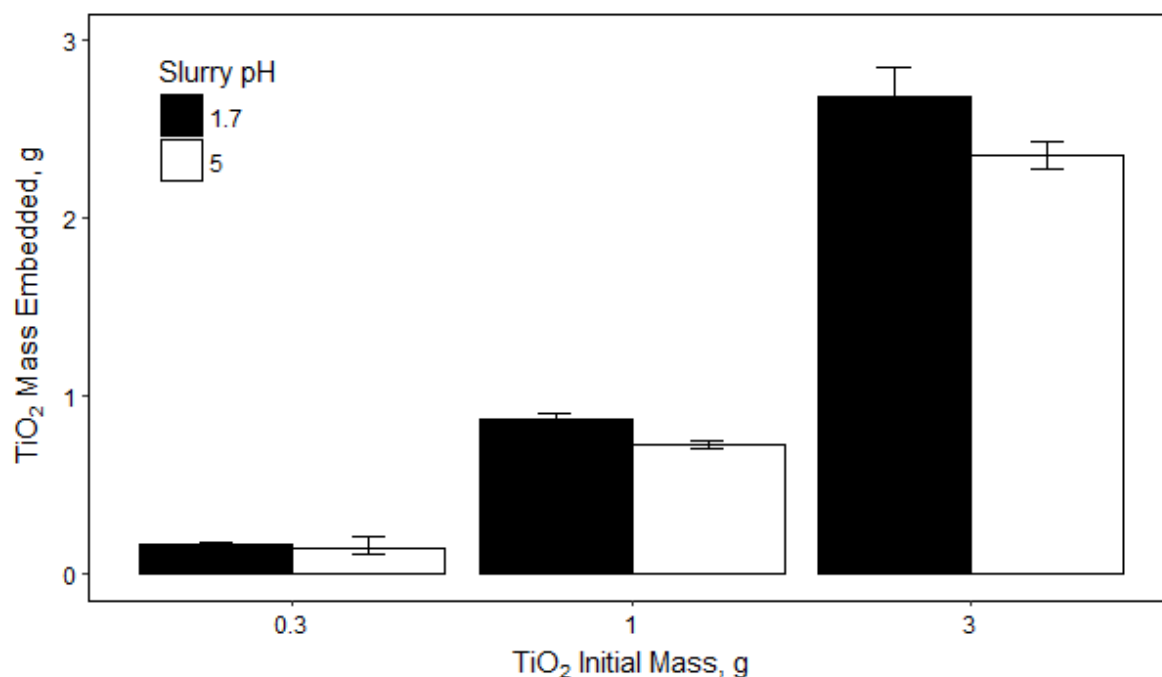


Figure 4-4. Total TiO_2 mass embedded onto the glass beads

A substantial influence of the TiO_2 initial mass on the sintering time and temperature of the dried TiO_2 and glass beads mixture was found. In general, the sintering time and temperature increases as the TiO_2 initial mass increases. The observed change in the sintering parameters may be explained by sintering theory. According to this theory, the sintering is achieved when the glass beads are compacted together. Since the contact between the glass beads is reduced as the TiO_2 mass increases, it is more difficult to achieve binding of the glass beads at lower sintering time and temperature. When using a starting TiO_2 quantity of 1 wt.% of the

total MG-30 mass for the GTC preparation, the TiO₂ and glass beads mixture were sintered at 950°C or 975°C for sintering times ranging from 60 to 90 minutes at 15 minutes intervals. An appropriate sintering was achieved under these conditions. However, it was found that the photocatalytic efficiency of this GTC was ineffective due to the capacity of the method to incorporate low amounts of TiO₂. Therefore, the initial TiO₂ mass was increased by a 10 percent.

The addition of 3.0 g of TiO₂ to the slurry led to further changes in sintering time and temperature. For the mixture with 3 g of TiO₂, a minimum of 5 hours were needed to sintering the TiO₂-glass beads mixture at 975°C. Furthermore, the sintering was accessed after implementing a reduction of the MG-30 mass by a 33 percent. Although the sintering of the GTC with 3.0 g of TiO₂ was achieve, the GTC exhibited a very weak strength since the mixture detached after sintering. This produced a total mass loss greater than 25% of the initial total weight. Therefore, the experimental conditions for producing the GTC under this method that exhibit the best properties are: 1.0 g of TiO₂, 20 g of MG-30, a sintering temperature of 975°C, and a sintering time of 90 minutes.

4.1.2 Immobilization by Gravitational Deposition and Evaporation

A second method for the immobilization of TiO₂ particles was assessed in order to improve the properties and photocatalytic activity of the GTC. The factorial experimental design was developed for this method to identify which parameters have the most influence on the TiO₂ mass immobilized. The factors selected for study in the experiments were sintering time, TiO₂

initial mass, pH value, ageing time and calcination temperature. A preliminary experiment was performed with the objective to select an optimal TiO₂ initial mass. Three different masses were evaluated: 1.0, 3.0 and 5.0 g and three replicate were conducted for each mass level.

Figure 4-5 shows the main result of how the initial mass can affect TiO₂ immobilization.

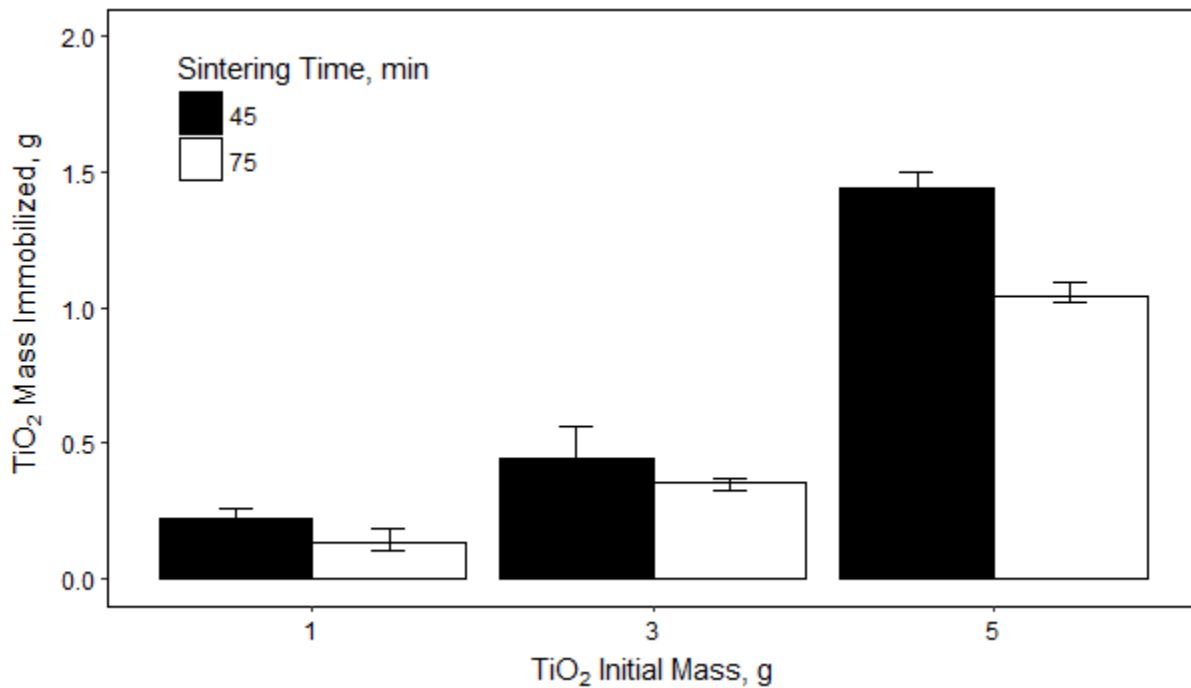


Figure 4-5. Effect of TiO₂ initial mass

The pH and the period time of immersion was kept constant with values of 5 and 6 hours, respectively. As expected, the studied GTC showed that the amount of TiO₂ immobilized increased with initial mass. These samples also showed considerable increases as the sintering time decreased. These results suggested that a lower sintering time an increment of 27% of immobilized mass could be achieved. A possible explanation is the higher porosity in

the SGS sintered at 45 minutes than the SGS obtained for 75 minutes. The SGS with greatest porosity encounters more sites to accommodate TiO₂ particles. Immobilization of TiO₂ decrease at 75 minutes due to the low porosity, which makes it harder for a large amount of TiO₂ particles to penetrate through the surface of the SGS. Furthermore, the detachment of TiO₂ particles from the SGS was observed when the initial TiO₂ mass was 5.0 g. A more stable TiO₂ layer with a good adhesion was observed for 3.0 g of initial TiO₂ mass. Therefore, an initial mass of 3.0 g was selected as a constant factor to perform further experiment with parameters that may exert some significant effect in the immobilization.

In order to optimize the total mass deposited onto the SGS surface, a second factorial design was use to investigate the effect of all possible combinations of the selected experimental factors. The objective was to find the levels of pH value, sintering time, ageing time and calcination temperature that maximize yield of the amount of TiO₂ immobilized. Figure 4-6 shows the response of the TiO₂ mass deposited onto the SGS. These results are based on 72 GTC that were prepared in randomized order. Taking all the previous experimental factors in consideration, the higher amount of mass deposited was achieved when the sintering time was 45 minutes, the ageing time was 24 hours and a pH value of 1.7. A total average mass of 1.49 ± 0.13 g of TiO₂ was not only deposited but also impregnated on the SGS under these conditions. Hence, these results are significantly correlated with the suspension stability and total porosity. The sintering time, pH value and ageing time that yield the lowest amount of TiO₂ deposited was 75 minutes, 5 and 6 hours, respectively. Around 0.42 ± 0.09 g of TiO₂ were deposited on the SGS.

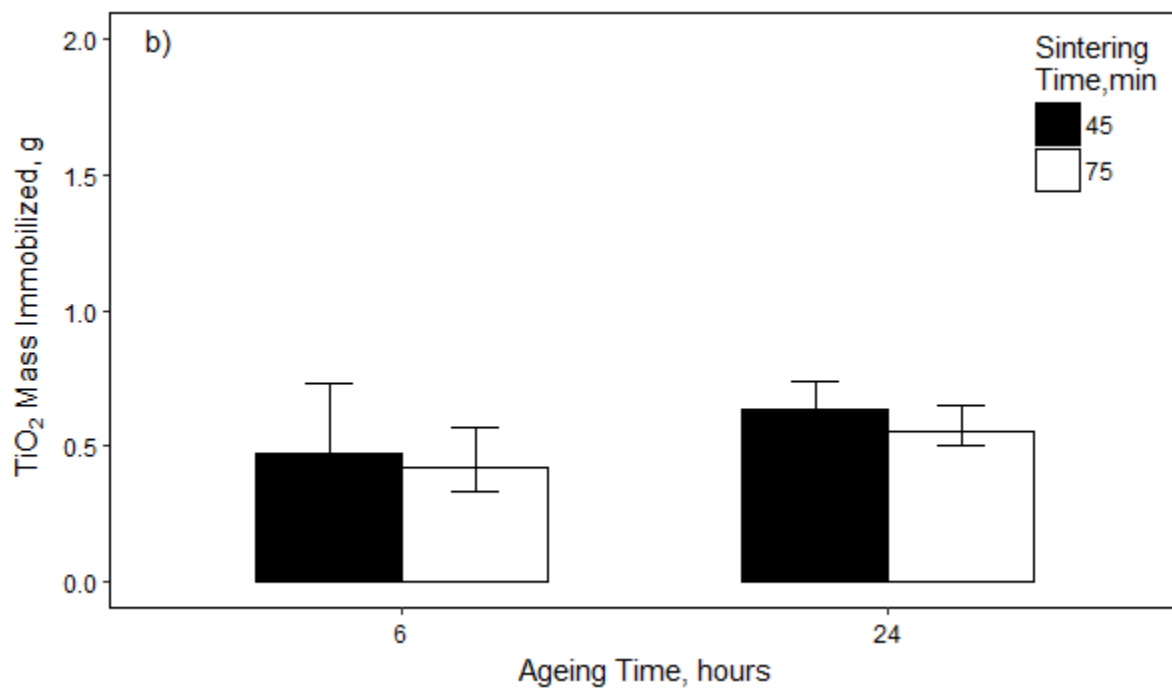
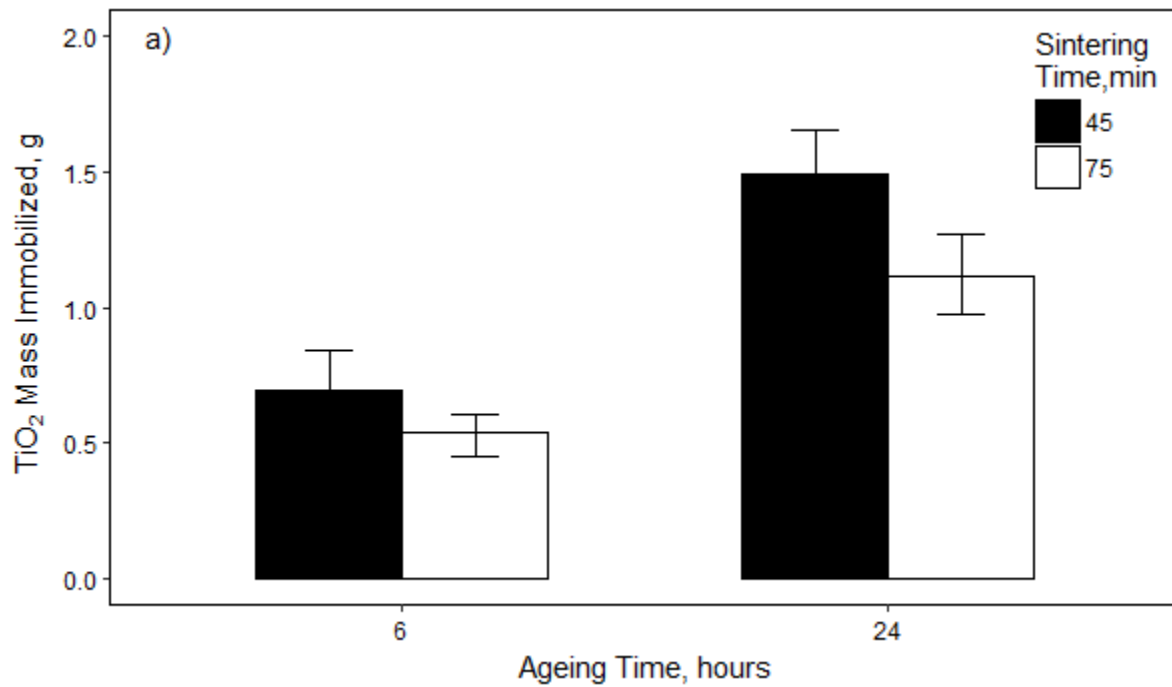


Figure 4-6. TiO₂ Mass deposited on the SGS: a) pH 1.7, and b) pH 5

In the deposition process, increasing the ageing time was a key factor that enhanced the yielding. The SGS's immersed for 24 hours have up to 53% more mass deposited than those immersed for 6 hours, especially when the slurry was prepared under highly acidic conditions. This observation is supported with the van der Waals attractive forces and electrical double layer forces theory since it is thought that the stability of the suspension as well as the aggregation of TiO₂ particles play an important role in the results. At pH 5, close to the zero point of charge, the TiO₂ suspension was unstable and particles flocculates into large clusters that tend to sediment out which limited their distribution in the SGS. Moreover, suspension of larger aggregates limits their penetration through the SGS pores leading to a lower amount of TiO₂ particles deposited. In contrast, at pH 1.7, TiO₂ suspensions were more stable and small particles aggregates were present. Due to the repulsive effect, the TiO₂ particles were considered to be spread evenly over the surface of the SGS. Therefore, the particles experience lower sedimentation rate leading to a deposition cause by evaporation as the immersion time increasing. Hence, the TiO₂ particles were deposited as the solvent evaporates. Furthermore, it was noted that when the evaporation of the solvent was restricted the suspension prepared at pH 1.7 was visually stable for almost 2 days.

Although a considerable mass were deposited on the SGS further thermal treatment was needed in order to immobilize the TiO₂ particles. After the TiO₂ particles were deposited on the SGS, the substrates were calcined at 800°C and 900°C for 3 hours. Calcination time below 3 hours were preliminary evaluated but the deposited TiO₂ was no adhered to the SGS surface. Control samples, heated only at 105°C, were prepared in order to evaluate the effect

of the calcination temperature in the adherence of the deposited TiO₂ particles. All samples were washed with acetone and deionized water with the intention of remove any TiO₂ particle that was not completely attached to the SGS surface. Figure 4-7 summarizes the percent of the total deposited mass completely adhere to the SGS surface. It was found that the thermal treatment at the investigated temperatures strengthen the attachment of the TiO₂ to the SGS. However, TiO₂-films of the GTC calcined at 900°C demonstrated better adherence to the one calcined at 800°C. At 900°C, only 2.39% and 7.17% of the deposited mass was loss at pH 1.7 and 5, respectively. In contrast, at 800°C, the mass loss was 5.38% at pH 1.7 and 15.20% at pH 5.

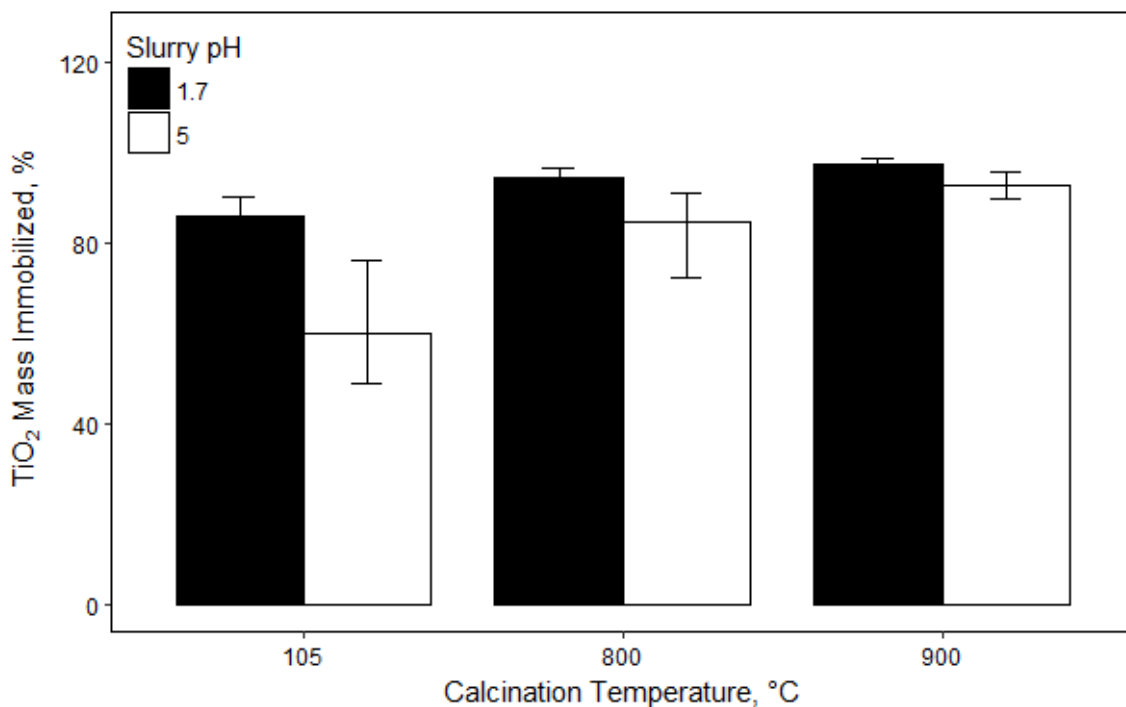


Figure 4-7. TiO₂ Mass Immobilized on the SGS for different temperatures

In addition, the results seem to indicate that the pH plays a vital role not only in the deposition of TiO₂ particles but also in their adherence to the SGS. The difference in final immobilized amount of TiO₂ in function of pH became more noticeable for control samples since the effect of the calcination temperature is negligible. From the Figure 4-7, it can be seen that the GTC prepared at pH 1.7 exhibited the highest immobilization. Moreover, mass loss for the control samples prepared at pH 5 was around 40%, which is almost 3 times greater than the mass loss for those prepared at pH 1.7. This may be attributed to the surface interaction between the TiO₂ and the SGS in strong acidic media (pH 1.7). As explained before, TiO₂ particles are smaller at this pH leading to an effective impregnation of the catalyst within the SGS pore, thus making more difficult the detachment of the deposited particles. Furthermore, Musić et al. (2011) found that under this condition the surface of the SiO₂ tends to have a neutral to negative charge thus the electrostatic attraction between the TiO₂ and SGS surface becomes much stronger. Even though that the calcination temperature produced a good adhesion of the TiO₂ particles, the results founded in this section suggest that surface charge is a key factor in the immobilization of TiO₂. However, from these results it was observed that the GTC was sensible to touch because when it was in contact with other surface the TiO₂ was easily transferred. For example, when the GTC was touched TiO₂ residues came off to the gloves.

4.1.3 Immobilization by TiO₂ Coating over the SGS surface

Previous results suggested that the TiO₂ adherence was enhanced under strong acidic conditions. To increase the adhesion of the TiO₂ film, the immobilization method discussed in Section 4.1.2 was investigated using HNO₃ as the solvent. The final coated SGS obtained by

using acid as the solvent was more stable than those produced with EtOH. It was observed a strong attachment with little mass loss (1.3%) of the TiO₂ particles in the GTC after the annealing process at 105°C. However, when the GTC was washed, the TiO₂ was completely removed from the SGS since the HNO₃ is soluble in water. A further evaluation of the immobilization using HNO₃-treated TiO₂ particles was conducted. The objective of this procedure was to investigate whether the acid treatment was able to produce a better immobilization of TiO₂ particles or not, hence, it was evaluated using a fixed value of the experimental parameters.

The adhesion of TiO₂ particles was significant enhanced by the acidic treatment. From the measurement, the amount of TiO₂ particles deposited to the SGS surface was significantly increased compared to the method using untreated TiO₂. The average treated TiO₂ particles deposited was 2.40 ± 0.29 g with a total immobilization of 99.37%. On the other hand, the average mass deposited with the untreated particle was 0.85 ± 0.17 g with a total immobilization of 63%. The results obtained with the untreated particles are very similar to those obtained in the previous section at pH 5.

A possibility for the reduction of mass loss may be that the electrostatic attraction between TiO₂ particles and SGS surface is optimized. It is believed that the TiO₂ particles adsorbed the HNO₃, thereby enhancing their physical properties. Indeed, Park et al. (2009) reported that when HNO₃ is adsorbed, the TiO₂ particles carry a positive charge with higher porosity and lower particle size compared to untreated particles. When the HNO₃-treated TiO₂ particles were mixed with EtOH, the pH of the suspension was between 2.5 and 3. Under

this condition, the SGS surface is considered to be negatively charge and its electrostatic interaction with positive TiO_2 is stronger, leading to a binding between them. It is assumed that the electrostatic interaction between the TiO_2 particles prepared at pH 1.7 and SiO_2 is weaker than the acid-treated TiO_2 particles and SiO_2 since at pH 1.7 the SGS can be barely charged due to proximity of pH_{zpc} . Based on these results, it is suggested that the interaction between the positively charge TiO_2 surface and negatively charge SiO_2 is necessary to induce binding and promote a better adhesion.

4.1.4 Immobilization with Polyvinyl Alcohol

As discussed, high calcination temperatures and times were required in order to promote the adherence of TiO_2 on the SGS. This presents a disadvantage since elevated temperatures and time may decreased the surface area and photocatalytic activity during thermal treatment. Therefore, the evaluation of a binding agent was carried out with the objective to immobilize the TiO_2 avoiding high calcination temperature. TiO_2 film on the SGS was prepared according to the method explained in Section 3.3.2.3. Using this method, further thermal treatment was not necessary; therefore, the GTC was ready after the annealing process. However, after washing the GTC in water the TiO_2 was completely gone. It is believed that the PVA got dissolved with the water due to its solubility. It was concluded that this method is not appropriate for the immobilization of TiO_2 particles on the SGS surface.

4.2 PHYSICAL AND STRUCTURAL PROPERTIES OF THE GLASS COMPOSITE

The data and results obtained from this investigation will establish the general principles for the development of a filter-like composite made out of sintered glass. Therefore, it was necessary to assess the physical and structural properties of the SGS as well as GTC. Of particular interest are the sintering parameters, which show how the properties of the porous matrix depend on the combination between these two parameters.

4.2.1 Percolation

The analysis of percolation of the porous matrix is essential to the broad understanding of the SGS physical properties. The purpose of this experiment was to investigate how sintering time and temperature affect the efficacy of SGS to percolate water. Hence, identify the optimal combination of sintering time and temperature for a better percolation. Percolation rate as a function of sintering time and temperature is presented in Figure 4-8. The percolation rate was measured for sintering temperature in the range of 950-1000°C with sintering time ranging from 45 to 75 minutes.

It was found that the percolation rate decreases with sintering temperature time. The main effect of the increment of sintering parameters is the reduction of the paths for the flux of water. The sintering theory may be used to interpret the water flux through the porous media. For instance, if the minor combination of sintering temperature and time is considered, which are 950°C and 45 minutes, an average percolation rate of 29.78 ± 4.46 gpm/ft² is obtained. This means that pores that are formed in the porous matrix possess a wide space between

the touching grains. If instead we consider the maximum combination of the sintering parameters, i.e., 1000°C and 75 minutes, will lead to an average percolation of 0.065 gpm/ft². Because this value is very close to 0, it is convenient to express that at 1000°C the SGS becomes a solid mass with little or no pore network in its surface. As consequence, the SGS loses its capacity to filtrate water.

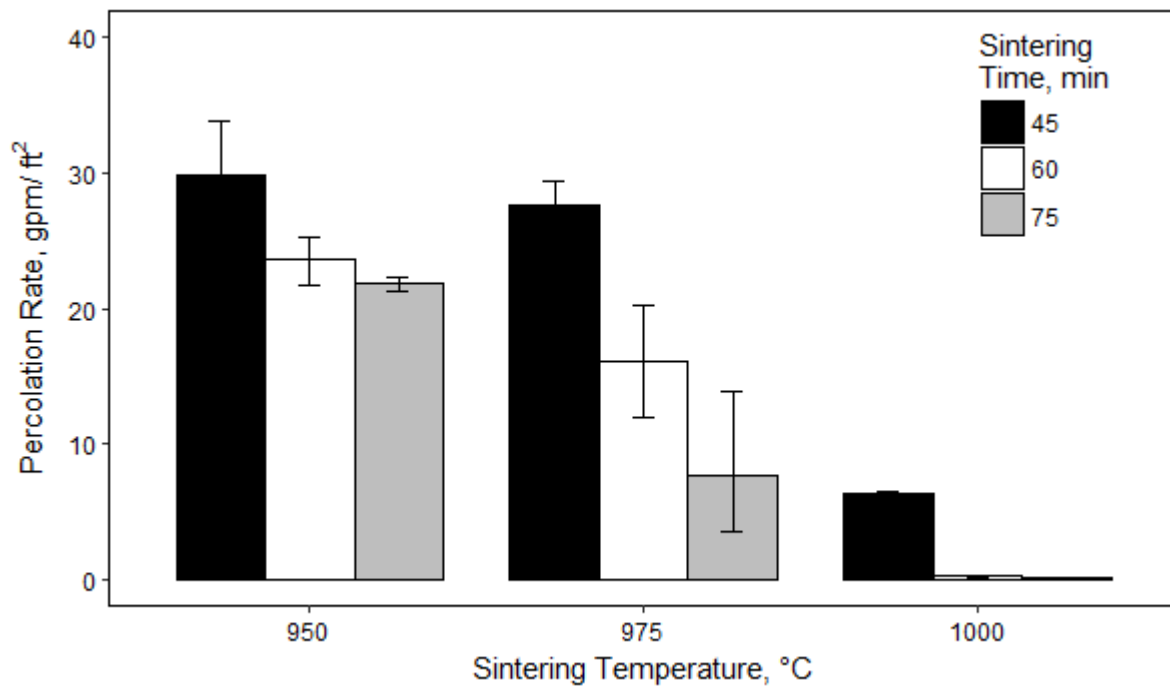


Figure 4-8. Percolation rate of SGS

A factorial experiment with two factors a three level was designed for this assessment with the purpose to evaluate the interaction effects of the sintering parameters on the percolation rate. For this study, statistical analysis of the data was conducted for the 9 combinations of the independent variables. Three replicates were performed for each of the combination, therefore a total of 27 samples were analyzed for percolation. In order to generate the

significance of the experimental variables an analysis of variance (ANOVA) has been performed. This allowed to determine the significant factors as well as their interactions with p -value ≤ 0.05 . According to the analysis, the sintering temperature and time have a statically significant effect on the percolation rate. However, it was observed that the interactions between the time and temperature did not present statistical significance since the p value was greater than 0.05. The response surface of the percolation rate is presented in Figure 4-9. A regression model was estimated for the percolation rate and it is presented in equation 4-2, in which Q is the percolation rate in gpm/ft^2 is, t is time in minutes, and T is the temperature in degrees Celsius.

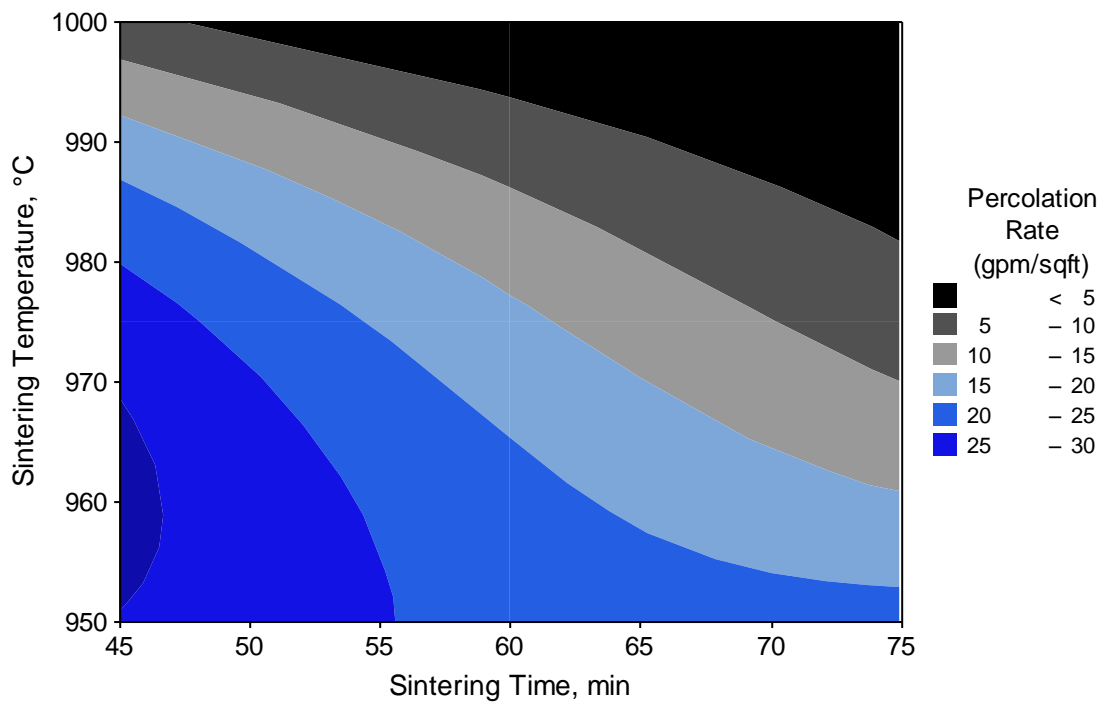


Figure 4-9. Response surface for the percolation rate of SGS

$$Q = 484.4 - 0.3787t - 0.4583T \quad (4-1)$$

In addition, the hydraulic conductivity of the SGS and its dependence on the sintering parameter was evaluated. The analysis involved Darcy's law since the flux of water through the SGS was measured using a system with a gravity-driven flow in a vertical column with a constant head. Hence, another approach to define the capacity of the SGS of passing a water flux through its porous network it is in terms of permeability, which is also known as hydraulic conductivity. Therefore, the hydraulic conductivity of the SGS was calculated according to the following equation:

$$k = \frac{QL}{A\Delta h} \quad (4-2)$$

In this case, Q is the flow rate, A is the SGS area, L is the SGS thickness, and Δh is the hydraulic head. In the percolation system (Figure 3-1), the hydraulic head was 1.5 ft, the average thickness of the SGS was 0.42 ± 0.023 in, and the average area was 2.81 ± 0.08 in². Figure 4-10 shows the results for the hydraulic conductivity of the SGS as function of the sintering temperature and time. An increase in the sintering parameters implied a reduction in the hydraulic conductivity, which defined the permeability of the porous matrix. Therefore, significant changes in the permeability of the tested specimens were observed as the sintering time and temperature increases. As explained before, this is due to the reduction in the pore size of the porous network. The highest average permeability was 3.01 ± 0.45 cm/min,

corresponding to a sintering temperature and time of 950°C and 45 minutes, respectively. The lowest permeability was approximately 0 at 1000°C for both 60 and 75 minutes.

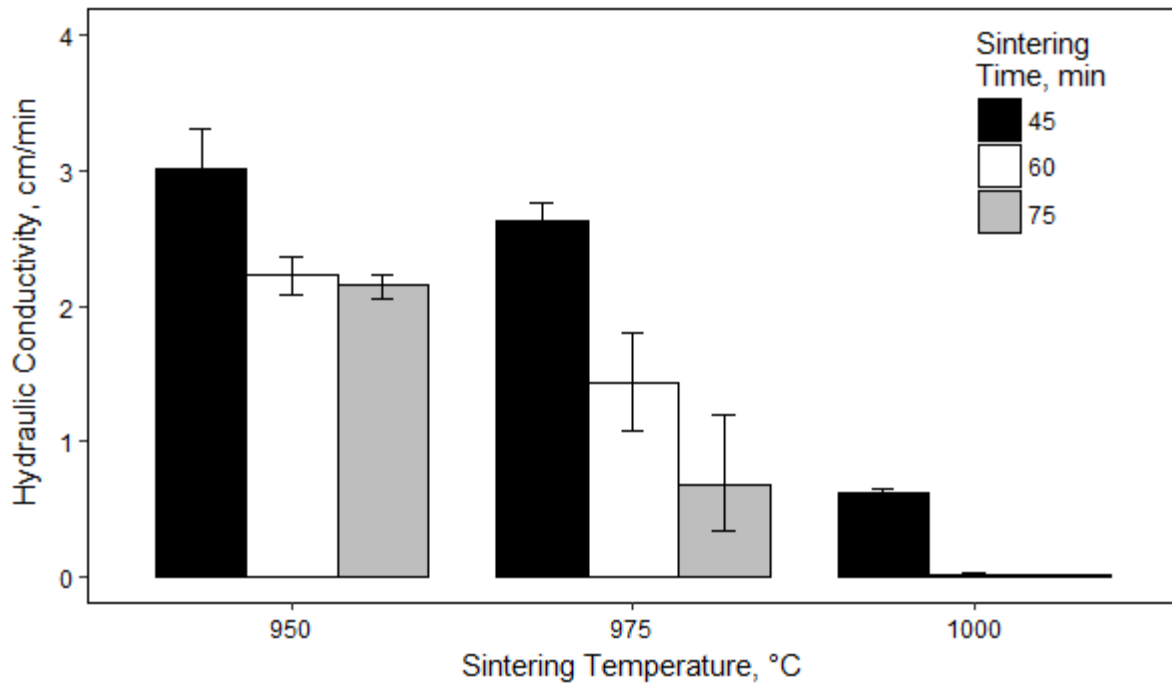


Figure 4-10. Hydraulic conductivity as a function of sintering parameters

4.2.2 Surface Porosity

To better control the percolation in SGS, it is necessary to understand how its porosity is affected during the sintering process. It is generally known that percolation in SGS is influenced by the sintering parameters but how they can combine to produce an SGS with an optimal porosity is the subject of research in this section. Therefore, the porosity assessment was performed to elucidate the relationship between the percolation and sintering parameters. SGS specimens were developed, for sintering time of 45, 60 and 75 minutes at

sintering temperature of 950 °C, 975 °C and 1000 °C. For the surface porosity evaluation, a total of 20 micrographs were obtained from each of the SGS produced. Micrographs in Figure 4-11 through Figure 4-13 present details of SGS porosity development that are in accordance to the theoretical principles. According to the sintering theory, the time and temperature selected to perform this process has a direct effect in the porosity of the sintered glass substrates. The results indicated changes in the porous network in response to the variations of sintering parameters, as shown on Figure 4-11 through Figure 4-13. A comparison of the micrographs demonstrates this behavior since a tendency to shrink pores becomes apparent.

The microstructural observation of the SGS further demonstrate the deformation of the grains shapes and rearrangement of the particle due to the continuous heating during the sintering process. In Figure 4-11 the large pores, label B, are surrounded by particles possessing irregular shapes, label A. It is important to note that the SGS were embedded in epoxy resin; hence, the pores were identified as the area of the SGS occupied by the resin. In Figure 4-12, a change in grain shape is observed in which the originally irregular shape has now become more flattened. The continuous change in particle shape suggest a grain growth where a flattening of the particle enclosed the pore area in the SGS. According to sintering theory, the densification and grain growth occur when there is a thermodynamic force, thus reducing the distance between neighboring grains. In Figure 4-13 it can be seen that the particle arrangement that occurs as the sintering parameters increase, progressively reduce the pores size until it reach a point in which the connection between adjacent glass particles is completely close as presented by the labeled position C. This label shows a crack in the

SGS surface, which is probably developed as a result of the continuous reduction of the pore size until the grains are compacted together. This last observation emphasizes that the thermal stress on the glass particles produced a grain growth that can eliminate any pores in the surface characterized by the formation of the neck between surrounding particles, i.e. grain boundary. Even though that the development of the porosity has a defined trend in terms of the sintering parameters it is difficult to defined a porous structure that includes pore size and distribution for the SGS due to the irregularities of the surface.

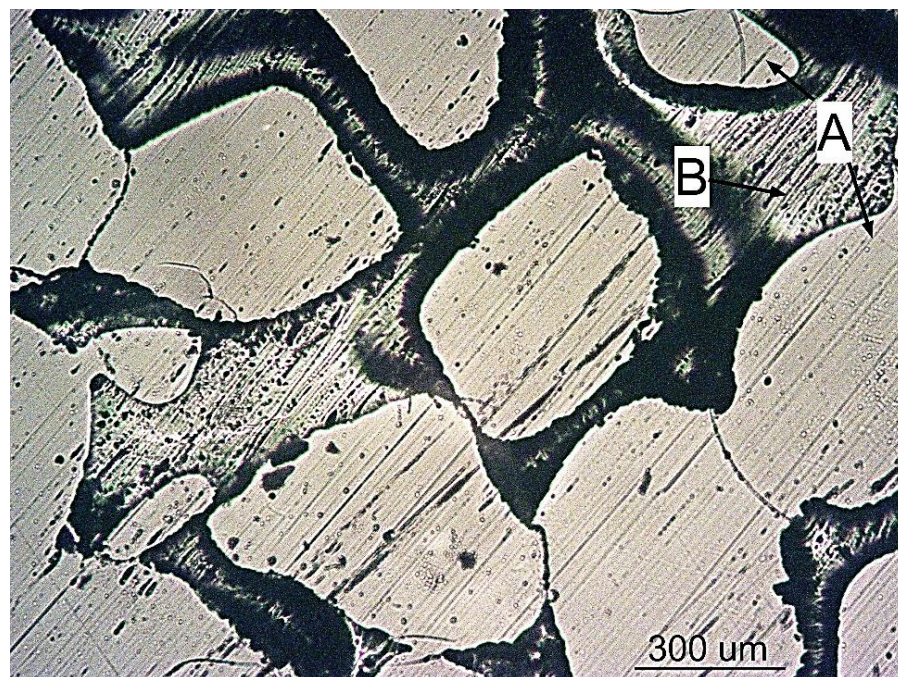


Figure 4-11. Surface micrograph for SGS sintered at 950°C for 45 minutes

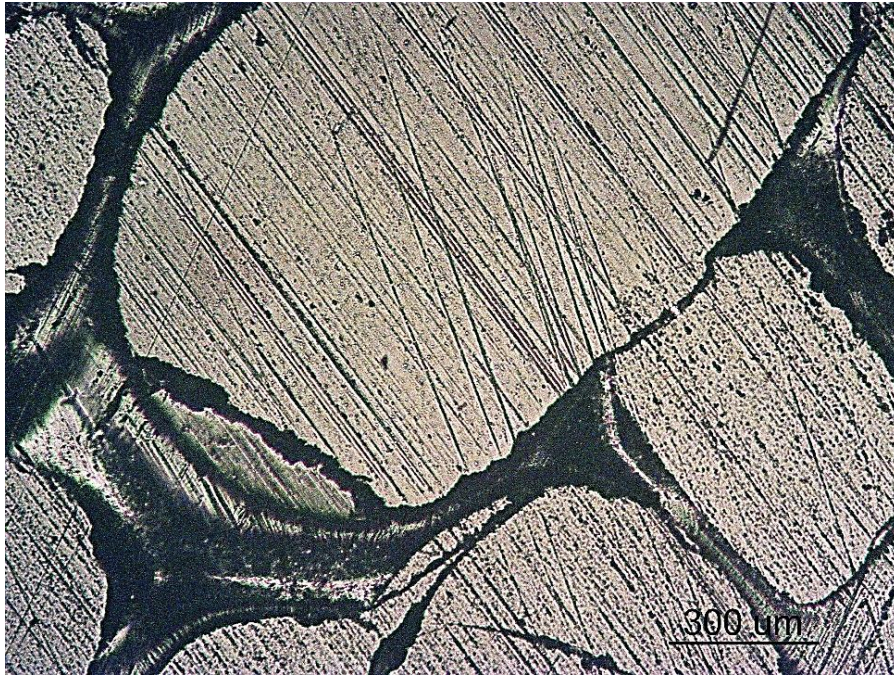


Figure 4-12. Surface micrograph for SGS sintered at 975°C for 45 minutes

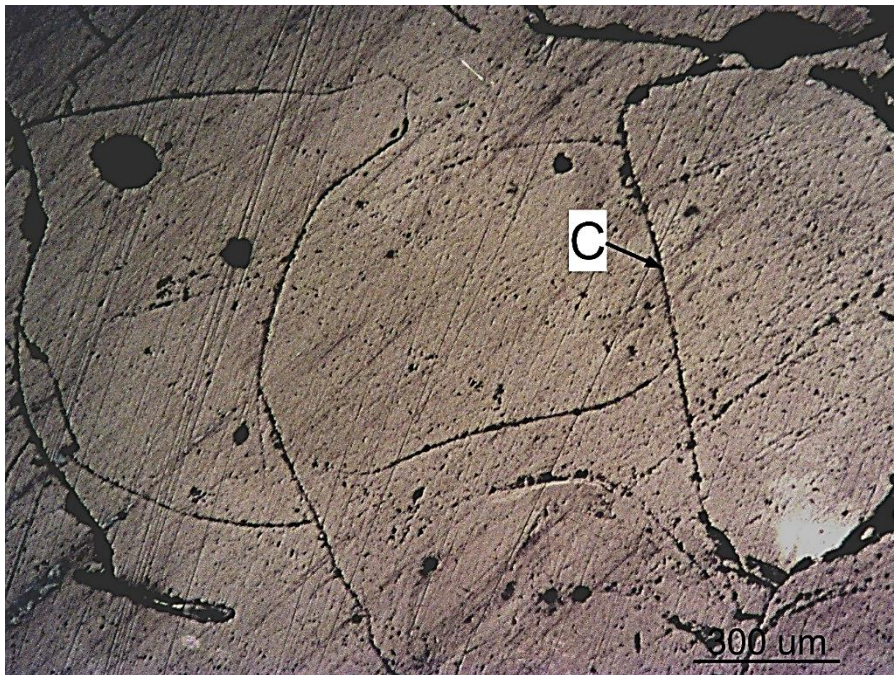


Figure 4-13. Surface micrograph for SGS sintered at 1000°C for 45 minutes

Figure 4-14 shows an example of a surface micrograph selected for the surface porosity assessment. The images processed for the surface porosity with manual selection and thresholding can discriminate very accurately between the pores and glass particles. The white regions in the images represent the pores and the black regions are the sintered glass particles.



Figure 4-14. Surface micrograph classified using ImageJ

Figure 4-15 shows the results, which represent the average surface porosity of 180 images analyzed. In general, the results seem to indicate that a reduction of the surface porosity occurs as the sintering parameter increases. A maximum porosity was obtained for the sintered glass substrates produced at sintering parameters of 45 minutes and 950°C. The means between the porosity of the samples are different; however, there is an overlap

between data. This may be attributed to the variability of the particle size distribution that comprises the RGP, which can affect the formation of the pores during the sintering process. The response surface of the surface porosity as a function of sintering parameters is presented in Figure 4-16. Notice that the reduction of the area occupied by the pores in the micrographs also results as the sintering time increase under a fixed temperature.

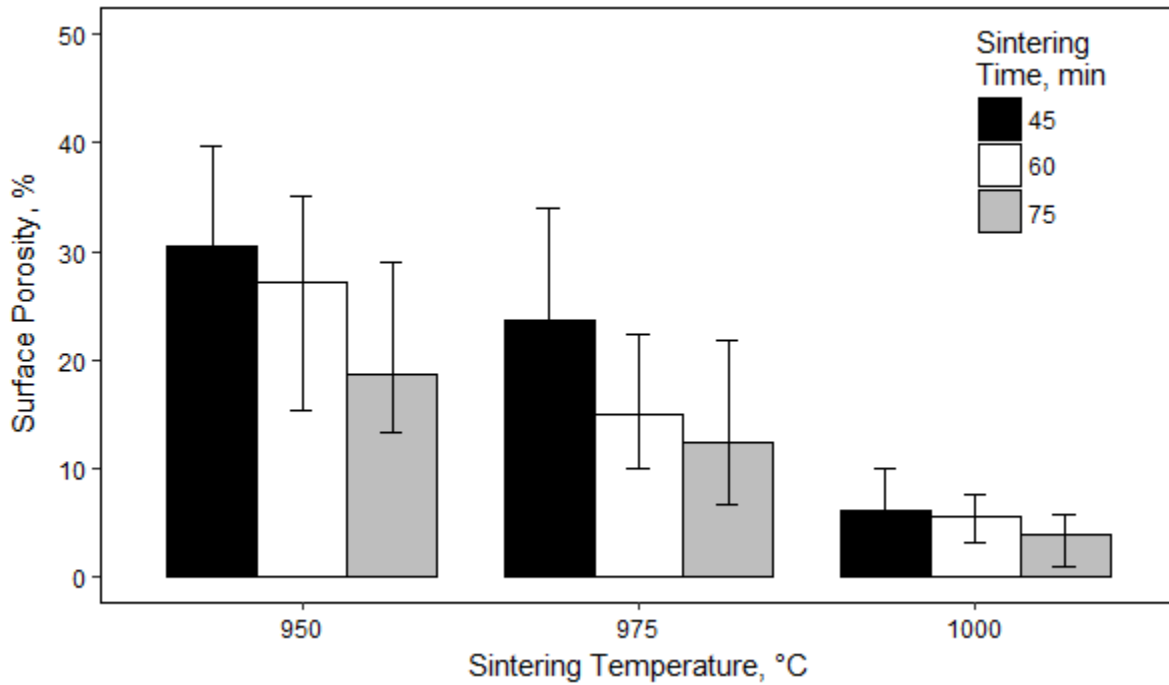


Figure 4-15. Characterization of the surface porosity of SGS samples

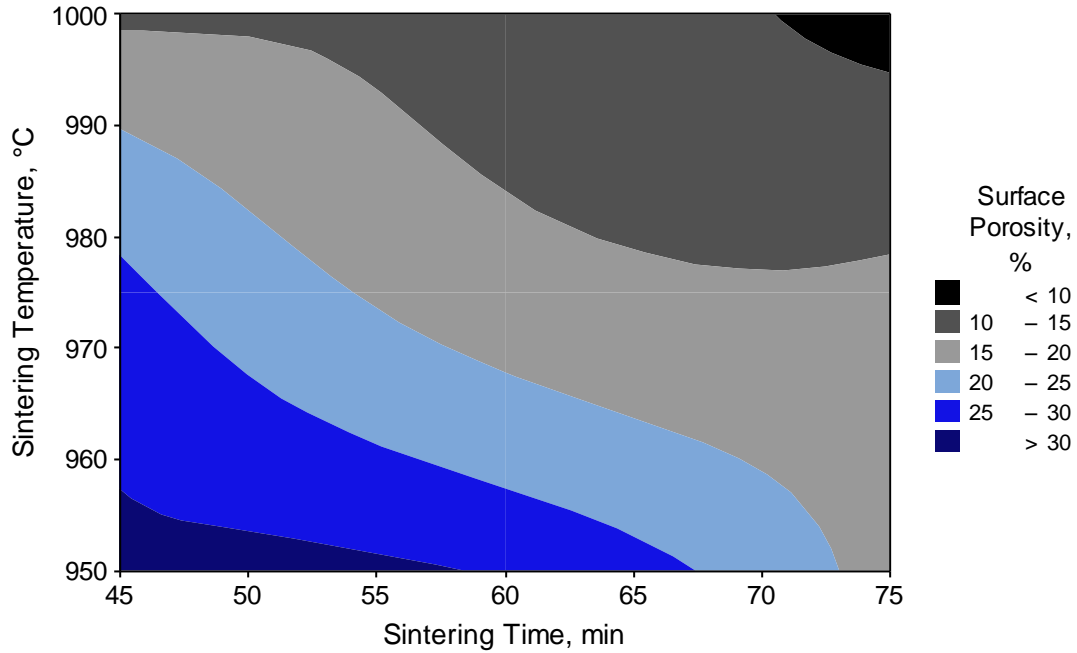


Figure 4-16. Response surface for surface porosity of SGS

4.2.3 General Porosity

The general porosity of the SGS was estimated using the procedure mentioned in Section 3.4.4. According to the literature, this method only consider the open pore networks in the SGS. Hence, its adaption for use in the assessment of total porosity would be incorrect since there is a probability that the SGS also comprises closed porosity. The open porosity results for the SGS are shown in Figure 4-17.

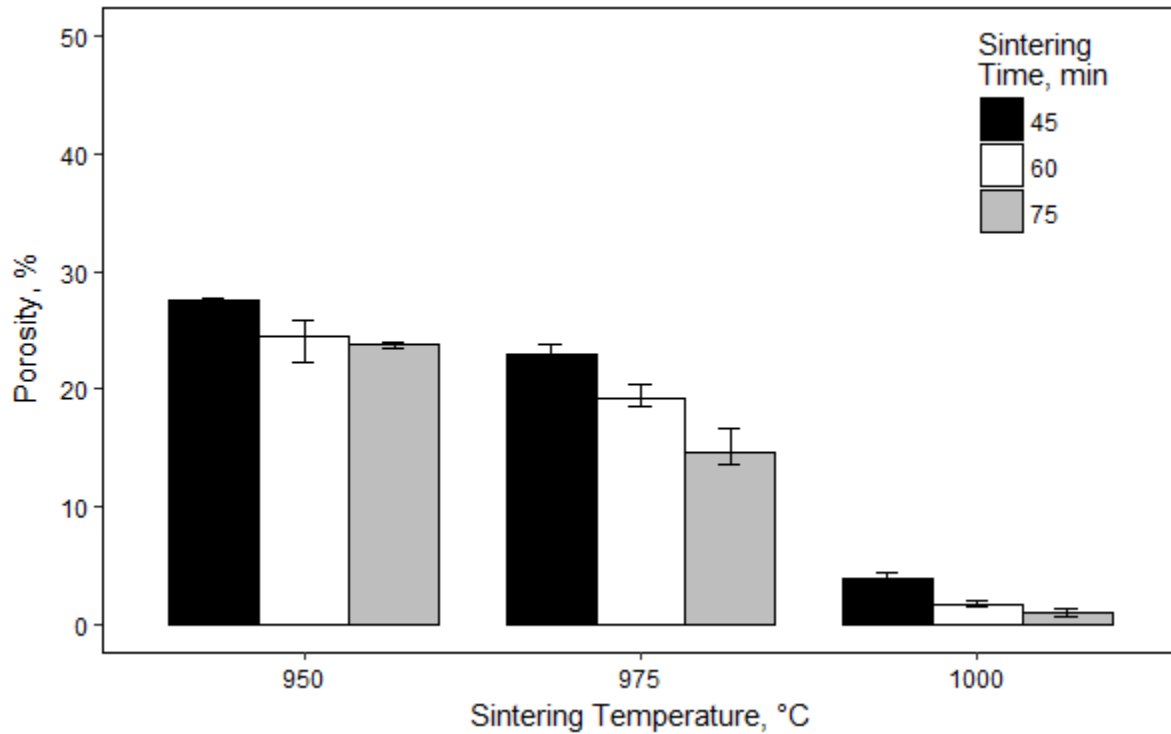


Figure 4-17. Characterization of the total porosity of SGS samples

In order to further understand the effect of the mass of TiO_2 immobilized in the open porosity, control specimens were elaborated to identify the modifications to the SGS open porosity generated by the TiO_2 films. To achieve this, control specimen, which are the uncoated SGS, were prepared by sintering at 975°C for 45 and 75 minutes followed by calcination at 800°C and 900°C for 3 hours. The influence of the calcination temperature in the porosity of the SGS was evaluated and the results are shown in Figure 4-18. A quantitative comparison between Figure 4-14 and 4-15 demonstrated that the SGS porosity gradually reduced with an increased in calcination temperature. The reason for the reduction of open porosity may be due to further connection of adjacent grain within the SGS produce by the atomic diffusion in

the solid-state sintering process. The open porosity for the SGS at 45 and 75 minutes before calcination were 22.91 ± 0.89 , and 14.69 ± 1.66 , respectively. After the calcination process, the open porosity reduced 16.28% and 20.18% for the SGS calcined at 900°C for 45 and 75 minutes, respectively. The reduction in open porosity for the SGS calcined at 800°C at 45 and 75 minutes were 8.90%, and 11.88%, respectively.

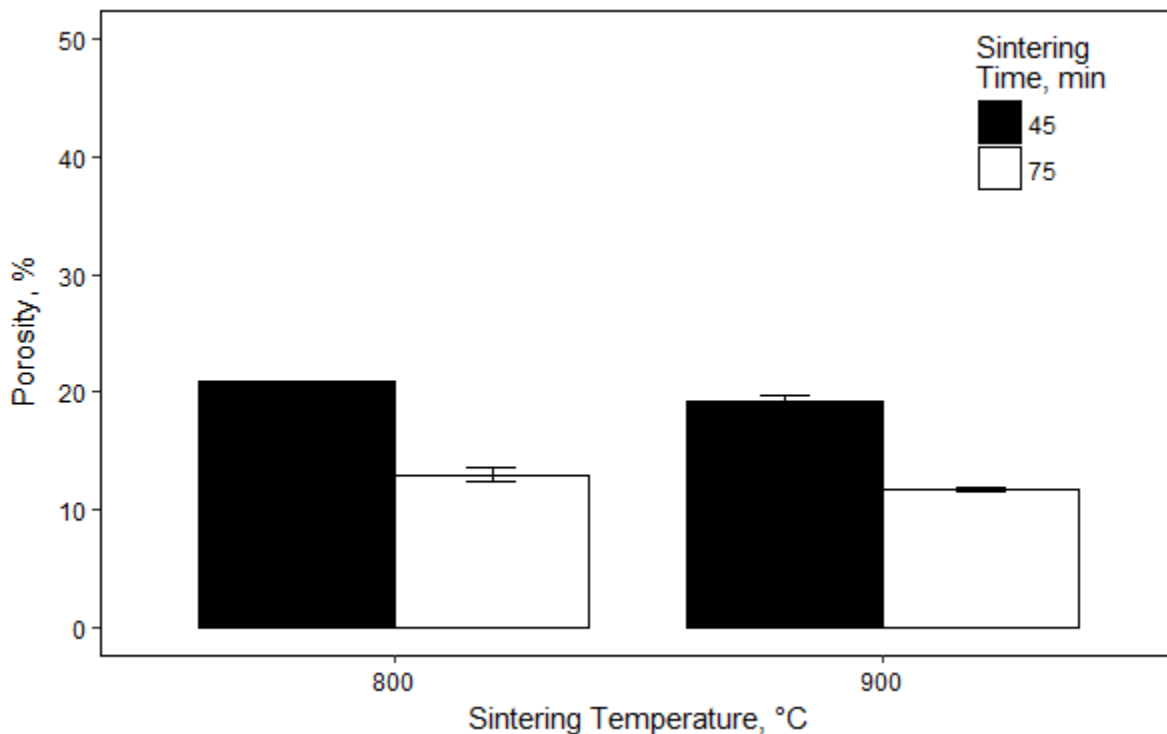


Figure 4-18. Porosity of the SGS as a function of calcination temperature

The effect of the TiO_2 -film in the open porosity of the SGS is presented in Table 4-3 and 4-4. The addition of TiO_2 to the SGS implied a reduction in the porosity. The reduction in porosity for both pH used for the immobilization were very similar, although the GTC prepared at pH 1.7 obtained slightly lower reduction percentages. The porosity reduction were ranging

between 20.10-25.76% and 21.78-30.78% for the GTC prepared at pH 1.7 and approximately 5, respectively. Despite the fact that the GTC prepared at pH 1.7 comprises a higher amount of TiO₂ immobilized, it is believed that the particles possess smaller size than those prepared at pH 5. Therefore, at pH 5 the porosity is generally more negatively affected considering that the TiO₂ agglomerates tends to saturate the pore area. It is noteworthy that the greatest effect on the porosity was produced by the addition of TiO₂ to the SGS. Thus, the above results indicate that the porosity of the SGS not only depends on the sintering temperature and time but on the on the calcination temperature, and the TiO₂ immobilized.

Table 4-3. Porosity of the GTC prepared at pH 1.7

Sintering Time, min	ϵ Average, %	
	Calcination Temperature, °C	
	800	900
45	16.19 ± 0.52	15.93 ± 1.04
75	9.61 ± 1.15	9.37 ± 0.03

Table 4-4. Porosity of the GTC prepared at pH 5

Sintering Time, min	ϵ Average, %	
	Calcination Temperature, °C	
	800	900
45	15.36 ± 2.33	13.34 ± 1.50
75	8.96 ± 0.31	9.17 ± 1.06

4.2.4 Polymorph Structure of TiO₂ Particles

An XRD analysis was conducted to assess the crystal structure of the TiO₂ powder and investigate if a phase transformation occurs due to calcination and sintering temperature. Figure 4-19 shows the XRD pattern of pure TiO₂ powder before thermal exposition, which confirms pure anatase crystal form. A qualitative phase analysis was performed using the D5000 XRD unit database in order to define the crystal structure and the peaks. The main diffraction peaks emerging at 2θ equal to 25.3°, 36.9°, 37.8°, 38.6°, 48.0°, 53.9°, 55.0°, 62.1°, 62.7°, 68.8°, and 70.3° can be identified as crystalline anatase peaks. The crystal lattice planes corresponding to the detected peaks are presented in Figure 4-19.

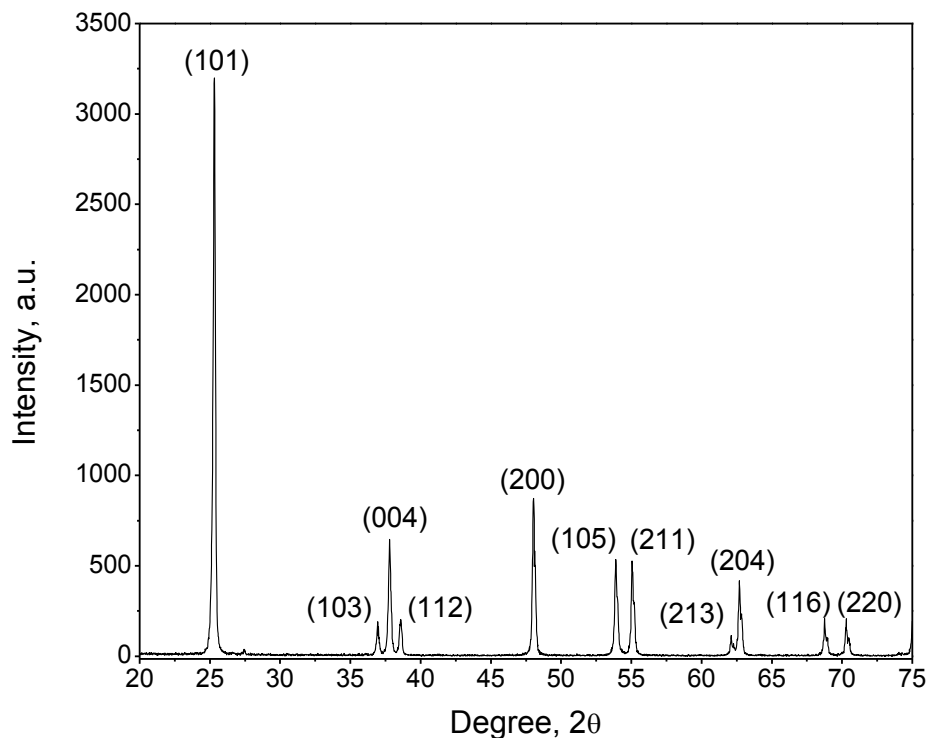


Figure 4-19. X-ray diffractogram of pure TiO₂ powder

Figure 4-20 shows the diffractogram of the TiO₂ calcinated at different temperatures for 3 hours. The results confirm that the crystal structure of the TiO₂ is not affected by the temperatures of thermal treatment used for the immobilization process. It can be seen that the emerging peaks for each sample are similar to those found in Figure 4-19 indicating the anatase structure. As it is seen from Figure 4-20 (f), the anatase to rutile transformation occurred at 1000°C. The primary diffraction peaks of rutile at 2θ equal to 27.8°, 36.4°, 41.5°, 54.6°, 56.9°, and 69.0° are indexed as (110), (101), (111), (211), (220), and (301), respectively.

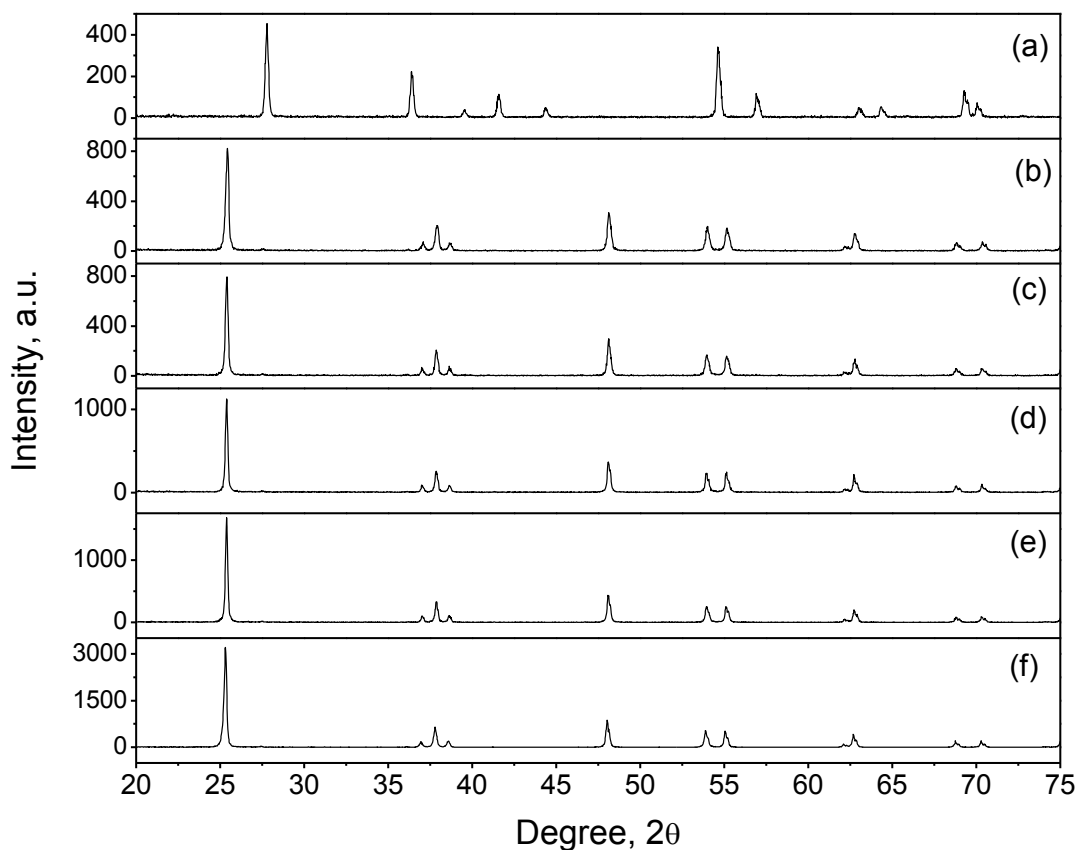


Figure 4-20. XRD diffractogram of TiO₂ particles calcinated at: (a) 1000°C, (b) 975°C, (c) 950°C, (d) 900°C, (e) 800°C, and (f) 105°C

A quantitative analysis using the Savitzky-Golay approach allowed the determination of relative crystallinity of the samples by separating the crystalline portion from the amorphous part. It was found that the relative crystallinity of the pure TiO₂ powder is approximately 97%. The relative crystallinity and crystallite size are plotted against calcination temperature in Figure 4-21. The correlation is very interesting and demonstrate that the crystallinity decreases as an effect of increasing the calcination temperature. Further increase in the calcination temperature led to an increase in the amount of amorphous phase, thus reducing the crystallinity. This effect also influenced the crystallite size of the TiO₂. A possible reason for changes in the crystallinity might be due to further phase transformation that can reduce the crystallinity of anatase to increase the crystallinity of the rutile phase.

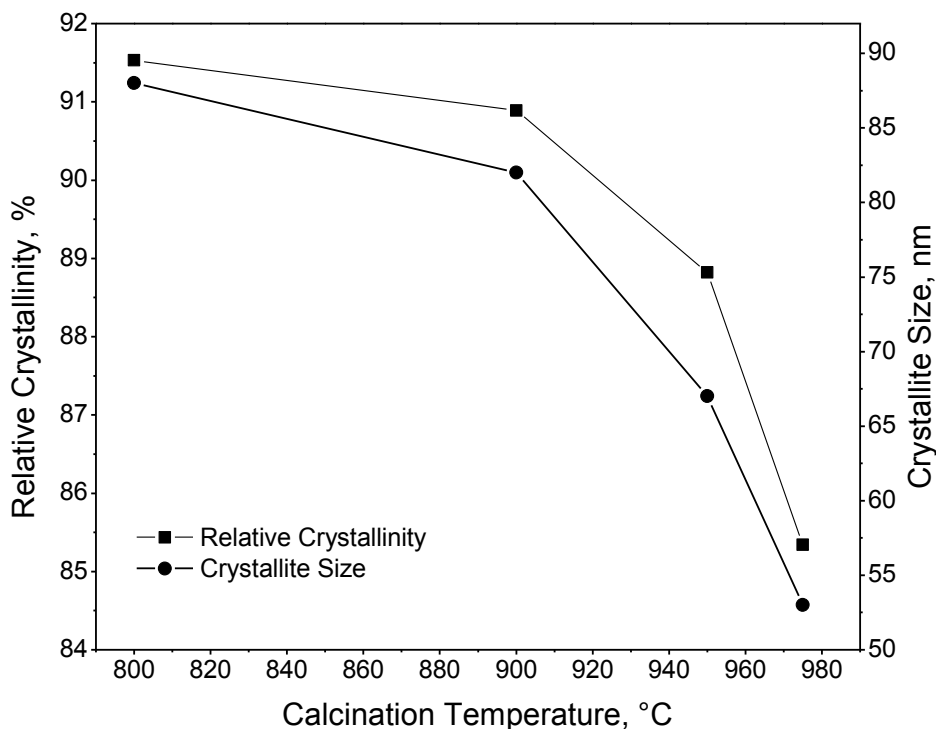


Figure 4-21. Effect of calcination temperature in TiO₂ crystallinity

Figure 4-22 presents the XRD patterns for samples of TiO₂-glass beads mixture containing 1, 3, and 10 wt.% TiO₂ content. The results confirm that an increase in the initial mass produces an increase in the TiO₂ particles deposited on the glass beads. This is observed by the reduction in the amorphous peaks as the TiO₂ wt.% increases. This means that the amount of TiO₂ deposited on the glass beads were large enough to interfere with the amorphous peaks that resulted from the glass beads. Thus, the optimization of the amount of TiO₂ particles deposited and embedded on the glass beads increases the relative crystallinity of the samples.

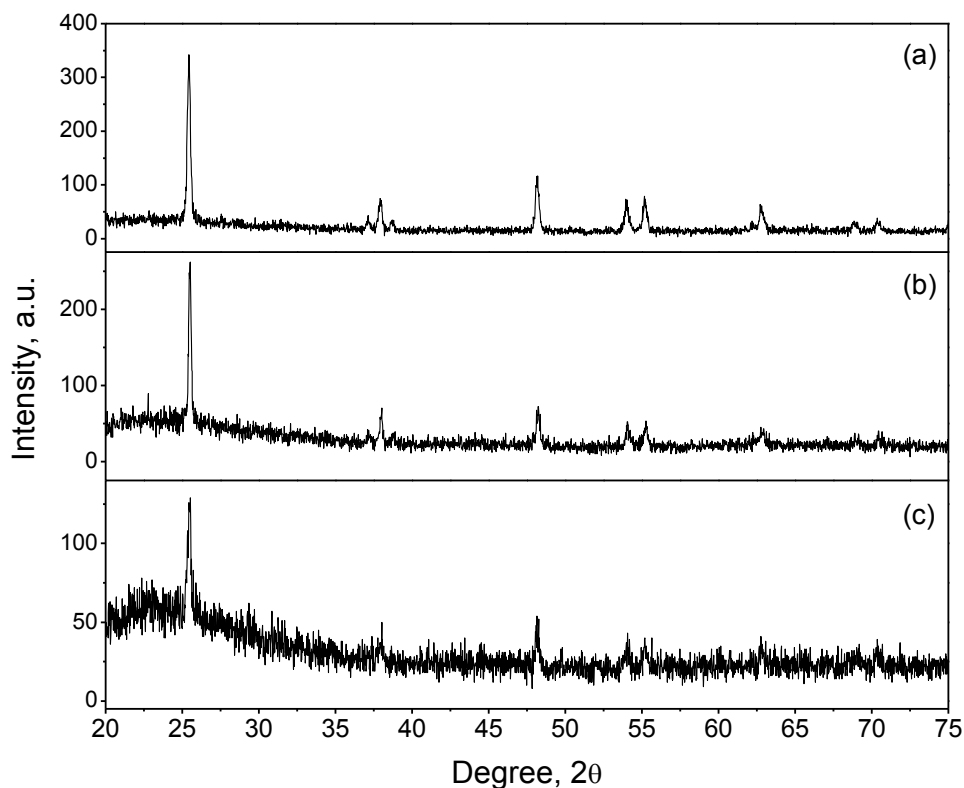


Figure 4-22. Effect of TiO₂ mass deposited onto glass beads in the relative crystallinity: a) 10wt.%, b) 3wt.%, and c) 1wt.%

Figure 4-23 and 4-24 shows the XRD pattern for the GTC that were prepared by the method discussed in Section 4.1.1. The XRD patterns exhibits a semi-crystalline structure with intense peak at 2θ equal to approximately 25.3° , which corresponds to the anatase plane (101). Furthermore, anatase peaks with less intensity are observed at 2θ equal to 37.8° and 48.0° corresponding to the (004) and (200) facets, respectively. This confirms that no further phase transformation occurred due to thermal treatment. Notice that the amorphous peaks in the patterns correspond to the glass beads in the GTC.

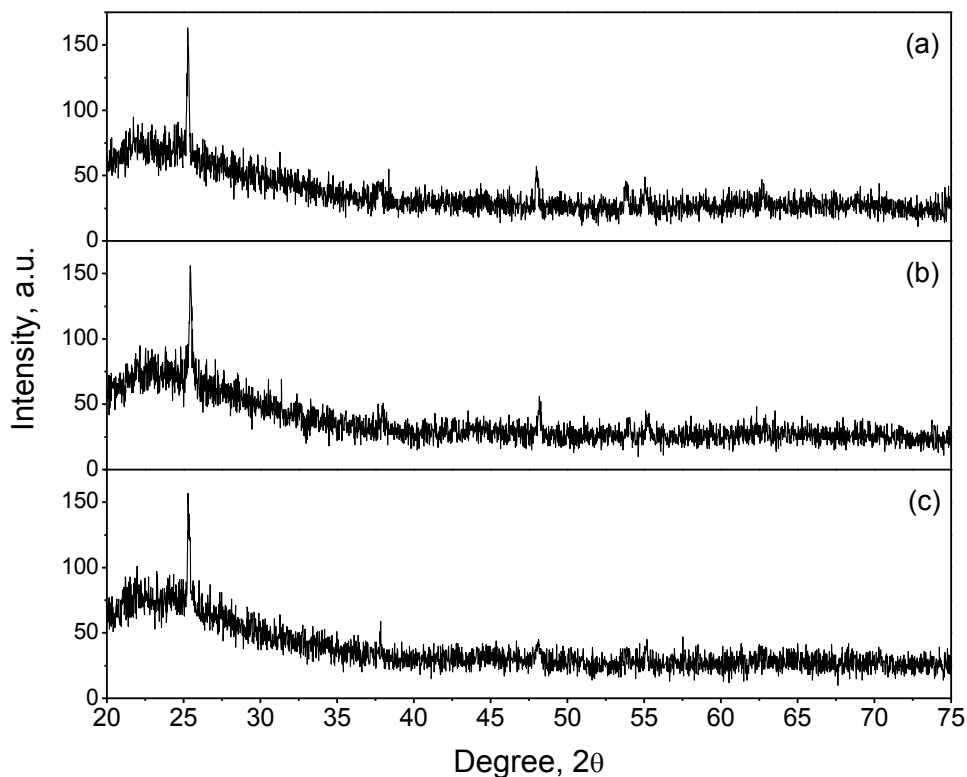


Figure 4-23. XRD diffractogram for TiO_2 -glass beads sintered at 950°C for: (a) 90 min, (b) 75 min, and (c) 60min

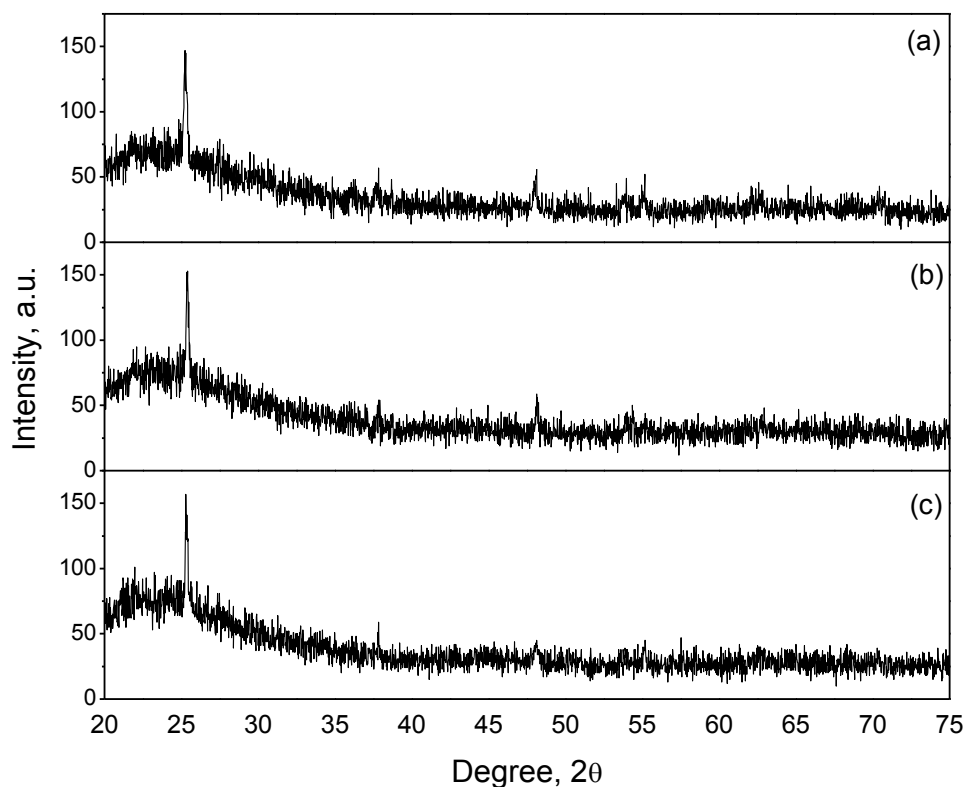


Figure 4-24. XRD diffractogram for TiO₂-glass beads sintered at 975°C for: (a) 90 min, (b) 75 min, and (c) 60min

The XRD diffraction measurements were performed also to evaluate the crystal structure of the TiO₂ films in the GTC prepared by the methods explained in Section 4.1.2 and 4.1.3. Figure 4-25 presents the diffraction patterns of this GTC and it can be seen that the obtained XRD peaks corresponds to the anatase phase. The XRD spectra indicated that the SGS is completely covered with TiO₂ since the amorphous peaks corresponding to the glass are not observed. A comparison of the XRD spectra from the different immobilization techniques clearly indicated that the GTC with TiO₂ particles embedded within the SGS retain the lower amount of TiO₂ in its surface.

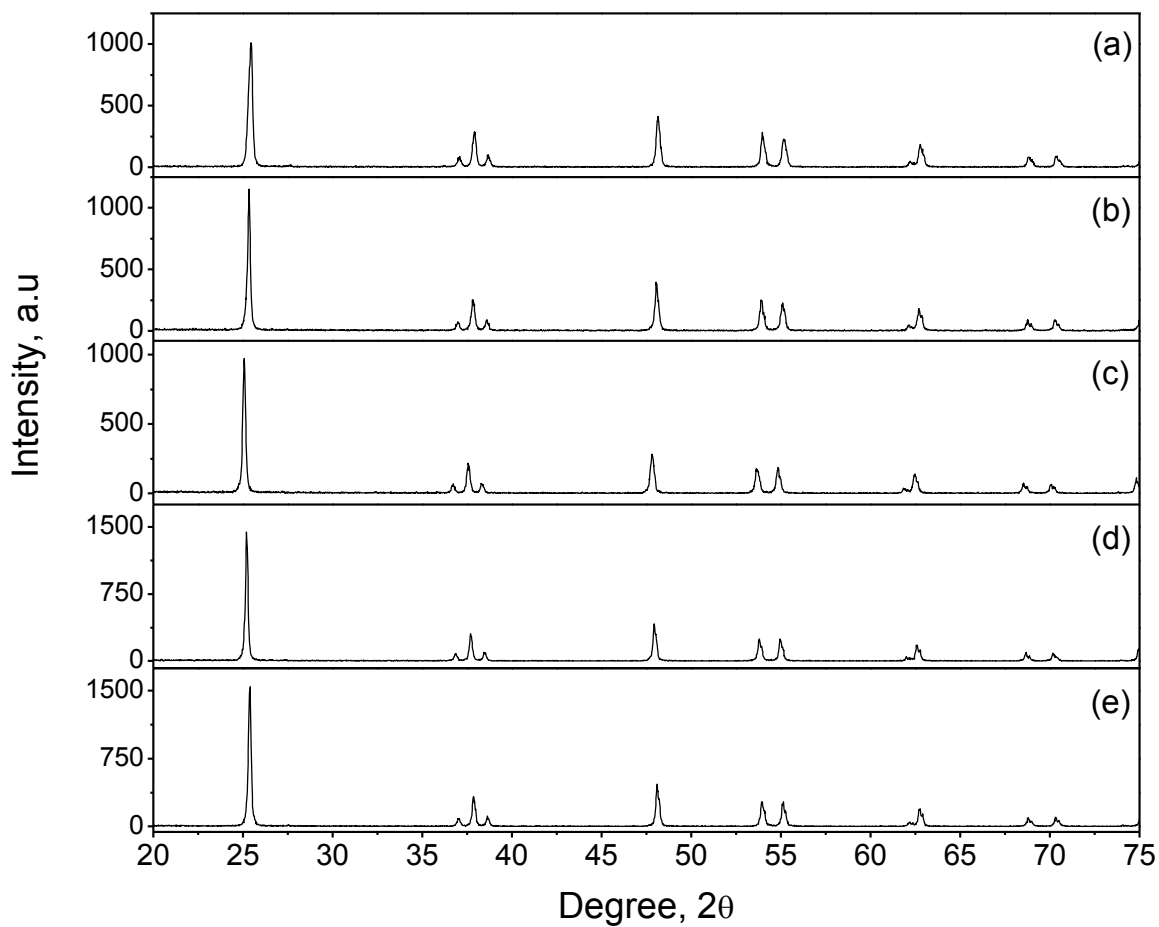


Figure 4-25. XRD diffractograms for GTC prepared by different TiO_2 immobilization methods: (a) immobilized on the SGS surface with pH 5 at 900°C , (b) immobilized on the SGS surface with pH 5 at 800°C , (c) immobilized on the SGS surface with pH 1.7 at 900°C , (d) immobilized on the SGS surface with pH 1.7 at 800°C , and (e) pasting the SGS at 800°C

4.2.5 Morphology

SEM micrographs were obtained to evaluate the changes in the surface of the SGS produced by the immobilization of the TiO_2 as well as surface of the TiO_2 films. Figure 4-26 shows a micrograph of the SGS sample (non- TiO_2 coated) where it can be observed that its surface is relatively smooth. The SGS presented in this micrograph was sintered at 975°C for 45 minutes. The SEM image also confirms the presence of what it is described as a neck represented as fissures or cracks in the SGS surface. Notice that this may be caused by the joint of neighboring sintered glass particles as discussed in Section 4.2.2. The resulting micrographs of the GTC prepared by the different evaluated methods for the immobilization of TiO_2 evaluated are shown in Figure 4-27. It is noticeable that there are significant changes detected in the morphology of the coating surface, which are attributed to the difference in conditions and parameters of preparation used in each immobilization method. For instance, the GTC involving HNO_3 -treated particles depicted in Figure 4-27 (b), presents the most homogenous coating over the surface of the SGS. By comparing micrographs 4-27 (b) and (c), one can observe the effect of the pH on the morphology of the coating; the GTC prepared at pH 1.7 shows a better distribution of the TiO_2 particles than the GTC prepared at pH 5.

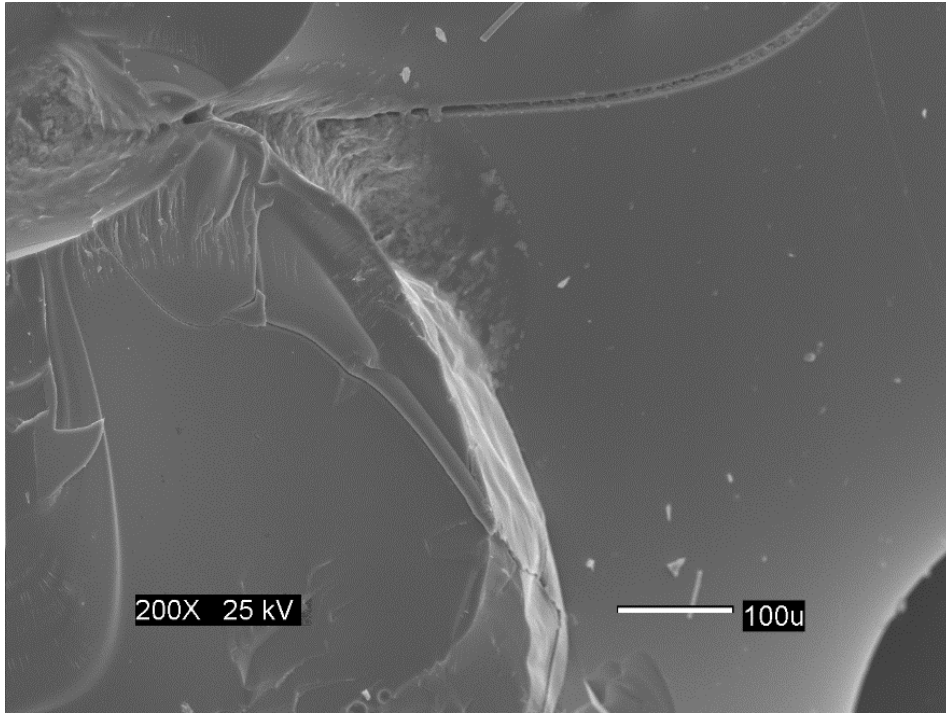


Figure 4-26. SEM micrographs of uncoated SGS

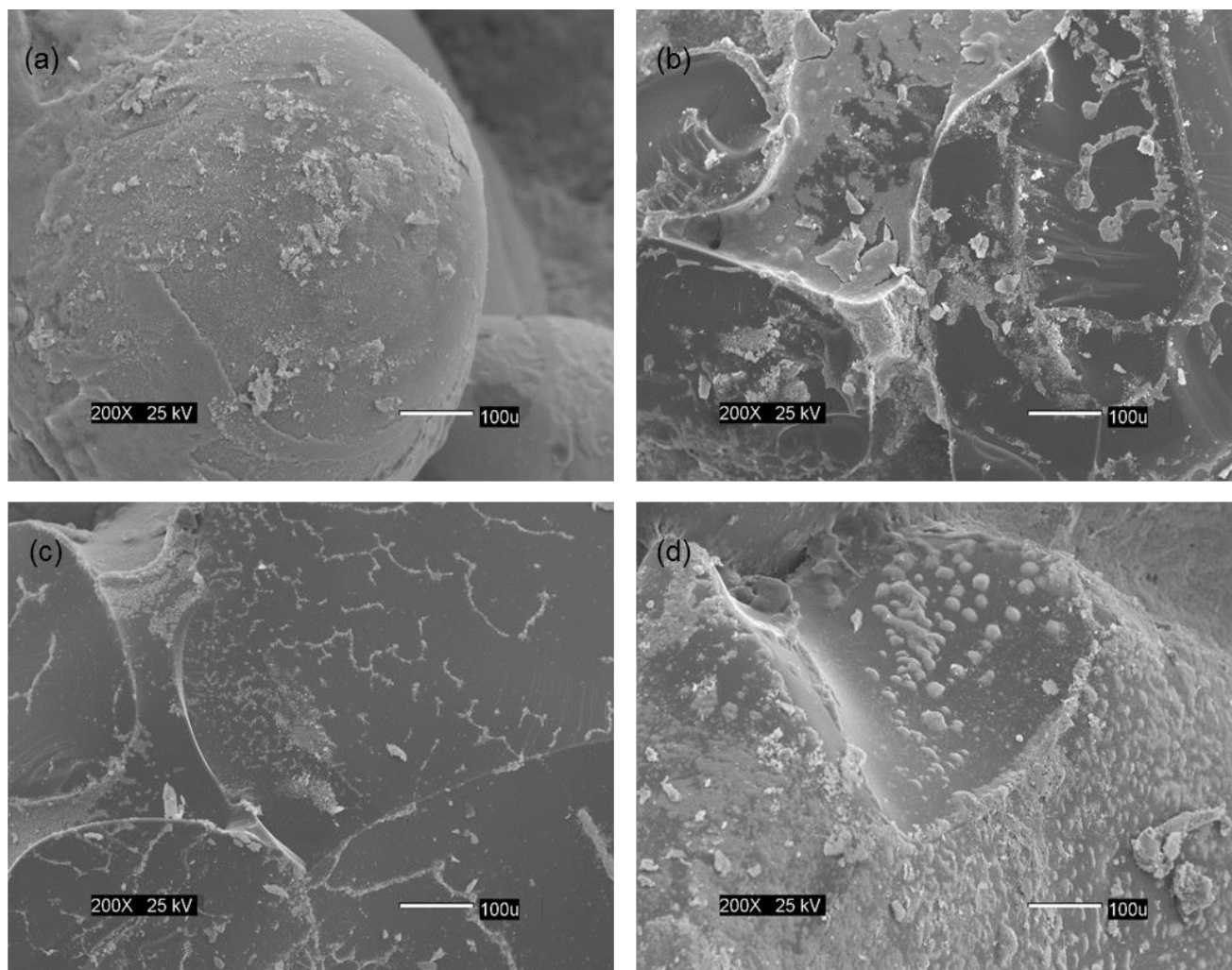


Figure 4-27. SEM micrographs of GTC prepared by method: (a) pasting the SGS, (b) immobilized on the SGS surface with pH 1.7, (c) immobilized on the SGS surface with pH 5, (d) TiO₂-glass beads sintered at 975°C with 1g of TiO₂

4.3 DEGRADATION OF HUMIC ACID

This section discusses the degradation of HA using TiO₂ particles both in suspension and immobilized onto the SGS. The experimental conditions used for the evaluation of TiO₂ particles in suspension were the same to the ones implemented in the evaluation of the GTC. It should be emphasized that the suspension system was employed in this study as a control to gain a better understanding of the photocatalytic process and the efficiency of the photocatalytic reactor. A direct comparison between these two approaches may be difficult because of the variability of operational parameters such as TiO₂ dosage, surface and contact area.

4.3.1 Photolysis

The study of the effect of the UV light irradiation on the concentration of HA may constitute one of the primary tasks in order to address any decomposition in the initial concentration. The process in which the HA molecule may decompose due to the influence of UV light illumination is referred as photolysis. Thus, the photolysis of the HA was investigated by monitoring HA concentrations of diluted solutions with respect of time in the presence of UV light. The UV-Vis absorbance in the wavelength of 254nm (UV₂₅₄) and TOC was used as a quantitative indicator of HA concentration. Figure 4-28 shows the HA concentration, in terms of absorbance, as a function of irradiation time. It is noticeable that the UV light transmitted to the solution is not capable of decompose or destroy the HA molecules. The variability in the values of absorbance may be due to the homogeneousness of the solution. Moreover, it

was found that the HA absorption capacity exhibits a direct relationship to its initial concentration. In general, an increase in HA concentration results in an increment of the amount of UV light absorbed. The correlation between the HA concentration and UV absorbance at 254nm is presented as a linear regression model in Equation 4-3. The relationship between the HA and the absorbance shows a high linear correlation with a $R^2 = 0.9989$.

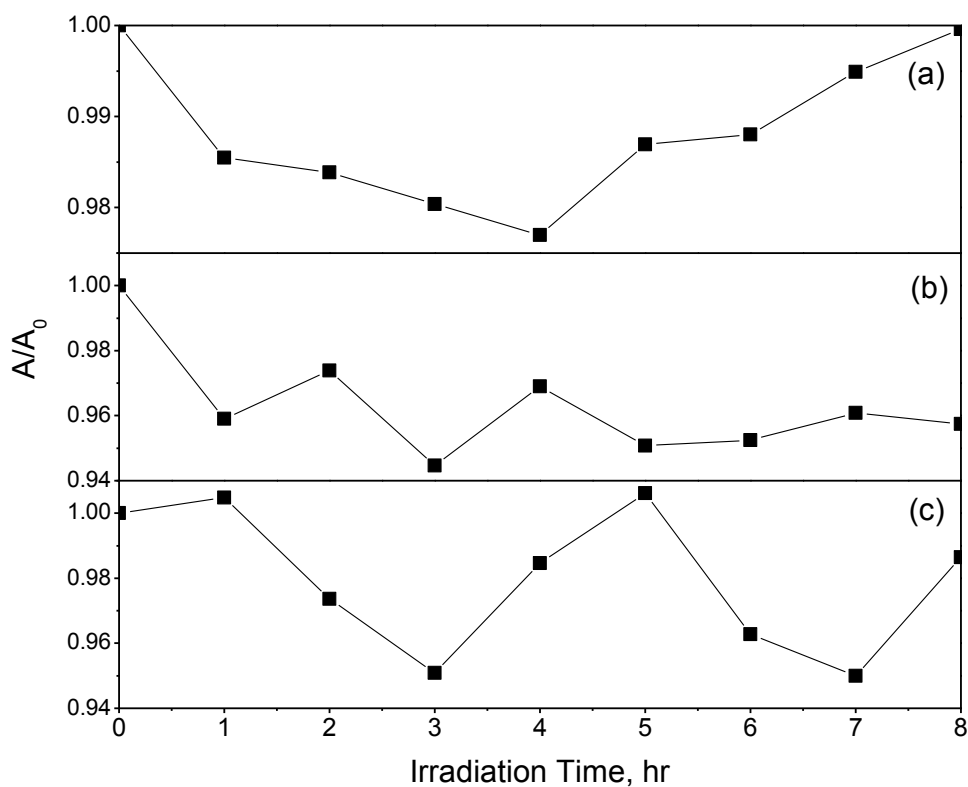


Figure 4-28. Evaluation of photolysis, in terms UV absorbance, of HA at: (a) 20 mg/L, (b) 15 mg/L, and (c) 10 mg/L

$$HA_{conc} = 31.063A_{254} - 2.9277 \quad (4-3)$$

Similarly, the influence of the UV light emitted in the concentration of the HA in terms of TOC was evaluated. Figure 4-29 shows the TOC concentrations as function of irradiation time. As explained, the discrepancy of the concentration with time can be attributed to the lack of uniformity in composition. No apparent degradation is observed with UV light. The data acquired in the range of HA concentration selected, i.e. 10-20 mg/L, was used to obtain the correlation between the TOC and HA concentration. The regression equation is presented in Equation 4-4 and possess a regression coefficient (R^2) of 0.9908.

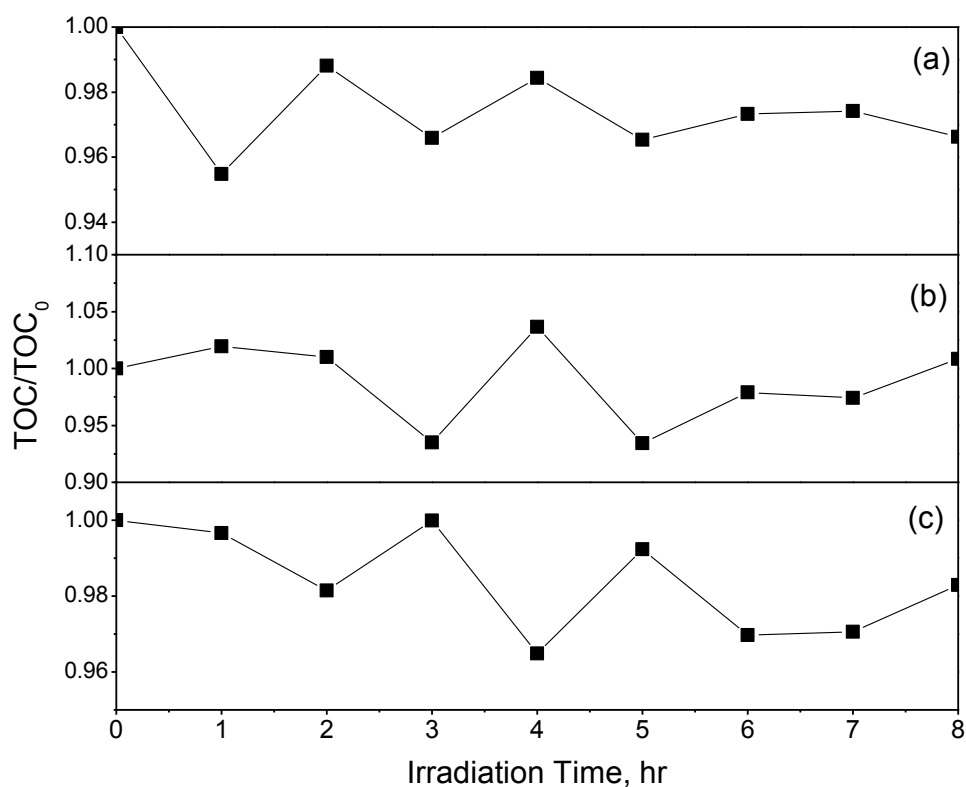


Figure 4-29. Evaluation of photolysis, in terms TOC, of HA at: (a) 10 mg/L, (b) 15 mg/L, and (c) 20 mg/L

$$HA_{conc} = 2.1338TOC - 0.7465 \quad (4-4)$$

4.3.2 Photodegradation of HA by TiO₂ Suspension

As mentioned earlier, the effectiveness of the TiO₂ photocatalytic oxidation and further mineralization of HAs was investigated using TiO₂ particles in suspension.

4.3.2.1 Influence of Initial HA concentration and pH

Photocatalytic degradation experiments were conducted at different concentration of HA under two different pH conditions in order to evaluate the effect of the initial pollutant concentration and the pH. The reduction in HA concentration in terms of UV absorbance is presented in Figure 4-30 and 4-31 for pH values of 3 and 6, respectively. In general, an increase in UV irradiation time results in a decrease of the absorbance levels. The photodegradation rate of HA increases with decreasing its initial concentration. For instance, in the first hour of reaction time, more than 57% UV₂₅₄ removal was obtained for the HA solution of 10 mg/L, while the initial HA concentration reduced only a 41% and 31% for the solution of 15 and 20 mg/L, respectively. Moreover, it was found that the removal efficiencies of HA at pH 6, in terms of UV₂₅₄, were 99%, 98% and 94% for 10, 15, and 20 mg/L, respectively. Significant pH dependent changes were observed in the photocatalytic degradation of the HA. Figure 4-31 and 4-32 demonstrates that at pH 3 the photomineralization of HA was significantly enhanced.

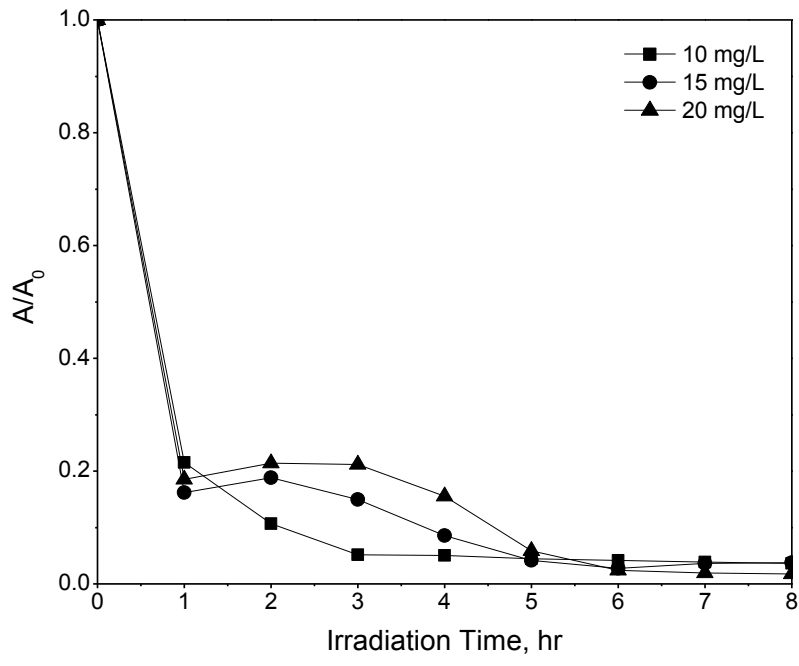


Figure 4-30. HA residuals levels in terms of absorbance as quantified by UV-vis spectrometry for three different initial HA concentrations in TiO₂ in suspension exposed to UV light at pH 3

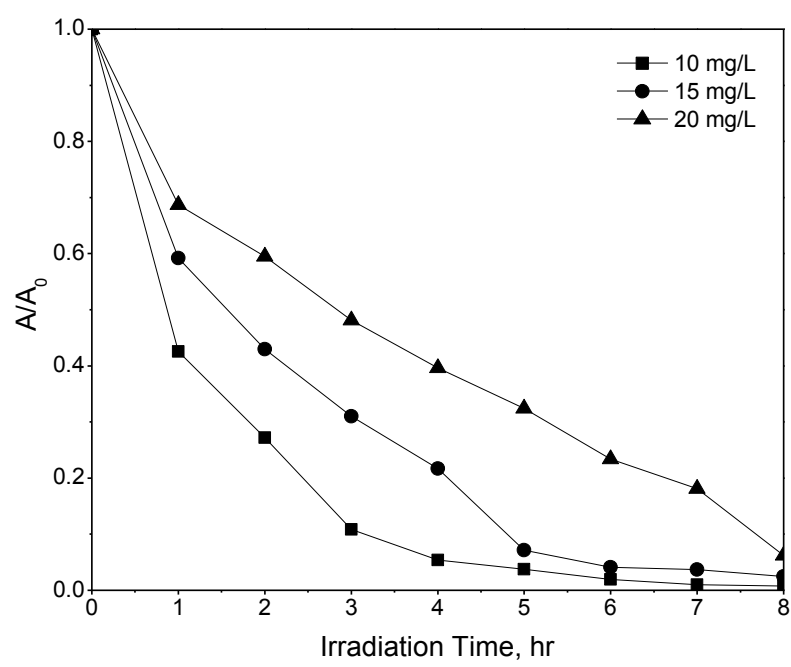


Figure 4-31. HA residuals levels in terms of absorbance as quantified by UV-vis spectrometry for three different initial HA concentrations in TiO₂ in suspension exposed to UV light at pH 6

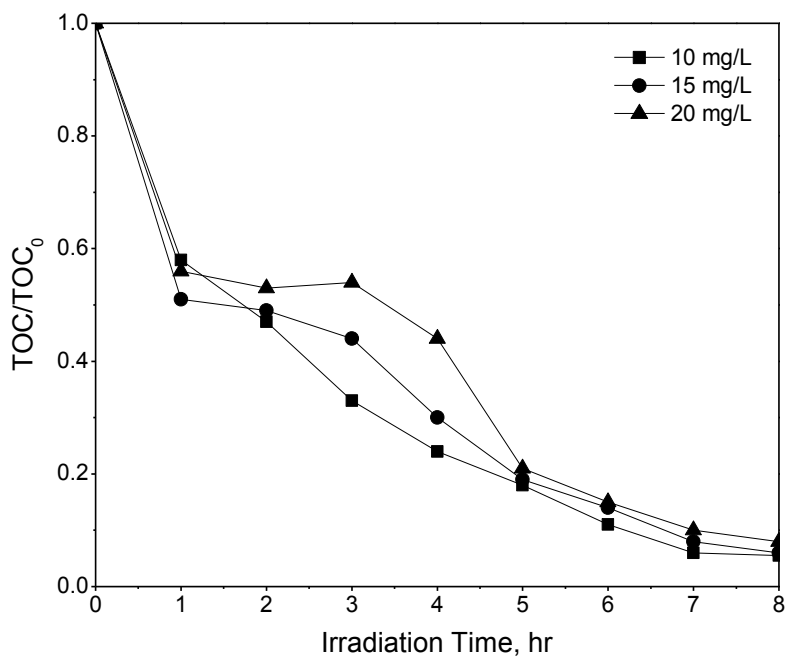


Figure 4-32. HA residuals levels in terms of TOC for three different initial HA concentrations in TiO₂ in suspension exposed to UV light at pH 3

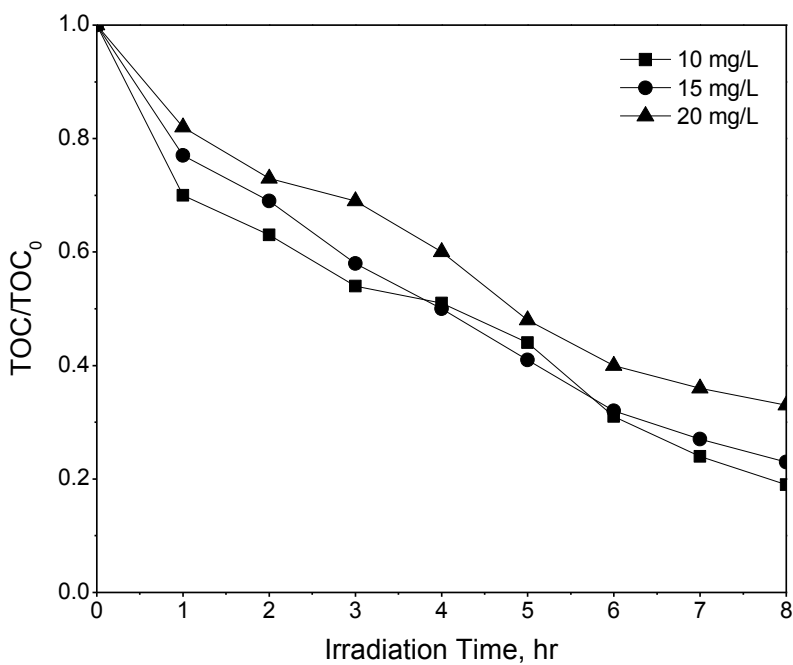


Figure 4-33. HA residuals levels in terms of TOC for three different initial HA concentrations in TiO₂ in suspension exposed to UV light at pH 6

The removal efficiency for 10 and 15 mg/L reaches approximately 96%, and for 20 mg/L was almost 98%. Furthermore, the degradation rate under acidic media is found to be faster considering that average removal of 80%, in terms of UV_{254} , was obtained within 1 hour of agitation. In contrast, at pH 6 the mineralization rate for each of the experimental conditions evaluated was slower. Although the TOC removal was slowly compared to the removal in terms of UV_{254} , at pH 3 a TOC removal of almost 94.5% was obtained. The reason may be attributed to the electrostatic attraction between the TiO_2 and HAs surface as explained in Section 2.2.4. Consequently, a decrease in the pH results in the adsorption of the reactant onto the catalyst surface and eventually a photodecomposition of HA. The above explanation implies that the optimum conditions for degradation is at pH 3.

It is noteworthy that the results observed for the UV-vis spectrometer (at UV_{254}) are quite different from those observed in the TOC analysis. The values of removal percent of UV_{254} are greater than the one reported for the TOC content. For instance, the degradation efficiency for HA with initial concentration of 20 mg/L at pH 6 was 94% for UV_{254} and 67% for TOC. The dissimilarity in the experimental data between the detections methods suggest that the aromatic groups in the HA are reduced faster than the other functional groups presented in the macromolecule. However, the continuous reduction in TOC content demonstrate that the degradation of HA leads to further mineralized it to CO_2 and H_2O . These experiments demonstrate that the TiO_2 as well as the photocatalytic reactor are adequate for the degradation of HAs.

4.3.3 Photodegradation of HA by GTC

This section includes a quantitative comparison of the photocatalytic activity of the TiO₂ films deposited on the glass substrate for each immobilization method. Several degradation experiments were implemented under different conditions of pH and initial HA concentration in order to determine which approach provides an efficient photodegradation. For explanation purposes, the immobilization method will be identified as follows:

- (i). **Method 1:** TiO₂ particles within the SGS body
- (ii). **Method 2:** Immobilization by gravitational deposition and evaporation
- (iii). **Method 3:** Immobilization by TiO₂ coating over the SGS surface

4.3.3.1 Influence of Initial HA concentration

The influence of the initial HA concentration on the photocatalytic efficiency of the coating was evaluated by preparing HA solutions with the following concentrations: 10, 15, and 20 mg/L. The Figure 4-34 through Figure 4-45 shows the resulted photoactivity of each of the immobilization method assessed. The first immobilization approach evaluated was the Method 1. As explained in Section 4.1.1, the GTC under this method was prepared using different amounts of TiO₂ masses. Preliminary experiments showed that the photocatalytic efficiency of the GTC prepared by this method is highly influenced by the amount of TiO₂ particles impregnated onto the glass beads. When using a starting TiO₂ quantity of 1 wt.%, of the total glass beads mass, the GTC did not have the ability of degrade the HA since only

a removal of 5% was achieved. Hence, the GTC prepared with 1 g of TiO₂ and 20 g of glass beads sintered at 975°C for 90 minutes was used for the degradation experiments. In Figure 4-34 through Figure 4-37 can be noticed that the sintered glass embedded with 1 g of TiO₂ particles possess the ability to degrade the HA molecules. The effect of the initial reactant concentration can be observed in the removal percentages presented in Table 4-5 and 4-6. According to the results, the removal efficiency of the GTC improve as the initial HA concentration decreases.

Table 4-5. Photocatalytic removal of HA by Method 1 at pH 3

Detection Method	Initial HA Concentration, mg/L		
	10	15	20
UV ₂₅₄	100	98	96
TOC	93	92	90

Table 4-6. Photocatalytic removal of HA by Method 1 at pH 6

Detection Method	Initial HA Concentration, mg/L		
	10	15	20
UV ₂₅₄	46	42	39
TOC	41	37	27

Similarly, the photoactivity of the GTC prepared by Method 2 was assessed. It should be mentioned that the GTC used under this method was prepared as follows: 3 g of TiO₂, SGS sintered at 975°C for 45 minutes, slurry at pH 1.7, and calcined at 800°C. Although the best TiO₂ adherence was obtained at a calcination temperature of 900°C, TiO₂-films of the GTC calcined at 800°C demonstrated better photocatalytic activity to the one calcined at 900°C.

The degradation of the HA in the presence of this GTC is presented in Figure 4-38 through 4-41. The experimental data shows a decrease in the initial concentration for each of the conditions evaluated. Meaning that the GTC has the capacity to degrade recalcitrant pollutants presents in water. Notice that the removal efficiency at pH does not present the trend expected since the greatest percentage was obtained with the solution of 15 mg/L and the lowest was for the solution with 10 mg/L. This may be attributed to the lack of uniformity in the characteristics of the GTC prepared since for each experimental condition a new GTC was used. Even though the GTC was prepared under the same conditions, the final TiO₂ film in the SGS could have dissimilarity in the particle distribution and size. Hence, affecting the final surface and contact area between the catalyst and the HA.

Table 4-7. Photocatalytic removal of HA by Method 2 at pH 3

Detection Method	Initial HA Concentration, mg/L		
	10	15	20
UV ₂₅₄	96	99	97
TOC	90	92	91

Table 4-8. Photocatalytic removal of HA by Method 2 at pH 6

Detection Method	Initial HA Concentration, mg/L		
	10	15	20
UV ₂₅₄	37	32	18
TOC	31	25	10

Figure 4-42 through 4-45 shows the decrement of HA concentration as a function of irradiation time obtained by method 3. The results indicate that the GTC possess a photoactive properties able to decomposed the HA a different levels of concentration. It is noteworthy that, in terms of total removal of HA, this method showed the best photocatalytic activity since a removal of 100% and 95% was achieved in UV₂₅₄ absorbance and TOC, respectively. In order to understand this behavior the preparation procedure of the catalyst films must be considered. In this method, HNO₃-treated TiO₂ particles were fixed in the surface of the SGS. As explained in Section 4.1.3, it is believed that the particles may absorbed the HNO₃ affecting the physical properties of the TiO₂. Hence, the surface of catalyst film can carry positive charges which increase the attraction of the HA molecules. Due to the adsorption of HA molecules on the GTC surface, the photocatalytic activity under this method seems to be more effective compared to the other methods even under the pH values evaluated.

Table 4-9. Photocatalytic removal of HA by Method 3 at pH 3

Detection Method	Initial HA Concentration, mg/L		
	10	15	20
UV ₂₅₄	100	100	100
TOC	95	94	95

Table 4-10. Photocatalytic removal of HA by Method 3 at pH 6

Detection Method	Initial HA Concentration, mg/L		
	10	15	20
UV ₂₅₄	78	60	58
TOC	55	48	43

4.3.3.2 Influence of Solution pH

The GTC photodegradation experiments were performed at two different pH levels in order to elucidate the influence of the solution pH in the decomposition and mineralization of HA. It can be noticed that the GTC efficiency change considerably according the pH value. Results presented in Figure 4-34 through Figure 4-45 shows that the decrease in the pH level considerably increase the rate of photocatalytic degradation. At the natural pH of the solution (pH 6) less than 20% of the initial HA concentration was degraded within the first hour, in contrast, at pH 3 up to 85% was decomposed in the first hour. It should be added that the total removal also was significantly affected by the pH conditions. Comparing the experimental results presented in Table 4-5 through 4-10 one can see that removal efficiency significantly improve at pH 3. This indicates that reducing the pH to acidic conditions increases the removal efficiency by a factor of almost 3.5.

The relationship between the degradation performance of the GTC and the solution pH can be explained considering the chemical characteristics developed in the system. Depending on the solution pH the TiO₂ particles as well as the HA macromolecule could be present as a negative, neutral or positive charges. As explained in detail in Section 2.2.4, this behavior is related to the protonation and deprotonation process of the catalyst and reactant surface. The natural pH of the solution is very similar to the p*H*_{pzc} of the TiO₂, hence the TiO₂ is considered to possess negative or no charge, while the HAs molecules are deprotonated and tend to have negative charges causing an increment in the electrostatic repulsion of HAs molecules and TiO₂ film. Consequently, promoting a colloidal suspension in the solution that affect the

contact between the HA molecules and the GTC surface. For an efficient photocatalytic process and further degradation, it is necessary to evade the repulsion between the TiO₂ and the HA. The primary photochemical reactions towards the photomineralization of the HA occurs in the surface of the catalyst. A reduction in contact between the TiO₂ and the HA is produced under this neutral to alkaline media, in which the TiO₂ film is not able to adsorb the pollutant. As a result, the generated holes, electrons and hydroxyl radicals are not capable to completely decompose the HAs macromolecules.

The opposite occurs in acidic conditions and the TiO₂ film in the GTC presents adsorptive characteristics since its surface develops an arrangement in which the positive charge particles are capable to attract the HAs. An increase in the contact between the TiO₂ and the HAs results in the degradation of the pollutant and eventually mineralized them to CO₂ and water H₂O. Consequently, the ideal conditions for the photodecomposition of the HAs is under acidic conditions. In addition, the TiO₂ particles may possess a smaller particle size under the acidic media, which can produce an increment in surface area.

The results obtained for each of the method shows significant differences between the degradation of HA in terms of UV₂₅₄ absorbance and in terms of TOC. Between these detection methods, degradation trends were similarly observed for each of the experimental conditions. However, decrease in UV₂₅₄ absorbance was faster. As mentioned early, this could be related to the rate of decomposition of the different functional groups in the HA macromolecule.

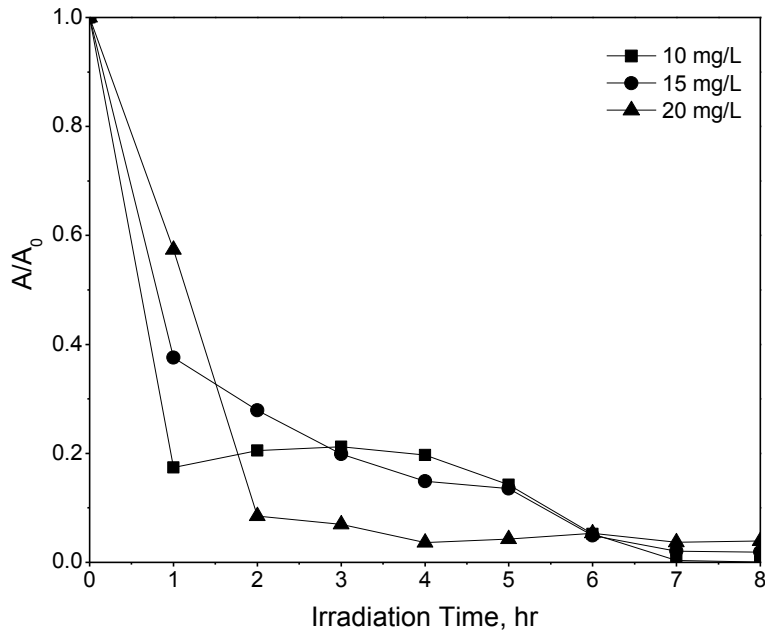


Figure 4-34. Effect of the photocatalytic degradation of different concentration of HA at pH 3 on the UV absorbance with TiO_2 particles within the SGS body

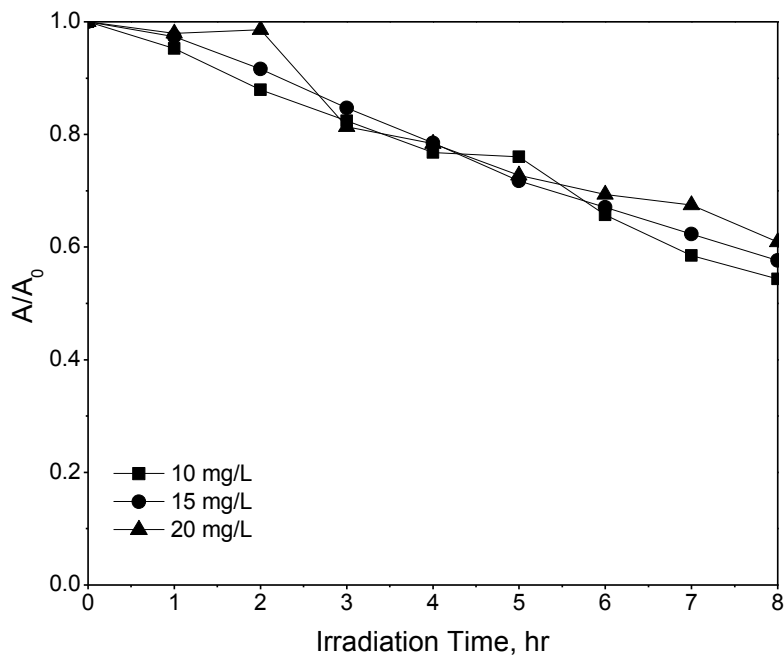


Figure 4-35. Effect of the photocatalytic degradation of different concentration of HA at pH 6 on the UV absorbance with TiO_2 particles within the SGS body

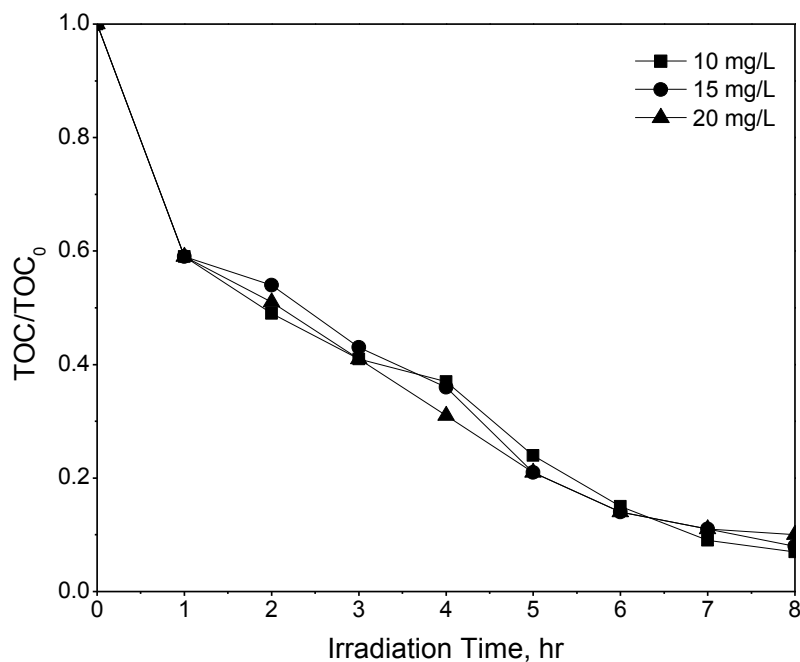


Figure 4-36. Effect of the photocatalytic degradation of different concentration of HA at pH 3 on the TOC with TiO₂ particles within the SGS body

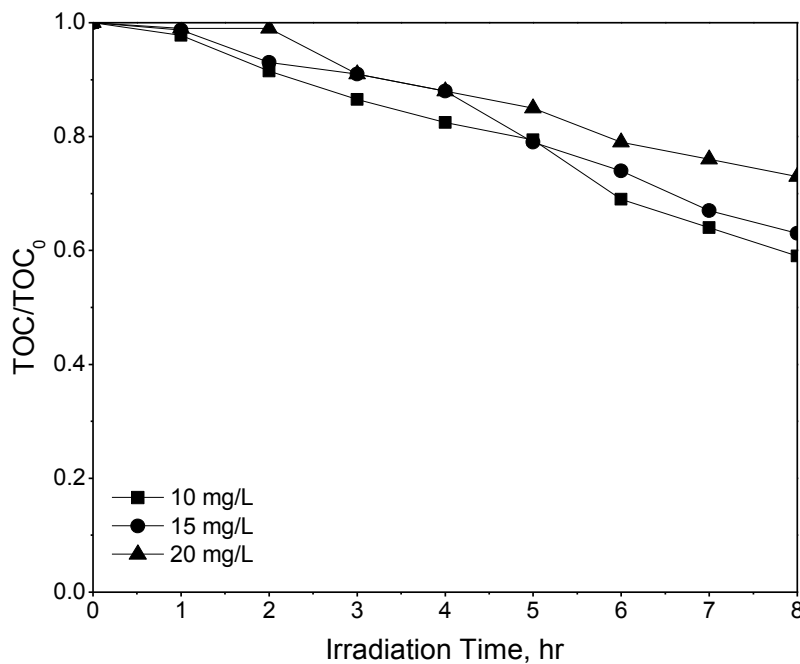


Figure 4-37. Effect of the photocatalytic degradation of different concentration of HA at pH 6 on the TOC with TiO₂ particles within the SGS body

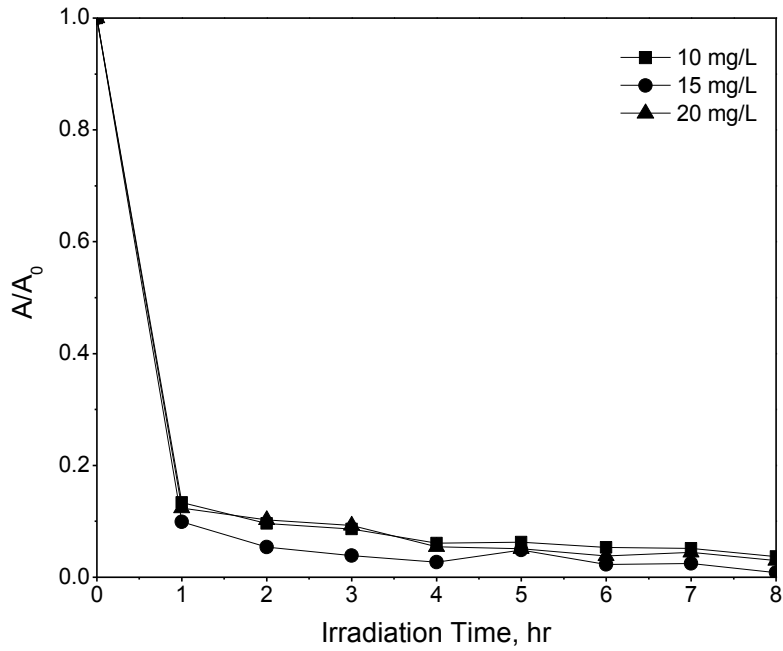


Figure 4-38. Effect of the photocatalytic degradation of different concentration of HA at pH 3 on the UV absorbance with TiO_2 particles immobilized by Method 2

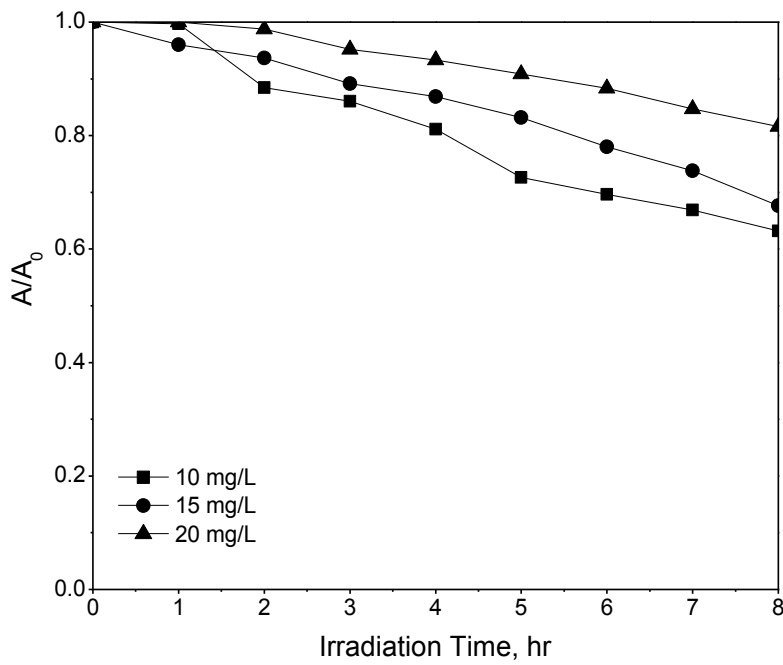


Figure 4-39. Effect of the photocatalytic degradation of different concentration of HA at pH 6 on the UV absorbance with TiO_2 particles immobilized by Method 2

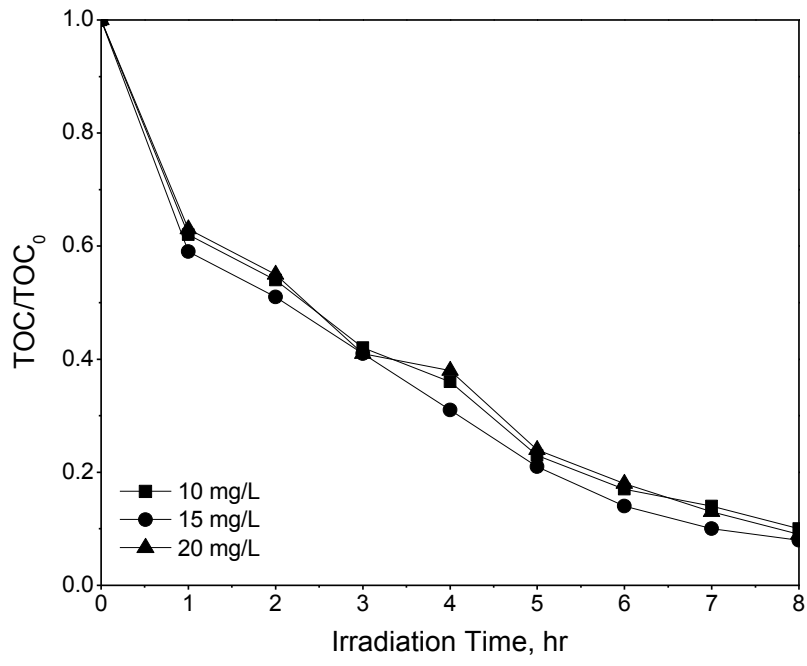


Figure 4-40. Effect of the photocatalytic degradation of different concentration of HA at pH 3 on the TOC with TiO₂ particles immobilized by Method 2

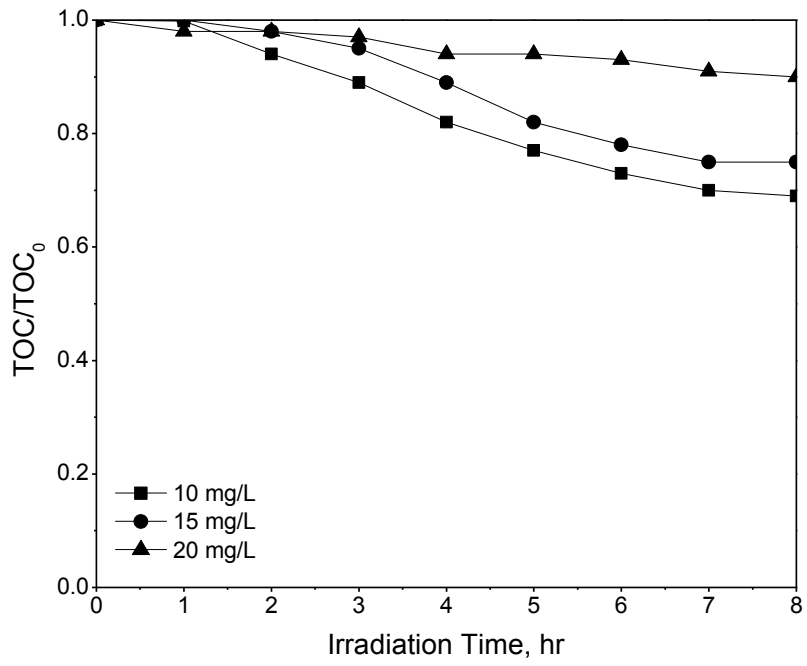


Figure 4-41. Effect of the photocatalytic degradation of different concentration of HA at pH 6 on the TOC with TiO₂ particles immobilized by Method 2

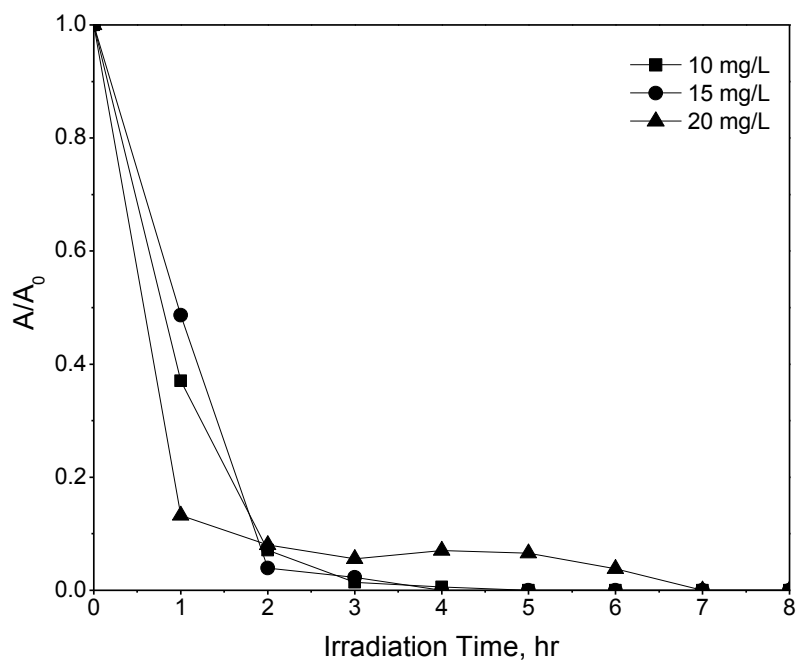


Figure 4-42. Effect of the photocatalytic degradation of different concentration of HA at pH 3 on the UV absorbance with TiO₂ particles immobilized by Method 3

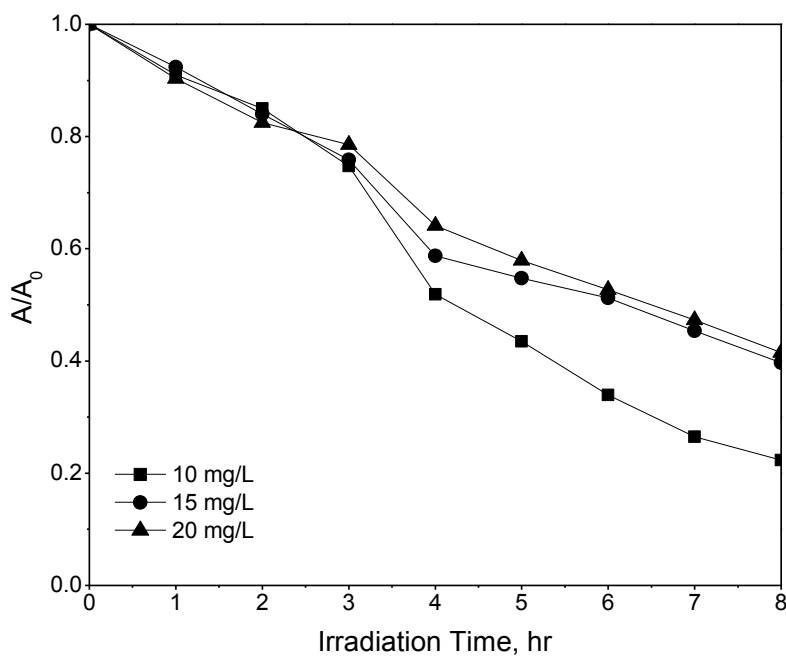


Figure 4-43. Effect of the photocatalytic degradation of different concentration of HA at pH 6 on the UV absorbance with TiO₂ particles immobilized by Method 3

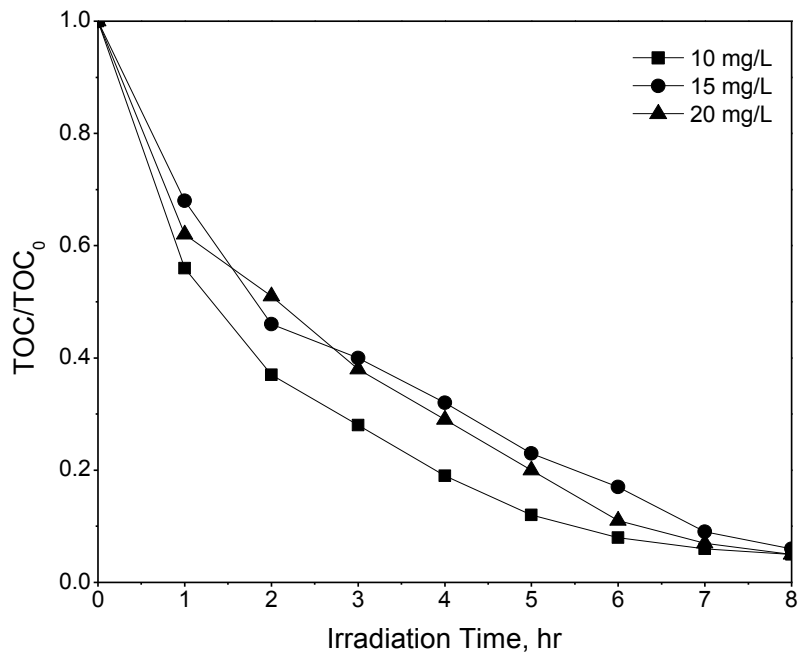


Figure 4-44. Effect of the photocatalytic degradation of different concentration of HA at pH 3 on the TOC with TiO₂ particles immobilized by Method 3

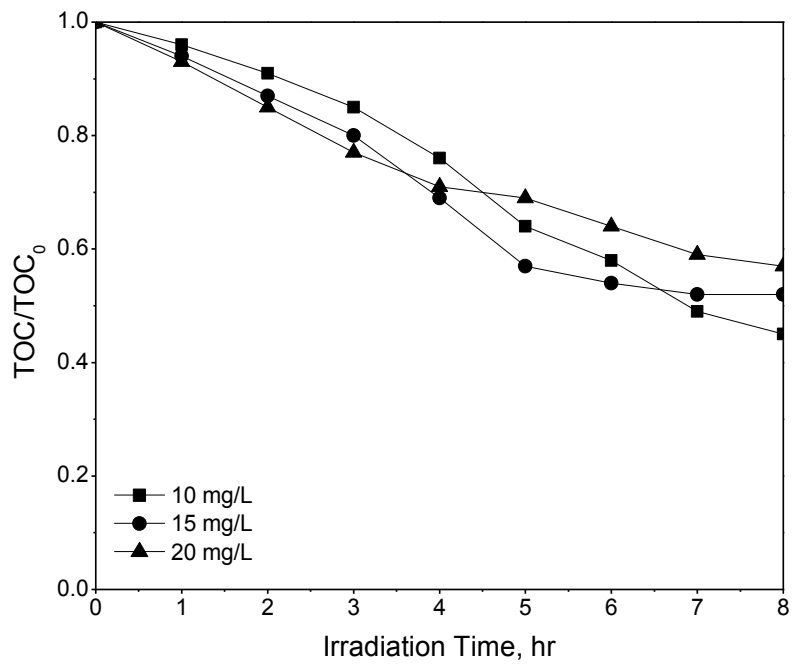


Figure 4-45. Effect of the photocatalytic degradation of different concentration of HA at pH 6 on the TOC with TiO₂ particles immobilized by Method 3

4.4 ADSORPTION OF NATURAL ORGANIC MATTER

The degradation of HAs was investigated in the absence of UV light irradiation at a concentration of 20 mg/L under two different conditions of pH. The experiments were conducted for 8 hours in order to provide a comparison with the photodegradation experiments. Figure 4-46 shows the degradation results for the experiments conducted in the absence of UV light at pH 6. It can be seen that the interaction between the HA and the GTC surface is weak under this pH of the reaction medium.

The lack of adsorption was expected since the electrostatic attraction at pH 6 between the catalyst and the reactant are considered negligible. However, it could be easily seen that the GTC prepared by method 3 demonstrate to have the capacity to attach HA molecules in its surface since a removal of 30% of the initial concentration was achieved. Due to the acid treatment conducted to the TiO₂ particles, the presence of positive charge particles are expected in the GTC surface. The presence of such particles are assumed to be responsible of the adsorptive capacity of the GTC. Even though the reaction medium was under natural pH conditions, it should be considered that the GTC surface is partially charge due to a possible protonation cause by the acid treatment. Therefore, in the aqueous medium the $TiOH_2^+$ might bond to molecules in the HAs.

Contradictory results were observed for the degradation experiment in absence of UV light under acidic conditions. The experimental results obtained are present in Figure 4-47. In this case, significant degradation was observed. Almost a 90% of removal was achieved in within

the first hour of reaction for the GTC prepared by the different immobilization method. This behavior could be explained taking in consideration the electrostatic attraction between the GTC surface and the HAs, which are strong under acidic media. The adsorptive property of the GTC demonstrate that they exhibit promising properties for the development of a filter.

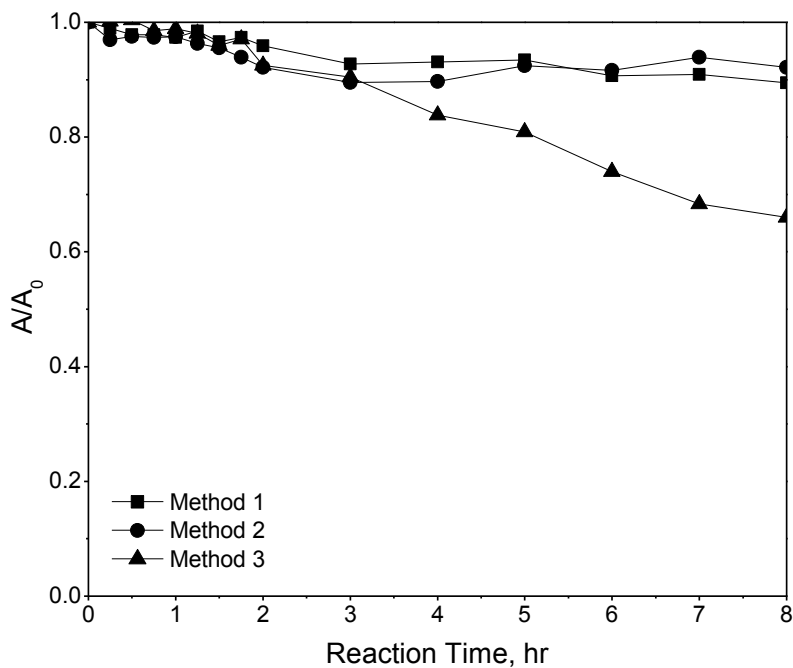


Figure 4-46. Degradation experiments in the absence of UV light with HA concentration of 20 mg/L at pH 6

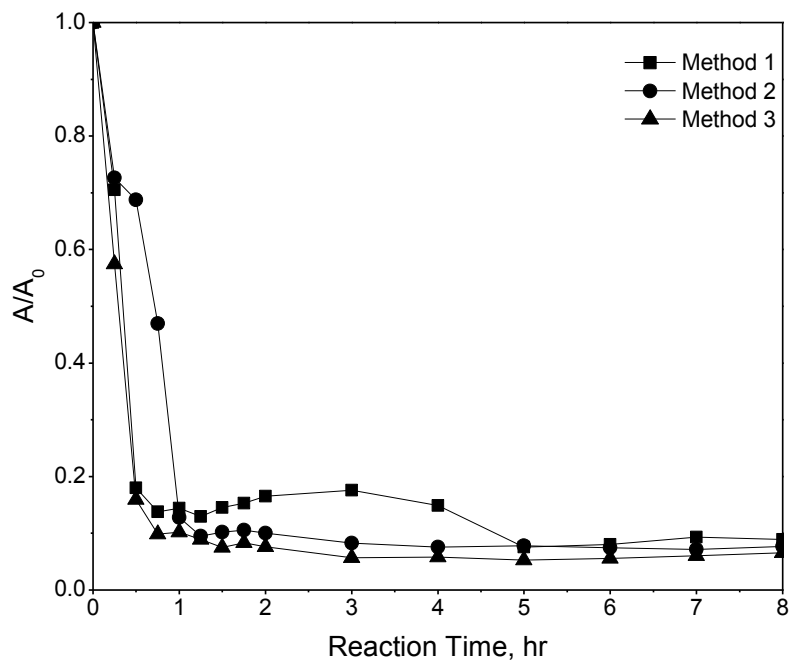


Figure 4-47. Degradation experiments in the absence of UV light with HA concentration of 20 mg/L at pH 3

4.5 FLUORESCENCE SPECTRA OF HAS

The effect of the degradation on the fluorescence spectra of the HAs was evaluated. Figure 4-48 shows the resulted spectra of a HA solution subjected to photodegradation. The results correspond to a degradation of HA under natural pH conditions. It is observed that the initial concentration of the HA solution has a broad peak around 460 nm with an intensity of 175. As the reaction time increases this peak become less intense until it completely disappears. The reduction in peak intensity indicates that the photocatalytic process are degrading the fluorophores that comprises the HAs molecules. Generally, this behavior was observed in all the degradation experiments conducted.

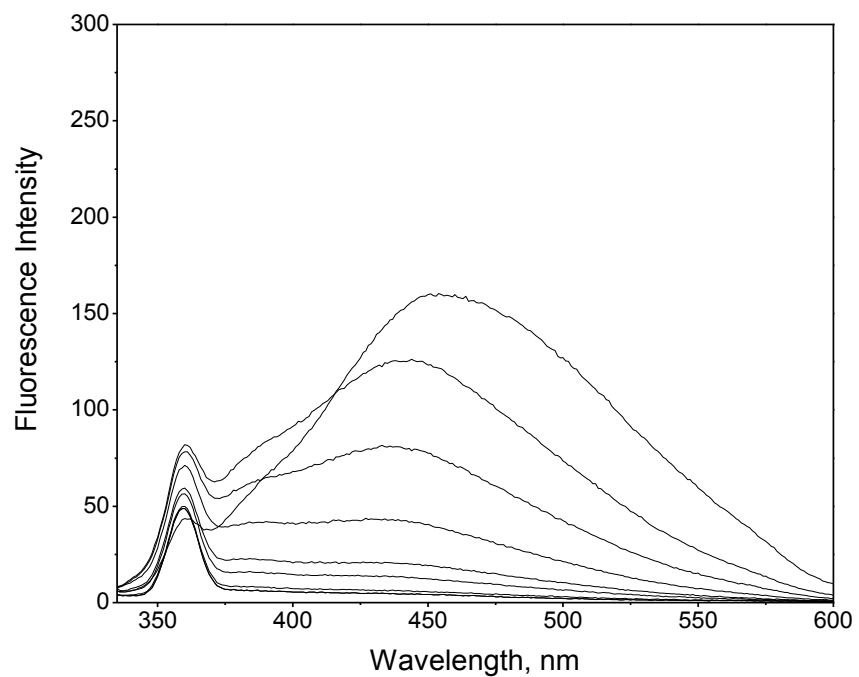


Figure 4-48. Fluorescence spectra of HA as a function of irradiation time

5 CONCLUSIONS

The excessive presence of HAs in natural waters may produce adverse health effects since they are considered one of the principal precursors of harmful compounds such as THMs. In view to suppress the formation of THMs due to chlorine-based disinfection process, the aim of this research was to investigate several alternative to remove HAs in an aqueous medium through the application of advanced oxidation processes. TiO_2 assisted photocatalytic degradation was selected for the removal of HAs due to its efficient photoactivity. In this matter, the catalyst was supported on a sintered glass substrates to undergo photodegradation of the HA solution.

The immobilization of TiO_2 particles was achieved by implementing three different techniques. The particles were attached on SGS possessing different characteristics according to the sintering time and temperature. Generally, the sintering time and temperature were identified as critical experimental parameters since a decrease in the SGS open porosity, total porosity, and percolation was observed as these parameters increases. Moreover, the addition of the TiO_2 particles to the SGS also reduced its porosity.

The TiO_2 particles were either embedded within the SGS body or immobilized on the SGS surface. It was demonstrated that the TiO_2 -glass immobilization is influenced by several parameters such as catalyst concentration, calcination temperatures, contact time between the TiO_2 slurry and the SGS, sintering parameters as well as slurry pH. In fact, the pH level

was an important parameter controlling the immobilization of TiO_2 in each of the techniques evaluated. It was observed that the total deposited and immobilized mass increased by decreasing the slurry pH. Furthermore, a better attachment was observed when the slurry was prepared at pH 1.7 since lower loss mass were found under this condition. In acidic media, the TiO_2 particles are protonated and tend to have positive charges causing an increment in the electrostatic repulsion of the particles. Hence, the stability of the slurry and attraction to the SGS was enhanced.

The photocatalytic degradation efficiencies of the prepared TiO_2 -immobilized substrate were evaluated using HA as the pollutant. Despite the discrepancy in the immobilization techniques, the photocatalytic degradation experiments showed that the performance and photoactivity of each GTC were very similar. There was a dependency between the adsorption and the photocatalytic performance of the GTC. The removal efficiency was greater under acid conditions due to effect of electrostatic attraction and further adsorption that leads to a photomineralization of HA. Among the proposed method for the immobilization of TiO_2 , the degradation and mineralization of HA was found to be more efficient in the method using HNO_3 -treated TiO_2 particles since a degradation of 100% of the concentration was observed.

Based on the results obtained from the degradation is prudent to suggest further investigation in order to achieve a more realistic schema of the problem. Although the GTC demonstrated a good photodegradation efficiency, experiments with natural water from different sources should be conducted. This should include the characterization of the natural organic matter

in the samples, isolation and extraction of the HAs. Characterization of the samples will provide a better understanding of their composition and degradation process.

In summary, some of the most relevant conclusions based on the obtained results in this research include the following:

- (i).** An increase in the sintering parameters implied a reduction in SGS porosity and water percolation.
- (ii).** The thermal treatment used for the immobilization process did not affected the crystal structure of the TiO_2 since the anatase phase was confirm in the XRD diffractogram.
- (iii).** It was demonstrated that highly photoactive TiO_2 films can be deposited and immobilized on glass substrates.
- (iv).** The pH conditions play an important role in the immobilization of TiO_2 as well as in the photocatalytic degradation.
- (v).** The GTC prepared by the method in which HNO_3 -treated particles were used showed the most homogenous coating over the surface of the SGS.
- (vi).** HNO_3 -treated TiO_2 particles can improved the photocatalytic degradation process under natural conditions since it is believed that the GTC could greatly adsorb the HA molecules and due to a possible increment of particle surface area.

(vii). The decomposition and mineralization of HAs can be enhanced by decreasing the pH of the aqueous medium due to a better adsorption of the HAs.

REFERENCES

- Amir, S., Hafidi, M., Merlina, G., Hamdi, H., & Revel, J.-C. (2004). Elemental Analysis, FTIR and ¹³C-NMR of humic acids from sewage sludge composting. *Italian Journal of Agronomy*, 3(3), 13–18. <https://doi.org/10.1051/agro>
- Andayani, W., & Bagyo, A. N. M. (2011). TiO₂ Beads for photocatalytic degradation of humic acid in peat water, 11(3), 253–257.
- Asing, J., Wong and Lau, N. S., Wong, N., Lau, S., Asing, J., Nan Chong, W., & Seng, L. (2009). Optimization of extraction method and characterization of humic acid derived from coals and composts. *J. Trop. Agric. and Fd. Sc*, 37(2), 211–223.
- Baghoth, S. A. (2012). CharaCterizing natural organiC matter in drinking water treatment proCesses and trains saeed abdallah baghoth, 178.
- Bahnemann, W., Muneer, M., & Haque, M. M. (2007). Titanium dioxide-mediated photocatalysed degradation of few selected organic pollutants in aqueous suspensions. *Catalysis Today*, 124(3–4), 133–148. <https://doi.org/10.1016/j.cattod.2007.03.031>
- Bekbolet, M., Suphandag, A. S., & Uyguner, C. S. (2002). An investigation of the photocatalytic efficiencies of TiO₂ powders on the decolourisation of humic acids. *Journal of Photochemistry and Photobiology A: Chemistry*, 148(1–3), 121–128. [https://doi.org/10.1016/S1010-6030\(02\)00081-3](https://doi.org/10.1016/S1010-6030(02)00081-3)
- Benítez, J. (1991). *Kinetics of trihalomethanes formation during chlorination of drinking water*. U.S. Geological Survey.
- Bernardo, E., Bonomo, E., & Dattoli, A. (2010). Optimisation of sintered glass-ceramics from an industrial waste glass. *Ceramics International*, 36(5), 1675–1680. <https://doi.org/10.1016/j.ceramint.2010.02.047>
- Boguta, P., D’Orazio, V., Sokołowska, Z., & Senesi, N. (2016). Effects of selected chemical and physicochemical properties of humic acids from peat soils on their interaction mechanisms with copper ions at various pHs. *Journal of Geochemical Exploration*, 168, 119–126. <https://doi.org/10.1016/j.gexplo.2016.06.004>
- Brigante, M., Zanini, G., & Avena, M. (2009). Effect of pH, anions and cations on the dissolution kinetics of humic acid particles. *Colloids and Surfaces A: Physicochemical and Engineering Aspects*, 347(1), 180–186. <https://doi.org/10.1016/j.colsurfa.2009.04.003>
- Cedillo-González, E. I., Riccò, R., Montorsi, M., Montorsi, M., Falcaro, P., & Siligardi, C. (2014). Self-cleaning glass prepared from a commercial TiO₂ nano-dispersion and its photocatalytic performance under common anthropogenic and atmospheric factors.

Building and Environment, 71, 7–14. <https://doi.org/10.1016/j.buildenv.2013.09.007>

- Chiu, C. Y., & Tian, G. (2011). Chemical structure of humic acids in biosolids-amended soils as revealed by NMR spectroscopy. *Applied Soil Ecology*, 49(1), 76–80. <https://doi.org/10.1016/j.apsoil.2011.06.013>
- Christl, I., Milne, C. J., Kinniburgh, D. G., & Kretzschmar, R. (2001). Relating ion binding by fulvic and humic acids to chemical composition and molecular Size. 2. metal binding. *Environmental Science & Technology*, 35(12), 2512–2517. <https://doi.org/10.1021/es0002520>
- Cuadrado, W. (2014). *Fabrication and characterization of sintered recycled glass designed for polluted soil filtering*. University of Puerto Rico Mayaguez Campus.
- de Melo, B. A. G., Motta, F. L., & Santana, M. H. A. (2015). Humic acids: Structural properties and multiple functionalities for novel technological developments. *Materials Science and Engineering C*, 62, 967–974. <https://doi.org/10.1016/j.msec.2015.12.001>
- Diebold, U. (2003). The surface science of titanium dioxide. *Surface Science Reports*, 48(5), 53–229. [https://doi.org/10.1016/S0167-5729\(02\)00100-0](https://doi.org/10.1016/S0167-5729(02)00100-0)
- Dong, H., Zeng, G., Tang, L., Fan, C., Zhang, C., He, X., & He, Y. (2015). An overview on limitations of TiO₂-based particles for photocatalytic degradation of organic pollutants and the corresponding countermeasures. *Water Research*, 79, 128–146. <https://doi.org/10.1016/j.watres.2015.04.038>
- Dziedzic, J., Wodka, D., Nowak, P., Warszyński, P., Simon, C., & Kumakiri, I. (2010). Photocatalytic degradation of the humic species as a method of their removal from water - comparison of UV and artificial sunlight irradiation. *Physicochemical Problems of Mineral Processing*, 45, 15–28.
- Furube, A., Asahi, T., Masuhara, H., Yamashita, H., & Anpo, M. (2001). *Direct observation of a picosecond charge separation process in photoexcited platinum-loaded TiO₂ particles by femtosecond diffuse reflectance spectroscopy*. *Chemical Physics Letters* (Vol. 336). [https://doi.org/10.1016/S0009-2614\(01\)00128-2](https://doi.org/10.1016/S0009-2614(01)00128-2)
- Gieguzynska, E., Amine-Khodja, A., Trubetskoj, O. A., Trubetskaya, O. E., Guyot, G., ter Halle, A., ... Richard, C. (2009). Compositional differences between soil humic acids extracted by various methods as evidenced by photosensitizing and electrophoretic properties. *Chemosphere*, 75(8), 1082–1088. <https://doi.org/10.1016/j.chemosphere.2009.01.047>
- Gondar, D., Lopez, R., Fiol, S., Antelo, J. M., & Arce, F. (2005). Characterization and acid-base properties of fulvic and humic acids isolated from two horizons of an ombrotrophic peat bog. *Geoderma*, 126(3–4), 367–374. <https://doi.org/10.1016/j.geoderma.2004.10.006>

- Hanaor, D. A. H., & Sorrell, C. C. (2011). Review of the anatase to rutile phase transformation. *Journal of Materials Science*, 46(4), 855–874. <https://doi.org/10.1007/s10853-010-5113-0>
- Hashimoto, K., Irie, H., & Fujishima, A. (2005). TiO₂ Photocatalysis: A historical overview and future prospects. *Japanese Journal of Applied Physics*, 44(12), 8269–8285. <https://doi.org/10.1143/JJAP.44.8269>
- Hidalgo, M. C., Sakthivel, S., & Bahnemann, D. (2004). Highly photoactive and stable TiO₂ coatings on sintered glass. *Applied Catalysis A: General*, 277(1–2), 183–189. <https://doi.org/10.1016/j.apcata.2004.09.011>
- Hoffmann, M. R., Martin, S. T., Choi, W., & Bahnemann, D. W. (1995). Environmental Applications of Semiconductor Photocatalysis. *Chemical Reviews*, 95(1), 69–96. <https://doi.org/10.1021/cr00033a004>
- Hosseini, S. N., Borghei, M., Vossoughi, M., & Taghavinia, N. (2008). Photocatalytic degradation of phenol in aqueous phase with TiO₂ immobilized on three different supports with a simple method. *Proceedings of the 3rd IASME/WSEAS International Conference on Energy & Environment*, 46–50.
- Hosseini, S. N., Borghei, S. M., Vossoughi, M., & Taghavinia, N. (2007). Immobilization of TiO₂ on perlite granules for photocatalytic degradation of phenol. *Applied Catalysis B: Environmental*, 74(1–2), 53–62. <https://doi.org/10.1016/j.apcatb.2006.12.015>
- Huang, X., Leal, M., & Li, Q. (2008). Degradation of natural organic matter by TiO₂ photocatalytic oxidation and its effect on fouling of low-pressure membranes. *Water Research*, 42(4–5), 1142–1150. <https://doi.org/10.1016/j.watres.2007.08.030>
- Janknecht, P., Proenc, F., Rodrigues, A., Brito, A., Janknecht, P., Proença, M. F., & Nogueira, R. (2009). Quantification of humic acids in surface water: effects of divalent cations, pH, and filtration. *Journal of Environmental Monitoring : JEM*, 11(2), 377–82. <https://doi.org/10.1039/b811942b>
- Kaliwoh, N., Zhang, J.-Y., & Boyd, I. W. (2002). Characterisation of TiO₂ deposited by photo-induced chemical vapour deposition. *Applied Surface Science*, 186, 241–245.
- Klavins, M., & Purmalis, O. (2010). Humic substances as surfactants. *Environmental Chemistry Letters*, 8(4), 349–354. <https://doi.org/10.1007/s10311-009-0232-z>
- Klavins, M., & Purmalis, O. (2013). Properties and structure of raised bog peat humic acids. *Journal of Molecular Structure*, 1050, 103–113. <https://doi.org/10.1016/j.molstruc.2013.07.021>
- Klučáková, M. (2016). Dissociation properties and behavior of active humic fractions dissolved in aqueous systems. *Reactive and Functional Polymers*, 109, 9–14.

<https://doi.org/10.1016/j.reactfunctpolym.2016.09.004>

- Krasner, S. W., Weinberg, H. S., Richardson, S. D., Pastor, S. J., Chinn, R., Scrimanti, M. J., ... Thruston, A. D. (2006). Occurrence of a New Generation of Disinfection Byproducts. *Environmental Science & Technology*, *40*(23), 7175–7185. <https://doi.org/10.1021/es060353j>
- Kumar, J., & Bansal, A. (2012). Photodegradation of amaranth in aqueous solution catalyzed by immobilized nanoparticles of titanium dioxide. *International Journal of Environmental Science and Technology*, *9*(3), 479–484. <https://doi.org/10.1007/s13762-012-0064-4>
- Lazar, M. A., Varghese, S., & Nair, S. S. (2012). Photocatalytic water treatment by Titanium Dioxide: Recent updates. *Catalysts*, *2*, 572–601. <https://doi.org/10.3390/catal2040572>
- Le-Clech, P., Lee, E. K., & Chen, V. (2006). Hybrid photocatalysis/membrane treatment for surface waters containing low concentrations of natural organic matters. *Water Research*, *40*(2), 323–330. <https://doi.org/10.1016/j.watres.2005.11.011>
- Li, X., Li, F., Fan, C., & Sun, Y. (2002). Photoelectrocatalytic Degradation of Humic Acid in Aqueous Solution Using a Ti/TiO₂ Mesh Photoelectrode. *Water Res.*, *36*, 2215–2224.
- Lin, H., Huang, C. P., Li, W., Ni, C., Shah, S. I., & Tseng, Y. H. (2006). Size dependency of nanocrystalline TiO₂ on its optical property and photocatalytic reactivity exemplified by 2-chlorophenol. *Applied Catalysis B: Environmental*, *68*(1–2), 1–11. <https://doi.org/10.1016/j.apcatb.2006.07.018>
- Liu, S., Lim, M., Fabris, R., Chow, C., Chiang, K., Drikas, M., & Amal, R. (2008). Removal of humic acid using TiO₂ photocatalytic process - Fractionation and molecular weight characterisation studies. *Chemosphere*, *72*(2), 263–271. <https://doi.org/10.1016/j.chemosphere.2008.01.061>
- Luttrell, T., Halpegamage, S., Tao, J., Kramer, A., Sutter, E., & Batzill, M. (2014). Why is anatase a better photocatalyst than rutile?--Model studies on epitaxial TiO₂ films. *Scientific Reports*, *4*, 4043. <https://doi.org/10.1038/srep04043>
- Mansilla, H. D., Mora, A., Pincheira, C., Mondaca, M. A., Marcato, P. D., Durán, N., & Freer, J. (2007). New photocatalytic reactor with TiO₂ coating on sintered glass cylinders. *Applied Catalysis B: Environmental*, *76*(1–2), 57–63. <https://doi.org/10.1016/j.apcatb.2007.04.025>
- Matilainen, A., Gjessing, E. T., Lahtinen, T., Hed, L., Bhatnagar, A., & Sillanpää, M. (2011). An overview of the methods used in the characterisation of natural organic matter (NOM) in relation to drinking water treatment. *Chemosphere*, *83*(11), 1431–1442. <https://doi.org/10.1016/j.chemosphere.2011.01.018>
- McDonald, S., Bishop, A. G., Prenzler, P. D., & Robards, K. (2004). Analytical chemistry of

freshwater humic substances. *Analytica Chimica Acta*, 527(2), 105–124.
<https://doi.org/10.1016/j.aca.2004.10.011>

- Mor, G. K., Varghese, O. K., Paulose, M., Shankar, K., & Grimes, C. A. (2006). A review on Highly Ordered, Vertically Oriented TiO₂ Nanotube Arrays: Fabrication, Material Properties, and Solar Energy Applications. *Sol. Energy Mater. Sol. Cells*, 90, 2011–2075.
- Mosteo, R., Miguel, N., Martin-Muniesa, S., Ormad, M. P., & Ovelleiro, J. L. (2009). Evaluation of trihalomethane formation potential in function of oxidation processes used during the drinking water production process. *Journal of Hazardous Materials*, 172(2–3), 661–666.
<https://doi.org/10.1016/j.jhazmat.2009.07.048>
- Motta, F. L., Melo, B. A. G., & Santana, M. H. A. (2016). Deprotonation and protonation of humic acids as a strategy for the technological development of pH-responsive nanoparticles with fungicidal potential. *New Biotechnology*, 33(6), 773–780.
<https://doi.org/10.1016/j.nbt.2016.07.003>
- Musić, S., Filipović-Vinceković, N., & Sekovanić, L. (2011). Precipitation of amorphous SiO₂ particules and their properties. *Brazilian Journal of Chemical Engineering*, 28(1), 89–94.
<https://doi.org/10.1590/S0104-66322011000100011>
- Nakata, K., & Fujishima, A. (2012). TiO₂ photocatalysis: Design and applications. *Journal of Photochemistry and Photobiology C: Photochemistry Reviews*, 13(3), 169–189.
<https://doi.org/10.1016/j.jphotochemrev.2012.06.001>
- Paez, L. R., & Matoušek, J. (2003). PREPARATION OF TiO₂ SOL-GEL LAYERS ON GLASS. *Ceramics*, 47(1), 28–31.
- Pansamut, G., Charinpanitkul, T., Biswas, P., & Suriyawong, A. (2013). Removal of Humic Acid by Photocatalytic Process: Effect of Light Intensity. *Engineering Journal*, 17(3), 25–32. <https://doi.org/10.4186/ej.2013.17.3.25>
- Park, K. H., Jin, E. M., Gu, H. B., Shim, S. E., & Hong, C. K. (2009). Effects of HNO₃ treatment of TiO₂ nanoparticles on the photovoltaic properties of dye-sensitized solar cells. *Materials Letters*, 63(26), 2208–2211. <https://doi.org/10.1016/j.matlet.2009.07.034>
- Peña-Méndez, M. E., Havel, J., & Patočka, J. (2005). Humic substances – compounds of still unknown structure : applications in agriculture , industry , environment , and biomedicine. *J. Appl. Biomed.*, 3, 13–24.
https://doi.org/https://assets.motherearthlabs.com/resources/4.humic_.substances.compn ds.of_.unkwn_.structure2005.pdf
- Pinar Gokdemir, F., Ece Yuzbasioglu, vecihe, Keskin, B., Ozdemir, O., & Kutlu, K. (2014). Formation Of TiO₂ Thin Films By A Modified Sol-gel Route And Characterization Of Structural, Optical And Electrochromic Properties. *Advanced Materials Letters*, 5(7), 367–

371. <https://doi.org/10.5185/amlett.2014.amwc.1007>

Reguero, V., López-Fernández, R., Feroso, J., Prieto, O., Pocostales, P., González, R., ... Villaverde, S. (2013). Comparison of conventional technologies and a Submerged Membrane Photocatalytic Reactor (SMPR) for removing trihalomethanes (THM) precursors in drinking water treatment plants. *Desalination*, 330, 28–34. <https://doi.org/10.1016/j.desal.2013.09.014>

Rice, J. A., & MacCarthy, P. (1991). Statistical evaluation of the elemental composition of humic substances. *Org. Geochem*, 17(5), 635–648.

Riungu, N. J., Home, P. G., & Nnegwa, G. M. (2012). Degradation of Humic Acid by Titanium Dioxide Catalyst, 1(1), 61–65.

Saito, B., & Seckler, M. M. (2014). Alkaline extraction of humic substances from peat applied to organic-mineral fertilizer production. *Brazilian Journal of Chemical Engineering*, 31(3), 675–682. <https://doi.org/10.1590/0104-6632.20140313s00002512>

Santacruz, I., Cabeza, A., Ibeh, P., Losilla, E. R., De La Torre, Á. G., & Aranda, M. A. G. (2012). Preparation of photocatalytic TiO₂ coatings by gel-dipping with polysaccharides. *Ceramics International*, 38(8), 6531–6540. <https://doi.org/10.1016/j.ceramint.2012.05.034>

Schulten, H., & Schnitzer, M. (1993). A State of the Art Structural Concept for Humic Substances. *Naturwissenschaften*, 29–30.

Shi, X., Wang, S., Dong, X., & Zhang, Q. (2009). Enhanced photocatalytic activity of titanium dioxide by nut shell carbon. *Journal of Hazardous Materials*, 167(1–3), 692–695. <https://doi.org/10.1016/j.jhazmat.2009.01.038>

Sillanpää, M. (2014). *NOM in water: Characterisation and treatment methods. Igarss 2014*. <https://doi.org/10.1007/s13398-014-0173-7.2>

Stathatos, E., Papoulis, D., Aggelopoulos, C. A., Panagiotaras, D., & Nikolopoulou, A. (2012). TiO₂/palygorskite composite nanocrystalline films prepared by surfactant templating route: Synergistic effect to the photocatalytic degradation of an azo-dye in water. *Journal of Hazardous Materials*, 211–212, 68–76. <https://doi.org/10.1016/j.jhazmat.2011.11.055>

Timofeevna Shirshova, L., Ghabbour, E. A., & Davies, G. (2006). Spectroscopic characterization of humic acid fractions isolated from soil using different extraction procedures. *Geoderma*, 133(3–4), 204–216. <https://doi.org/10.1016/j.geoderma.2005.07.007>

Trubetskaya, O. E., Trubetskoj, O. A., Voyard, G., & Richard, C. (2013). Determination of hydrophobicity and optical properties of soil humic acids isolated by different methods.

Journal of Geochemical Exploration, 132, 84–89.
<https://doi.org/10.1016/j.gexplo.2013.06.004>

- Tseng, T. K., Lin, Y. S., Chen, Y. J., & Chu, H. (2010). A review of photocatalysts prepared by sol-gel method for VOCs removal. *International Journal of Molecular Sciences*, 11(6), 2336–2361. <https://doi.org/10.3390/ijms11062336>
- Umar, M., & Aziz, H. A. (2013). Photocatalytic Degradation of Organic Pollutants in Water.
- United States Environmental Protection Agency. (2012). Stage 2 DBP Rule. Retrieved from <http://water.epa.gov/lawsregs/rulesregs/sdwa/stage2/basicinformation.cfm>
- Uyguner-Demirel, C. S., & Bekbolet, M. (2011). Significance of analytical parameters for the understanding of natural organic matter in relation to photocatalytic oxidation. *Chemosphere*, 84(8), 1009–1031. <https://doi.org/10.1016/j.chemosphere.2011.05.003>
- Uyguner, C. S., & Bekbolet, M. (2005). Evaluation of humic acid photocatalytic degradation by UV-vis and fluorescence spectroscopy. *Catalysis Today*, 101(3–4 SPEC. ISS.), 267–274. <https://doi.org/10.1016/j.cattod.2005.03.011>
- Valencia, S., Marín, J. M., Restrepo, G., & Frimmel, F. H. (2013). Evaluations of the TiO₂/simulated solar UV degradations of XAD fractions of natural organic matter from a bog lake using size-exclusion chromatography. *Water Research*, 47(14), 5130–5138. <https://doi.org/10.1016/j.watres.2013.05.053>
- van Rensburg, C. E. J. (2015). The Antiinflammatory Properties of Humic Substances: A Mini Review. *Phytotherapy Research*, 29(6), 791–795. <https://doi.org/10.1002/ptr.5319>
- Wan Ngah, W. S., Hanafiah, M. A. K. M., & Yong, S. S. (2008). Adsorption of humic acid from aqueous solutions on crosslinked chitosan-epichlorohydrin beads: Kinetics and isotherm studies. *Colloids and Surfaces B: Biointerfaces*, 65(1), 18–24. <https://doi.org/10.1016/j.colsurfb.2008.02.007>
- Wang, J., Bi, L., Ji, Y., Ma, H., & Yin, X. (2014). Removal of humic acid from aqueous solution by magnetically separable polyaniline: Adsorption behavior and mechanism. *Journal of Colloid and Interface Science*, 430, 140–146. <https://doi.org/10.1016/j.jcis.2014.05.046>
- Wang, M.-Q., Yan, J., Cui, H.-P., & Du, S.-G. (2013). Low temperature preparation and characterization of TiO₂ nanoparticles coated glass beads by heterogeneous nucleation method. *Materials Characterization*, 76(97), 39–47. <https://doi.org/10.1016/j.matchar.2012.12.002>
- Wang, Z., Helmersson, U., & Käll, P.-O. (2002). Optical properties of anatase TiO₂ thin films prepared by aqueous sol-gel process at low temperature. *Thin Solid Films*, 405(1–2), 50–54. [https://doi.org/10.1016/S0040-6090\(01\)01767-9](https://doi.org/10.1016/S0040-6090(01)01767-9)

- Wiszniewski, J., Robert, D., Surmacz-Gorska, J., Miksch, K., & Weber, J.-V. (2002). Photocatalytic decomposition of humic acids on TiO₂. *Journal of Photochemistry and Photobiology A: Chemistry*, 152(1–3), 267–273. [https://doi.org/10.1016/S1010-6030\(02\)00022-9](https://doi.org/10.1016/S1010-6030(02)00022-9)
- Xu, J., Zhao, B., Chu, W., Mao, J., & Zhang, J. (2017). Chemical nature of humic substances in two typical Chinese soils (upland vs paddy soil): A comparative advanced solid state NMR study. *Science of the Total Environment*, 576, 444–452. <https://doi.org/10.1016/j.scitotenv.2016.10.118>
- Yigit, Z., & Inan, H. (2009). A study of the photocatalytic oxidation of humic acid on anatase and mixed-phase anatase-rutile TiO₂ nanoparticles. *Water, Air, and Soil Pollution: Focus*, 9(3), 237–243. <https://doi.org/10.1007/s11267-009-9213-2>
- Zaleska, A. (2008). Doped-TiO₂: A Review. *Recent Patents on Engineering 2008*, 2, 157-164, (1), 157–164. https://doi.org/10.1007/978-1-4020-8121-0_8
- Zhang, S., Yuan, L., Li, W., Lin, Z., Li, Y., Hu, S., & Zhao, B. (2017). Characterization of pH-fractionated humic acids derived from Chinese weathered coal. *Chemosphere*, 166, 334–342. <https://doi.org/10.1016/j.chemosphere.2016.09.095>
- Zhang, Y., Xiong, X., Han, Y., Zhang, X., Shen, F., Deng, S., ... Peng, H. (2012). Photoelectrocatalytic degradation of recalcitrant organic pollutants using TiO₂ film electrodes: An overview. *Chemosphere*, 88(2), 145–154. <https://doi.org/10.1016/j.chemosphere.2012.03.020>
- Zhu, M., Wang, H., Keller, A. A., Wang, T., & Li, F. (2014). The effect of humic acid on the aggregation of titanium dioxide nanoparticles under different pH and ionic strengths. *Science of the Total Environment*, 487(1), 375–380. <https://doi.org/10.1016/j.scitotenv.2014.04.036>
- Zhuang, J., Dai, W., Tian, Q., Li, Z., Xie, L., Wang, J., ... Wang, D. (2010). Photocatalytic degradation of RhB over TiO₂ bilayer films: Effect of defects and their location. *Langmuir*, 26(12), 9686–9694. <https://doi.org/10.1021/la100302m>